Technical Report No. 32-464

The Determination and Characteristics of Ballistic Interplanetary Trajectories Under the Influence of Multiple Planetary Attractions

Michael A. Minovitch

T. W. Hamilton, *Chief*
Systems Analysis Section

JET PROPULSION LABORATORY
CALIFORNIA INSTITUTE OF TECHNOLOGY
PASADENA, CALIFORNIA

October 31, 1963

CONTENTS

CONTENTS (Cont'd)

TABLES

TABLES (Cont'd)

FIGURES

FIGURES (Cont'd)

ACKNOWLEDGMENTS

The author wishes to express deep appreciation to the Computing Facility of the University of California at Los Angeles for carrying out many of the calculations. If this facility or its operational policies did not exist, the numerical results describing these advanced interplanetary missions would have been greatly delayed. The program for the IBM 7090 digital computer corresponding to the solution given in Part III was written at UCLA, whereupon the extensive calculations took place at UCLA and at the Jet Propulsion Laboratory. The author wishes to convey his gratitude to all the computer operators at both facilities for their kind and thoughtful assistance. The author also expresses his appreciation to Victor C. Clarke, Jr., of the Systems Analysis Section at the Jet Propulsion Laboratory, who was closely associated with the project and provided a great deal of valuable information aiding the numerical computation. The secretarial work of Miss Corinne Ward, also in the Systems Analysis Section at JPL, is also appreciated.

ABSTRACT

When an interplanetary space vehicle approaches a planet on a free-fall trajectory, the gravitational influence of the planet can radically change the vehicle's trajectory about the Sun. The vehicle can take advantage of this influence if it passes the planet on a precisely calculated trajectory that will place it on an intercept trajectory with another planet. These trajectories will, in general, require very long flight times; however, there are some trajectories involving Mercury, Venus, Earth, and Mars that have relatively short flight times and low launch energies. Since the favorable launch periods for missions to a given planet do not occur often, trajectories that take one free-fall vehicle to several planets are particularly attractive.

The determination of free-fall trajectories to several planets is essentially the well-known, unsolved n-body problem. Thus, in order to calculate these trajectories, certain simplifying assumptions must be made. This Report is based upon one fundamental assumption: At any instant, one, and only one, gravitating body influences the vehicle's motion. Under this assumption, almost all of the vehicle's trajectory will consist of arcs of different ellipses with the Sun at a focus; however, when the vehicle comes sufficiently close to a passing planet, its trajectory with respect to this planet will be hyperbolic while the Sun's influence is neglected.

This Report contains the results of a study of such conic trajectories performed at the Jet Propulsion Laboratory during the summer of 1961. It also contains results of a numerical study performed at the Computing Facility of the University of California at Los Angeles and the computing complex at the Jet Propulsion Laboratory. These calculations show that, by utilizing multiple planetary trajectories, many interplanetary missions requiring very large launch vehicles can be carried out with much smaller vehicles by simply changing their mission profiles. This is particularly true for missions to Mercury and manned missions to Mars. The numerical study is confined to the decade beginning in 1965.

I. INTRODUCTION

It has been discovered that conic trajectories give excellent first approximations to actual flight paths of free-fall interplanetary space vehicles. Thus it is natural, while studying space trajectories, to assume that the vehicle moves along conic paths. The primary goal of the theoretical portion of this Report is to determine a conic trajectory in the vicinity of a passing planet that will enable the vehicle to pass out of its gravitational sphere of influence on a conic trajectory about the Sun to intercept another predetermined planet. Thus we shall assume that the missions begin and end at the centers of massless planets. The initial conditions are given by specifying the order in which the vehicle is to rendezvous with the given planets along with the launch date and the first planetary closest approach date. If these initial conditions are arbitrarily given, a solution may not exist or may be physically unrealizable; that is, the resulting trajectory may require the vehicle to pass closer to a particular planet than its own radius.

This Report includes the results of a numerical study of multiple planetary trajectories performed at the Computing Facility of the University of California at Los Angeles and at the computing complex at the Jet Propulsion Laboratory. These calculations show that, by utilizing multiple planetary trajectories, many interplanetary missions requiring very large launch vehicles can be carried out with much smaller vehicles by simply changing their mission profiles.

The quantitative study of forces, velocities, and positions in a three-dimensional space is most conveniently made by using vector analysis. With this technique, no assumptions regarding the geometry of the solar system will be necessary; indeed, it will not matter how eccentric the planets' orbits are or how much their planes of motion differ from each other. Thus, before attacking the above problem, we shall construct a convenient mathematical technique for handling conic trajectories in three-dimensional space.

II. CONIC TRAJECTORIES

We begin our study of conic trajectories in three-dimensional space by equating the dynamic force on a space vehicle of mass m with the force of gravitational attraction set up by the presence of a body of mass M. If Σ is any inertial frame, this equation becomes

$$m \frac{d\mathbf{V}}{dt} = -G \frac{Mm}{R^2} \hat{\mathbf{R}}$$

where $\mathbf{V}$ is the velocity of the vehicle and $\hat{\mathbf{R}}$ is a unit vector directed from the center of the body to the vehicle separated by a distance R. We shall adhere to the convention of denoting a unit vector by placing $\wedge$ over a letter.

Since the ratio m/M is very small, we may assume that the body is at rest in Σ. We shall take the center of this body as the origin of Σ. By setting $GM = \mu$ and dividing both sides of the above equation by m, we obtain

$$\frac{d\mathbf{V}}{dt} = -\frac{\mu}{R^2} \hat{\mathbf{R}} \qquad (1)$$

A. The e and h Vectors of Conic Trajectories

By using the differentation formula for the cross product of two vectors, we write

$$\frac{d}{dt}(\mathbf{R}\times\mathbf{V}) = \frac{d\mathbf{R}}{dt}\times\mathbf{V} + \mathbf{R}\times\frac{d\mathbf{V}}{dt}$$

Hence, with the aid of Eq. (1), we have

$$\frac{d}{dt}(\mathbf{R}\times\mathbf{V}) = 0$$

since the cross product of parallel vectors vanishes. This result implies

$$\mathbf{R}\times\mathbf{V} = \int \frac{d}{dt}(\mathbf{R}\times\mathbf{V})\,dt + \mathbf{h} = \mathbf{h}$$

where $\mathbf{h}$ is a constant vector of integration; therefore,

$$\mathbf{R}\times\mathbf{V} = \mathbf{h} \tag{2}$$

From this important relation it follows that $\mathbf{R}$ always remains perpendicular to $\mathbf{h}$; consequently, the motion remains confined to a fixed plane in Σ. The angular momentum of the vehicle about the body is simply $m\mathbf{h}$.

We now express Eq. (2) in a slightly different form:

$$\mathbf{h} = \mathbf{R}\times\frac{d\mathbf{R}}{dt} = \mathbf{R}\times\frac{d}{dt}(R\hat{\mathbf{R}}) = \mathbf{R}\times\left(\frac{dR}{dt}\hat{\mathbf{R}} + R\frac{d\hat{\mathbf{R}}}{dt}\right)$$

Thus

$$\mathbf{h} = R^2\hat{\mathbf{R}}\times\frac{d\hat{\mathbf{R}}}{dt}$$

By combining this result with Eq. (1), we find

$$\frac{d\mathbf{V}}{dt}\times\mathbf{h} = -\mu\hat{\mathbf{R}}\times\left(\hat{\mathbf{R}}\times\frac{d\hat{\mathbf{R}}}{dt}\right)$$

After applying the vector triple product formula of vector analysis, we obtain

$$\frac{d\mathbf{V}}{dt}\times\mathbf{h} = -\mu\left[\left(\hat{\mathbf{R}}\cdot\frac{d\hat{\mathbf{R}}}{dt}\right)\hat{\mathbf{R}} - (\hat{\mathbf{R}}\cdot\hat{\mathbf{R}})\frac{d\hat{\mathbf{R}}}{dt}\right]$$

Now, since $\hat{\mathbf{R}}\cdot\hat{\mathbf{R}} = 1$, it follows that

$$\hat{\mathbf{R}}\cdot\frac{d\hat{\mathbf{R}}}{dt} = \frac{1}{2}\left(\hat{\mathbf{R}}\cdot\frac{d\hat{\mathbf{R}}}{dt} + \frac{d\hat{\mathbf{R}}}{dt}\cdot\hat{\mathbf{R}}\right) = \frac{1}{2}\frac{d}{dt}(\hat{\mathbf{R}}\cdot\hat{\mathbf{R}}) = 0$$

Consequently,

$$\frac{d\mathbf{V}}{dt}\times\mathbf{h} = \mu\frac{d\hat{\mathbf{R}}}{dt}$$

By noting that $\mathbf{h}$ is a constant vector and μ is a constant scalar, this equation may be written as

$$\frac{d}{dt}(\mathbf{V}\times\mathbf{h}) = \frac{d}{dt}(\mu\hat{\mathbf{R}})$$

Upon integration, this leads to

$$\mathbf{V}\times\mathbf{h} = \mu\hat{\mathbf{R}} + \mathbf{c}$$

where $\mathbf{c}$ is another constant vector of integration. By setting

$$\mathbf{c} = \mu\mathbf{e}$$

we obtain

$$\mathbf{V}\times\mathbf{h} = \mu(\hat{\mathbf{R}} + \mathbf{e}) \tag{3}$$

where $\mathbf{e}$ is a constant vector of integration. It follows from Eq. (3) that this vector can be expressed as

$$\mathbf{e} = \frac{1}{\mu}\mathbf{V}\times\mathbf{h} - \hat{\mathbf{R}} \tag{4}$$

Since $\mathbf{V}\times\mathbf{h}$ is a vector lying in the plane of motion, the above relation implies that $\mathbf{e}$ also lies in the plane of motion.

Let θ be the angle measured from $\mathbf{e}$ in the positive direction (i.e., counterclockwise) to $\mathbf{R}$. Hence, in view of Eq. (2) and (3), we find that

$$h^2 = \mathbf{h}\cdot\mathbf{h} = \mathbf{h}\cdot\mathbf{R}\times\mathbf{V} = \mathbf{R}\cdot\mathbf{V}\times\mathbf{h} = \mathbf{R}\cdot\mu(\hat{\mathbf{R}} + \mathbf{e})$$

Thus

$$\frac{h^2}{\mu} = R + Re\cos\theta = R(1 + e\cos\theta)$$

and

$$R = \frac{h^2/\mu}{1 + e\cos\theta} \tag{5}$$

This is the general equation of a conic with eccentricity e, semilatus rectum l, and radius R, where

$$l = \frac{h^2}{\mu} \tag{6}$$

and

$$R = \frac{l}{1 + e\cos\theta} \tag{7}$$

which demonstrate the well-known fact that the trajectory is a conic section.

Since Eq. (7) implies that R is smallest when $\theta = 0$, the direction of $\mathbf{e}$ is along the direction of perihelion. An example of the geometric properties of these vectors is given in Fig. 1, where F^* represents the vacant focus.

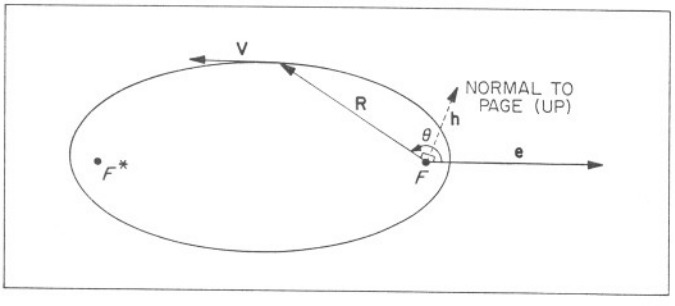

Fig. 1. Orientation of the e and h vectors

B. The Calculation of e and h Vectors From Two Position Vectors

If two position vectors on an elliptic trajectory are known, as well as its semimajor axis a and eccentricity e, the $\mathbf{e}$ and $\mathbf{h}$ vectors can be calculated. The $\mathbf{h}$ vector can easily be obtained from

$$\mathbf{h} = \pm\frac{\mathbf{R}_1 \times \mathbf{R}_2}{|\mathbf{R}_1 \times \mathbf{R}_2|}\left(a\mu\,|\,1 - e^2\,|\right)^{1/2} \tag{8}$$

where the choice of signs depends upon $\measuredangle(\mathbf{R}_1, \mathbf{R}_2)$ and the direction of motion. The $\mathbf{e}$ vector can be calculated from

$$\mathbf{e} = \alpha\,\mathbf{R}_1 + \beta\,\mathbf{R}_2 \tag{9}$$

where

$$\alpha = \frac{\begin{vmatrix} b_1 & a_{12} \\ b_2 & a_{22} \end{vmatrix}}{D} \qquad \beta = \frac{\begin{vmatrix} a_{11} & b_1 \\ a_{21} & b_2 \end{vmatrix}}{D} \tag{10}$$

with

$$\begin{aligned} b_i &= \frac{l}{R_i} + e^2 - 1 \\ a_{ii} &= l \\ a_{ij} &= \hat{\mathbf{R}}_i \cdot \mathbf{R}_j + l - R_j \quad (i \neq j) \end{aligned} \tag{11}$$

and

$$D = \begin{vmatrix} a_{11} & a_{12} \\ a_{21} & a_{22} \end{vmatrix} \tag{12}$$

The derivation of Eq. (8) is obvious, but the derivation of Eq. (9), along with Eq. (10), (11), and (12), is more involved. These formulas can be established by first noting that, since the $\mathbf{e}$ vector lies in the plane of motion, two scalars α and β exist such that Eq. (9) holds. If we denote the vehicle's velocity vectors at $\mathbf{R}_1$ and $\mathbf{R}_2$ by $\mathbf{V}_1$ and $\mathbf{V}_2$, respectively, and if we dot each side of Eq. (9) by $[(1/\mu)\,\mathbf{V}_1 \times \mathbf{h}]$ and $[(1/\mu)\,\mathbf{V}_2 \times \mathbf{h}]$, we obtain the following equations:

$$\frac{1}{\mu}\,\mathbf{V}_1 \times \mathbf{h} \cdot \mathbf{e} = \frac{1}{\mu}\,\mathbf{V}_1 \times \mathbf{h} \cdot \mathbf{R}_1\,\alpha + \frac{1}{\mu}\mathbf{V}_1 \times \mathbf{h} \cdot \mathbf{R}_2\,\beta$$

and

$$\frac{1}{\mu}\,\mathbf{V}_2 \times \mathbf{h} \cdot \mathbf{e} = \frac{1}{\mu}\,\mathbf{V}_2 \times \mathbf{h} \cdot \mathbf{R}_1\,\alpha + \frac{1}{\mu}\mathbf{V}_2 \times \mathbf{h} \cdot \mathbf{R}_2\,\beta$$

By employing Eq. (3) and noting that Eq. (7) implies

$$\hat{\mathbf{R}} \cdot \mathbf{e} = \frac{l}{R} - 1$$

the formulas of Eq. (10), (11), and (12) easily follow.

C. Velocity Vector as a Function of e, h, and R

We now come to a very useful formula that expresses the vehicle's velocity vector in terms of the $\mathbf{e}$ and $\mathbf{h}$ vec-

tors and its unit position vector $\hat{\mathbf{R}}$. By using the vector triple product formula, we write

$$\mathbf{h} \times (\mathbf{V} \times \mathbf{h}) = (\mathbf{h} \cdot \mathbf{h})\,\mathbf{V} - (\mathbf{h} \cdot \mathbf{V})\,\mathbf{h}$$

Since V is perpendicular to **h**, we have

$$h^2\,\mathbf{V} = \mathbf{h} \times (\mathbf{V} \times \mathbf{h})$$

and, by employing Eq. (3), we obtain

$$\mathbf{V} = \frac{\mu}{h^2}\,\mathbf{h} \times (\hat{\mathbf{R}} + \mathbf{e}) \tag{13}$$

As an immediate application of Eq. (13), we now derive the well-known energy equation. With the aid of Eq. (13) and (6), we may write

$$V^2 = \frac{1}{l}\,(\mathbf{V} \cdot \mathbf{h} \times \hat{\mathbf{R}} + \mathbf{V} \cdot \mathbf{h} \times \mathbf{e})$$

By the box product formulas, this becomes

$$V^2 = \frac{1}{Rl}\,[\mathbf{h} \cdot \mathbf{R} \times \mathbf{V} + R\,(\mathbf{e} \cdot \mathbf{V} \times \mathbf{h})]$$

Making use of Eq. (2) and (3), this can be written as

$$V^2 = \frac{1}{Rl}\,[h^2 + \mu\,(R\,e\cos\theta + R\,e^2)]$$

Consequently, employing Eq. (5), this is expressible as

$$V^2 = \frac{1}{Rl}\,[2h^2 + \mu R\,(e^2 - 1)]$$

and, by using Eq. (6), we obtain the familiar energy equation

$$V^2 = \mu\left(\frac{2}{R} \mp \frac{1}{a}\right) \tag{14}$$

The negative or positive sign is chosen according to whether the trajectory is elliptic or hyperbolic.

D. Relations Between the e and h Vectors and the Classical Orbital Elements

The vectors **e** and **h** and the time of perihelion passage T_F completely determine the conic trajectory. These vectors represent six constant scalars, five of which are independent. To an astronomer, who is primarily interested in knowing where to point his telescope, the classical method of defining an orbit by giving its classical orbital elements Ω, i, ω, a, e, T_P is very convenient. In astronautics, on the other hand, velocity vectors are very important. The determination of velocity vectors of celestial bodies having orbits defined by the classical osculating elements usually requires slow and cumbersome numerical differentiation of position vectors; however, if the trajectories are defined in terms of osculating **e** and **h** vectors, velocity vectors can be immediately calculated from Eq. (13) (see Appendix A).

The classical orbital elements can easily be calculated for a trajectory described by **e**, **h**, and T_P by referring to Fig. 2 where, for illustration, Σ is taken to be an ecliptic coordinate system, although it could as well be any other convenient system such as Earth equatorial. We take M to denote the point where the vehicle rises above the ecliptic, which is in the X-Y plane, and **n** as a unit vector directed toward M. The point of perihelion is denoted by P. The X-axis is directed toward the vernal equinox for some epoch.

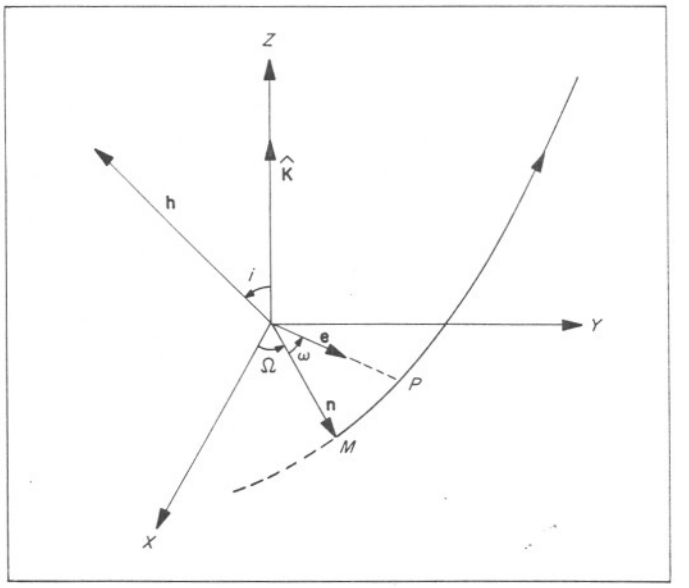

Fig. 2. Relation between the e and h vectors and the classical orbital elements

The time of perihelion passage T_P has already been given, and $|\mathbf{e}| = e$. Thus, only four of the six orbital elements remain to be calculated. From Eq. (6), the semimajor axis a can be obtained by

$$a = \frac{h^2}{\mu\,|\,1 - e^2\,|}$$

The inclination i of the trajectory can be calculated from the relation

$$\cos i = \frac{h_3}{h} \tag{15}$$

where we write

$$\mathbf{h} = (h_1, h_2, h_3) \qquad \text{and} \qquad \mathbf{e} = (e_1, e_2, e_3)$$

The unit vector $\hat{\mathbf{n}}$ is given by

$$\hat{\mathbf{n}} = (\cos \Omega, \sin \Omega, 0)$$

Since

$$\hat{\mathbf{k}} \times \mathbf{h} = h \sin i \, \hat{\mathbf{n}}$$

the longitude of the ascending node Ω can be obtained by

$$\sin \Omega = \frac{h_1}{h \sin i} \qquad \text{and} \qquad \cos \Omega = \frac{-h_2}{h \sin i} \tag{16}$$

The argument of perihelion ω may be calculated from

$$\cos \omega = \frac{\hat{\mathbf{n}} \cdot \mathbf{e}}{e} \tag{17}$$

Similarly, if a trajectory is defined by the classical orbital elements, the **e** and **h** vectors can readily be calculated by the following formulas:

$$e_1 = e (\cos \Omega \cos \omega - \cos i \sin \Omega \sin \omega) \tag{18}$$

$$e_2 = e (\sin \Omega \cos \omega + \cos i \cos \Omega \sin \omega) \tag{19}$$

$$e_3 = e \sin i \sin \omega \tag{20}$$

$$h_1 = h \sin i \sin \Omega \tag{21}$$

$$h_2 = -h \sin i \cos \Omega \tag{22}$$

$$h_3 = h \cos i \tag{23}$$

where

$$h = \left(\mu a \left| 1 - e^2 \right| \right)^{1/2}$$

E. Lambert's Theorem

We now use a fundamental theorem of celestial mechanics, known as Lambert's theorem, which plays an important role in the determination of interplanetary trajectories. The theorem states that the time required for a body to move from a point P, with position vector $\mathbf{R}_1$, to a point Q, with position vector $\mathbf{R}_2$, depends only on $R_1 + R_2$ and the distance c between P and Q. Since proof of this theorem can be found in any advanced text on celestial mechanics (for example, see Ref. 1), we shall merely state the associated equations that correspond to elliptic trajectories.

Let a body moving on an elliptic path be at the points P at time T_1 and Q at time T_2. If the arc $\overset{\frown}{PQ}$ traversed by the body during the time interval $T = T_2 - T_1$ is less than 180 deg, and if F and F^* denote the primary and vacant foci, respectively, then

$$T = \left(\frac{a^3}{\mu}\right)^{1/2} \left[\left(1 - x_2^2\right)^{1/2} + \sin^{-1} x_2 - \left(1 - x_1^2\right)^{1/2} - \sin^{-1} x_1 \right] \tag{24}$$

if the line segment $\overline{PQ}$ does not intersect $\overline{FF^*}$; however, if $\overline{PQ}$ does intersect $\overline{FF^*}$, then

$$T = \left(\frac{a^3}{\mu}\right)^{1/2} \left[\pi + \left(1 - x_2^2\right)^{1/2} + \sin^{-1} x_2 + \left(1 - x_1^2\right)^{1/2} + \sin x_1 \right] \tag{25}$$

In Eq. (24) and (25),

$$x_1 = 1 - \frac{s}{a}$$

$$x_2 = 1 - \frac{s - c}{a}$$

and

$$s = \frac{1}{2} (\overline{FP} + \overline{FQ} + c)$$

where s is the semiperimeter of the triangle PQF. The geometry of these two situations is shown in Fig. 3. By taking P and Q to be perihelion and aphelion, we find that the period P of the trajectory is

$$P = 2\pi \left(\frac{a^3}{\mu}\right)^{1/2}$$

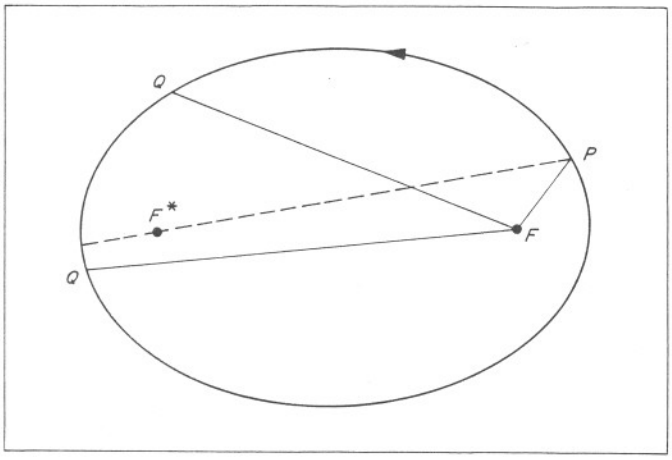

Fig. 3. Geometry for Lambert's theorem

If the arc $\widehat{PQ}$ subtended by P and Q lies in the range [180 deg, 360 deg], Eq. (24) becomes

$$T = \left(\frac{a^3}{\mu}\right)^{1/2}\left[2\pi - \left(1 - x_2^2\right)^{1/2} - \sin x_2 + \left(1 - x_1^2\right)^{1/2} + \sin x_1\right] \tag{26}$$

and Eq. (25) becomes

$$T = \left(\frac{a^3}{\mu}\right)^{1/2}\left[\pi - \left(1 - x_2^2\right)^{1/2} - \sin x_2 - \left(1 - x_1^2\right)^{1/2} - \sin^{-1} x_1\right] \tag{27}$$

If, on the other hand, we assume that the angle subtended by P and Q lies in the range [360 deg, 540 deg], Eq. (24) and (25) become

$$T = \left(\frac{a^3}{\mu}\right)^{1/2}\left[2\pi + \left(1 - x_2^2\right)^{1/2} + \sin^{-1} x_2 - \left(1 - x_1^2\right)^{1/2} - \sin^{-1} x_1\right] \tag{28}$$

and

$$T = \left(\frac{a^3}{\mu}\right)^{1/2}\left[3\pi + \left(1 - x_2^2\right)^{1/2} + \sin^{-1} x_2 + \left(1 - x_1^2\right)^{1/2} + \sin^{-1} x_1\right] \tag{29}$$

respectively. The eccentricity of the elliptic path (corresponding to the case where $\overline{PQ}$ does not intersect $\overline{FF}^*$) is given by

$$e = \left\{1 - \frac{2}{c^2}\left(s - \overline{FP}\right)\left(s - \overline{FQ}\right)\left[1 - x_1 x_2 + \left(1 - x_1^2\right)^{1/2}\left(1 - x_2^2\right)^{1/2}\right]\right\}^{1/2} \tag{30}$$

If $\overline{PQ}$ does intersect $\overline{FF}^*$, then

$$e = \left\{1 - \frac{2}{c^2}\left(s - \overline{FP}\right)\left(s - \overline{FQ}\right)\left[1 - x_1 x_2 - \left(1 - x_1^2\right)^{1/2}\left(1 - x_2^2\right)^{1/2}\right]\right\}^{1/2} \tag{31}$$

Interplanetary conic trajectories of free-fall space vehicles in the foreseeable future will be elliptic. Thus, if such a vehicle is to move along an elliptical path leaving P at time T_1 and arriving at Q at time T_2, the semimajor axis a of the trajectory may be calculated by one of the formulas of Eq. (24) to (29), provided, of course, that the angle subtended by P and Q is not greater than 540 deg. The eccentricity can then be calculated from Eq. (30) or (31). Recalling Section B of Part II, the corresponding $\mathbf{e}$ and $\mathbf{h}$ vectors can then be calculated; hence, the trajectory can be completely determined.

Now let us suppose that the point P represents a launch planet moving with velocity $\mathbf{V}_P$ at time T_1 when the vehicle is launched. If, at this moment, the vehicle's velocity vector is $\mathbf{V}$ with respect to the Sun and $\mathbf{V}'$ with respect to P, we have

$$\mathbf{V} = \mathbf{V}_P + \mathbf{V}'$$

Consequently,

$$V'^2 = \mathbf{V}' \cdot \mathbf{V}' = (\mathbf{V} - \mathbf{V}_P) \cdot (\mathbf{V} - \mathbf{V}_P)$$

$$= V^2 - 2\mathbf{V} \cdot \mathbf{V}_P + V_P^2$$

or, if $\measuredangle(\mathbf{V}, \mathbf{V}_P) = \theta$,

$$V'^2 = V^2 - 2V V_P \cos\theta + V_P^2 \tag{32}$$

Thus, by the energy equation, Eq. (32) may be expressed as

$$V'^2 = \left[\mu\left(\frac{2}{\overline{FP}} - \frac{1}{a}\right)\right]^{1/2}\left\{\left[\mu\left(\frac{2}{\overline{FP}} - \frac{1}{a}\right)\right]^{1/2} - 2V_P \cos\theta\right\} + V_P^2$$

implying that V' is minimum when $\theta = 0$ and a is minimum. From the definition of an ellipse, we may write

$$\overline{FP} + \overline{F^*P} = 2a$$

and

$$\overline{FQ} + \overline{F^*Q} = 2a$$

It follows that

$$2s = \overline{FP} + \overline{FQ} + c = (\overline{FP} + \overline{F^*P}) + (\overline{FQ} + \overline{F^*Q}) + (c - \overline{F^*P} - \overline{F^*Q})$$

or

$$2s + \overline{F^*P} + \overline{F^*Q} - c = 4a$$

Since the sum of any two sides of a plane triangle is greater than or equal to the third side, we find

$$a \geq \frac{s}{2}$$

The results given above show that minimum launch energy trajectories have $\theta = 0$ and $a = s/2$ (when $s = \overline{FP} + \overline{FQ}$ or equivalently when $c = \overline{FP} + \overline{FQ}$). These minimum launch energy trajectories are also referred to as Hohmann transfers. Figure 4 describes Hohmann transfers to Venus and Mars. It is important to have a general idea of the properties of the functions in Eq. (24) to (29). It is particularly important to know how these functions compare with each other.

Consider the set of all pairs of points P, Q such that $\overline{FP} + \overline{FQ}$ and c remain unchanged along with the primary focus F. Through each pair of points let us pass all possible elliptical paths such that $0 \text{ deg} \leq \measuredangle PFQ \leq 540$ deg by varying the semimajor axis and the eccentricity. The graphs of T vs. a of the six functions can then be plotted for identical values of $\overline{FP} + \overline{FQ}$ and c.

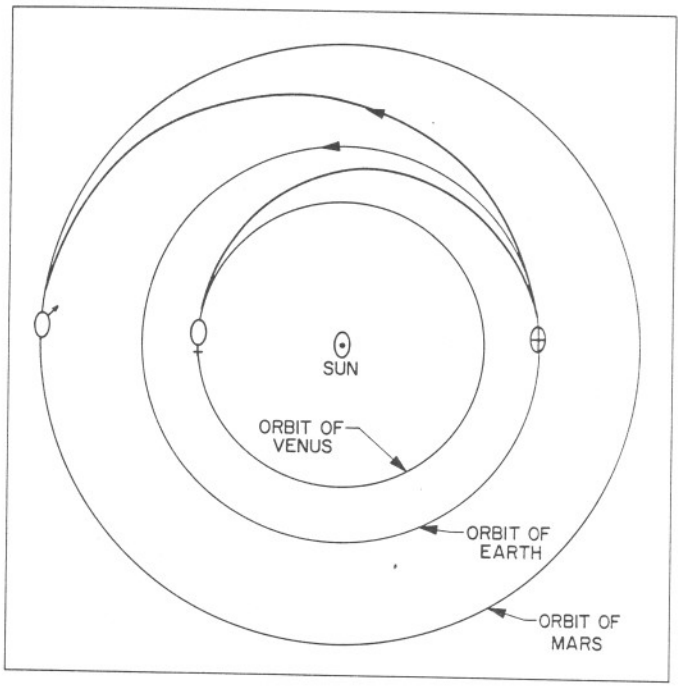

Fig. 4. Hohmann transfers to Mars and Venus

Figure 5 is an example of how these functions behave. In Fig. 5, T_{A1} and T_{A2} are asymptotic values that can be shown to be

$$T_{A1} = \frac{1}{3}\left(\frac{2}{\mu}\right)^{1/2}\left[s^{3/2} - \left(s-c\right)^{3/2}\right]$$

$$T_{A2} = \frac{1}{3}\left(\frac{2}{\mu}\right)^{1/2}\left[s^{3/2} + \left(s-c\right)^{3/2}\right]$$

When a = minimum $= s/2$, the graph of Eq. (24) joins Eq. (25) at time T_{M1}, the graph of Eq. (26) joins Eq. (27) at time T_{M2}, and the graph of Eq. (28) joins Eq. (29) at time T_{M3}. By substituting $a = s/2$ into Eq. (24) or (25), we find

$$T_{M1} = \left(\frac{s^3}{2\mu}\right)^{1/2}\left\{\left[\frac{c}{s}\left(1 - \frac{c}{s}\right)\right]^{1/2} + \frac{1}{2}\sin^{-1}\left(\frac{2c}{s} - 1\right) + \frac{\pi}{4}\right\}$$

and substituting $a = s/2$ into Eq. (26) or (27) yields

$$T_{M2} = \left(\frac{s^3}{2\mu}\right)^{1/2}\left\{\frac{3\pi}{4} - \left[\frac{c}{s}\left(1 - \frac{c}{s}\right)\right]^{1/2} - \frac{1}{2}\sin^{-1}\left(\frac{2c}{s} - 1\right)\right\}$$

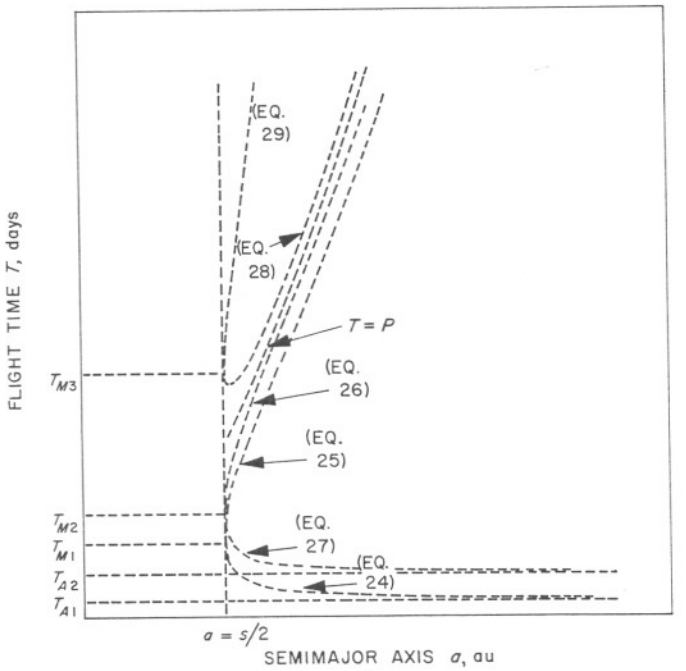

Fig. 5. Flight time vs. semimajor axis for six functions from Lambert's theorem

Since $T_{M3} = T_{M1} + P \mid_{a=s/2}$, we have

$$T_{M3} = \left(\frac{s^3}{2\mu}\right)^{1/2} \left\{\left[\frac{c}{s}\left(1 - \frac{c}{s}\right)\right]^{1/2} + \frac{1}{2}\sin^{-1}\left(\frac{2c}{s} - 1\right) + \frac{5}{4}\pi\right\}$$

F. Extension of Kepler's Second Law of Planetary Motion

The second of Kepler's three laws of planetary motion states that the radius vector from the Sun to a planet sweeps out equal areas in equal times. We shall now show that this law also applies to parabolic and hyperbolic paths.

Let π denote the plane of motion of a body moving under the influence of one, and only one, other body. Let $\mathbf{h}$ denote the angular momentum vector of the conic trajectory as defined previously. (See Fig. 6.) Let S denote the area of π bounded by the arc of the trajectory and the radius vectors $\mathbf{R}$ (T_1) and $\mathbf{R}$ (T_2). If C denotes the boundary of S, Stokes' theorem gives

$$\oint_C \mathbf{f} \cdot d\mathbf{R} = \iint_S \hat{\mathbf{h}} \cdot (\nabla \times \mathbf{f})\, dS$$

where $\mathbf{f}$ is any vector function having continuous gradient $\nabla \mathbf{f}$ over S. Letting

$$\mathbf{f} = \boldsymbol{\zeta} \times \mathbf{R}$$

where $\boldsymbol{\zeta}$ is any arbitrary constant vector, we may write

$$\oint_C (\boldsymbol{\zeta} \times \mathbf{R}) \cdot d\mathbf{R} = \iint_S \hat{\mathbf{h}} \cdot \nabla \times (\boldsymbol{\zeta} \times \mathbf{R})\, dS \tag{33}$$

With the aid of the box product formulas, it follows that

$$\boldsymbol{\zeta} \times \mathbf{R} \cdot d\mathbf{R} = d\mathbf{R} \cdot \boldsymbol{\zeta} \times \mathbf{R} = \boldsymbol{\zeta} \cdot \mathbf{R} \times d\mathbf{R}$$

Applying the formula for the curl of a cross product of two vector functions, we write

$$\nabla \times (\boldsymbol{\zeta} \times \mathbf{R}) = \mathbf{R} \cdot \nabla \boldsymbol{\zeta} - \boldsymbol{\zeta} \cdot \nabla \mathbf{R} + \boldsymbol{\zeta} \nabla \cdot \mathbf{R} - \mathbf{R} \nabla \cdot \boldsymbol{\zeta}$$

Since $\boldsymbol{\zeta}$ is a constant vector, the dyadic $\nabla \boldsymbol{\zeta}$ and the scalar $\nabla \cdot \boldsymbol{\zeta}$ vanish. Also, since $\mathbf{R} = x\hat{\mathbf{i}} + y\hat{\mathbf{j}} + z\hat{\mathbf{k}}$, the dyadic $\nabla \mathbf{R}$ is the idemfactor $\mathbf{I}$ for

$$\nabla \mathbf{R} = \frac{\partial \mathbf{R}}{\partial x}\hat{\mathbf{i}} + \frac{\partial \mathbf{R}}{\partial y}\hat{\mathbf{j}} + \frac{\partial \mathbf{R}}{\partial z}\hat{\mathbf{k}} = \hat{\mathbf{i}}\hat{\mathbf{i}} + \hat{\mathbf{j}}\hat{\mathbf{j}} + \hat{\mathbf{k}}\hat{\mathbf{k}} = \mathbf{I}$$

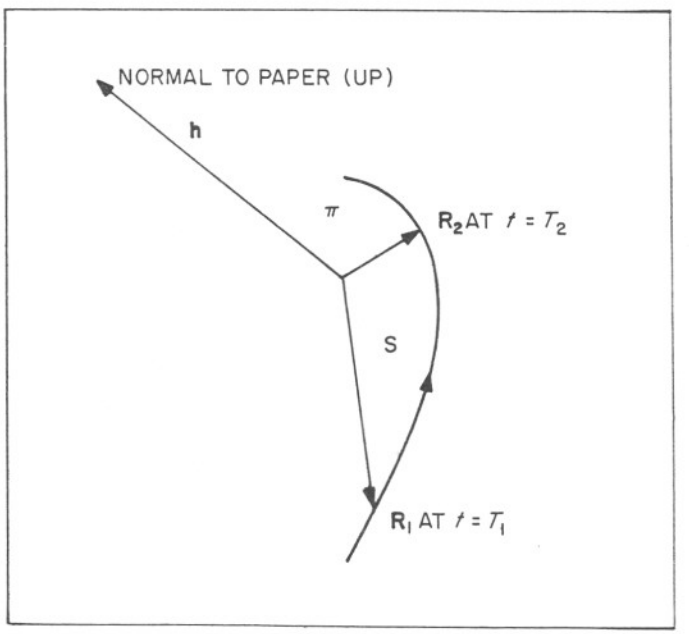

Fig. 6. Geometry for Kepler's second law

Noting that $\nabla \cdot \mathbf{R} = 3$, we obtain

$$\nabla \times (\boldsymbol{\zeta} \times \mathbf{R}) = -\boldsymbol{\zeta} \cdot \mathbf{I} + 3\boldsymbol{\zeta} = 2\boldsymbol{\zeta}$$

Substituting these results into Eq. (33), one finds

$$\boldsymbol{\zeta} \cdot \oint_C \mathbf{R} \times d\mathbf{R} = 2\boldsymbol{\zeta} \cdot \hat{\mathbf{h}} \iint_S ds = 2\boldsymbol{\zeta} \cdot \hat{\mathbf{h}}\, S$$

Now $\boldsymbol{\zeta}$ is any arbitrary constant vector; hence, it follows from the above equation that

$$\oint_C \mathbf{R} \times d\mathbf{R} = 2\hat{\mathbf{h}}\, S$$

Since

$$d\mathbf{R} = \frac{d\mathbf{R}}{dt}\, dt = \mathbf{V} dt$$

the equation can be written as

$$\int_{T_1}^{T_2} \mathbf{R} \times \mathbf{V}\, dt = 2\hat{\mathbf{h}}\, S$$

By employing Eq. (2), this result reduces to

$$h\,(T_2 - T_1) = 2S$$

Hence, Kepler's second law of planetary motion holds for all conic trajectories.

Let $T = T_2 - T_1$, where T_1 is the time of perihelion passage. Then by the above result we may write

$$T = \frac{2S}{h} = \frac{1}{h} \int_0^{\theta} R^2\, d\theta \tag{34}$$

Since Eq. (5) and (6) imply

$$d\theta = \frac{l}{R^2\, e \sin\theta}\, dR$$

we obtain

$$T = \frac{l}{eh} \int_{R_0}^{R} \frac{dR}{\left\{1 - \left(\frac{l}{R} - 1\right)^2 \frac{1}{e^2}\right\}^{1/2}} \tag{35}$$

where $R_0 = a\,(1 - e)$ for elliptical trajectories and $R_0 = a\,(e - 1)$ for hyperbolic trajectories. The integral can be integrated in closed form.

III. USING THE GRAVITATIONAL INFLUENCE OF A PASSING PLANET[1]

The effort to develop space vehicles designed for the exploration of the solar system is rapidly gaining momentum. Recent advances in many fields, such as metallurgy, chemistry, and electronics, are being applied to actual hardware as soon as they become available. With the arrival of new, sophisticated long-life interplanetary spacecraft, many new, complex deep-space operations will be possible. If such a vehicle were equipped with an advanced planetary-approach guidance system, it could accurately control its flight path in the vicinity of a passing planet. If the mission does not require the vehicle to land or to orbit the planet, the planet's gravitational influence gives the vehicle the potential of radically changing its trajectory about the Sun.

We now consider the problem of finding a conic approximation of the trajectory of a free-fall vehicle in the vicinity of a passing planet such that its influence will enable the vehicle to rendezvous with another planet. Let Σ denote any Cartesian inertial frame with the Sun's center as its origin. Let Σ' be a parallel translation of Σ with new origin located at the center of a planet influencing the motion of the vehicle. Let τ denote the region of gravitational influence about the planet. It can be shown that τ can be taken as a spherical region with center at the planet's center and with radius ρ^* given by

$$\rho^* = \left(\frac{m}{M}\right)^{2/5} R$$

[1]Proposed as a means for meeting energy requirements (see Ref. 2).

where R is the distance between the Sun of mass M and the planet of mass m.

The problem is formally stated as follows: Suppose a free-fall interplanetary space vehicle leaves a planet P_1 at time T_1 and makes a closest approach to a planet P_2 at time T_2. As illustrated in Fig. 7, the influence of P_2 then causes the vehicle to rendezvous with a third planet P_3. (P_3 may or may not be P_1; indeed, it may be another space vehicle orbiting the Sun.) The planets P_1, P_2, and P_3 along with the times T_1 and T_2 are given. The elliptic transfer trajectory from P_1 to P_2, the hyperbolic trajectory in τ, and the elliptic transfer trajectory from P_2 to P_3 are to be determined.

The following notation shall be employed throughout this Part:

$\overset{\frown}{P_1 P_2}$ = the elliptical transfer trajectory from P_1 to P_2

$\overset{\frown}{P_2 P_3}$ = the elliptical transfer trajectory from P_2 to P_3

$\mathbf{R}_i\,(t)$ = position vector of P_i with respect to Σ at time t $(i = 1, 2, 3)$

$\mathbf{R}\,(t)$ = position vector of vehicle with respect to Σ at time t

$\boldsymbol{\rho}\,(t)$ = position vector of vehicle with respect to Σ' at time t

$\mathbf{V}_i\,(t)$ = velocity vector of P_i with respect to Σ at time t $(i = 1, 2, 3)$

$\mathbf{V}\,(t)$ = velocity vector of vehicle with respect to Σ at time t

$\mathbf{V}'\,(t)$ = velocity vector of vehicle with respect to Σ' at time t

T_1^*, T_2^* = time at which vehicle enters and leaves τ, respectively

$a_1, l_1; a_3, l_3$ = semimajor axis and semilatus rectum of $\overset{\frown}{P_1 P_2}$ and $\overset{\frown}{P_2 P_3}$, respectively

$\mathbf{e}_1, \mathbf{h}_1; \mathbf{e}_3, \mathbf{h}_3$ = $\mathbf{e}$ and $\mathbf{h}$ vectors of $\overset{\frown}{P_1 P_2}$ and $\overset{\frown}{P_2 P_3}$, respectively

$a_2, \mathbf{e}_2, \mathbf{h}_2$ = semimajor axis and $\mathbf{e}$ and $\mathbf{h}$ vectors of hyperbolic trajectory in τ with respect to Σ' (With respect to Σ, the trajectory in τ is not a conic; hence, these quantities have no meaning.)

d = distance of closest approach to the surface of P_2

μ_2 = $m_2 G$, where m_2 is the mass of P_2 and G is the gravitational constant

For definiteness we shall assume that $\measuredangle\,[\mathbf{R}_1\,(T_1), \mathbf{R}_2\,(T_2)]$ and $\measuredangle\,[(\mathbf{R}_2\,(T_2), \mathbf{R}_3\,(T_3)]$ are not greater than 540 deg so that one of the formulas of Eq. (24) to (29) will always be applicable.

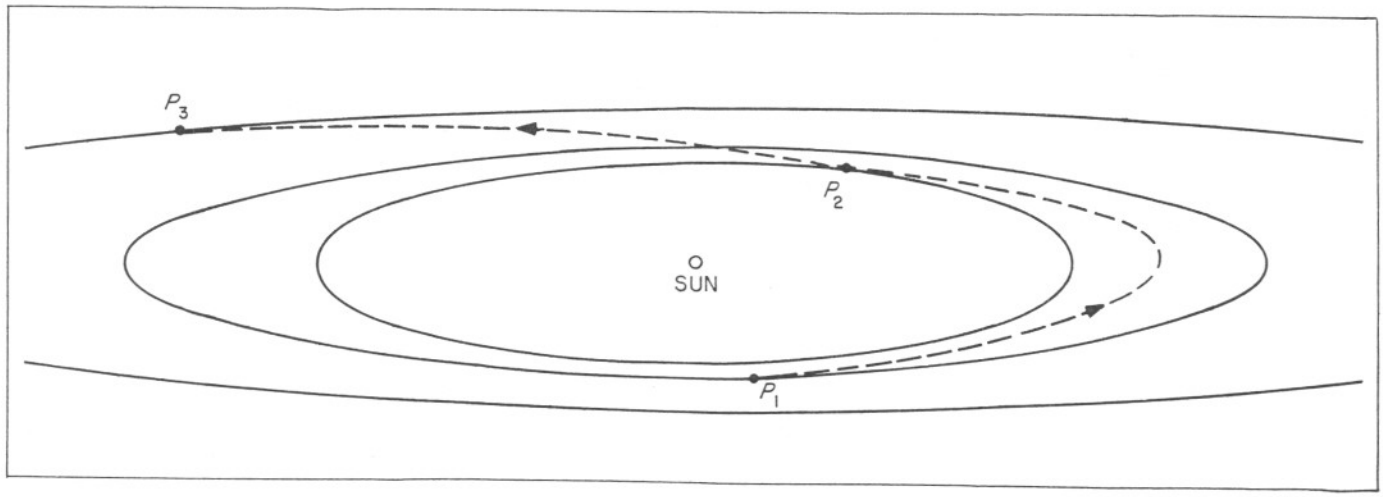

Fig. 7. Typical multiple planetary trajectory

A. The Fundamental Equation

If $T_1^* < t < T_2^*$, it follows from the above notations that

$$\mathbf{R}(t) = \mathbf{R}_2(t) + \boldsymbol{\rho}(t)$$

By differentiation,

$$\mathbf{V}(t) = \mathbf{V}_2(t) + \mathbf{V}'(t)$$

Since half of the total time that the vehicle spends in τ is very small compared to the period of P_2 about the Sun, we may write

$$\mathbf{V}(t) = \mathbf{V}_2 + \mathbf{V}'(t)$$

where $\mathbf{V}_2 = \mathbf{V}_2(T_2)$; consequently

$$\mathbf{V}(T_i^*) = \mathbf{V}_2 + \mathbf{V}'(T_i^*) \qquad (i = 1,2) \qquad (36)$$

Since $V^2 = \mathbf{V} \cdot \mathbf{V}$, these equations yield

$$V^2(T_i^*) = V_2^2 + 2\mathbf{V}_2 \cdot \mathbf{V}'(T_i^*) + V'^2(T_i^*) \qquad (37)$$

By employing Eq. (14), the energy equation for hyperbolic trajectories, we write

$$V'^2(T_i^*) = \mu_2 \left[\frac{2}{\rho(T_i^*)} + \frac{1}{a_2} \right]$$

The radius of τ at T_1^*, which is $\rho(T_1^*)$, is almost identical with the radius of τ at T_2^*, which is $\rho(T_2^*)$. Thus, the above equation implies that the vehicle's energy with respect to Σ' as it enters τ is the same as its energy as it leaves τ, or

$$V'^2(T_1^*) = V'^2(T_2^*) \qquad (38)$$

Upon substituting this result into the difference of the equations given by evaluating Eq. (37) at times T_2^* and T_1^*, we find

$$V^2(T_2^*) - V^2(T_1^*) = 2\mathbf{V}_2 \cdot [\mathbf{V}'(T_2^*) - \mathbf{V}'(T_1^*)] \qquad (39)$$

Taking the difference of the two equations given by evaluating Eq. (36) at times T_2^* and T_1^*, we obtain

$$\mathbf{V}'(T_2^*) - \mathbf{V}'(T_1^*) = \mathbf{V}(T_2^*) - \mathbf{V}(T_1^*)$$

Substituting this result into Eq. (39), we obtain an important equation by which all three parts of the total trajectory can be determined:

$$V^2(T_2^*) - V^2(T_1^*) = 2\mathbf{V}_2 \cdot [\mathbf{V}(T_2^*) - \mathbf{V}(T_1^*)] \qquad (40)$$

It should be borne in mind that this equation, in essence, says nothing more than Eq. (38). Its value lies in its form, where the quantities are given with respect to Σ rather than Σ'. This equation represents the amount of energy exchanged between the planet P_2 and the vehicle.

B. The Determination of the Elliptical Orbits Associated With the Transfer Trajectories

By the orbits associated with the transfer trajectories we mean the two closed elliptical orbits about the Sun, where $\overset{\frown}{P_1 P_2}$ and $\overset{\frown}{P_2 P_3}$ are sections. The elliptic trajectory $\overset{\frown}{P_1 P_2}$ begins at the center of P_1, with position vector $\mathbf{R}_1(T_1)$, and ends at a point on the surface of τ at T_1^*, with position vector $\mathbf{R}(T_1^*)$. The elliptic trajectory $\overset{\frown}{P_2 P_3}$ begins at a point on the surface of τ at T_2^*, with position vector $\mathbf{R}(T_2^*)$, and ends at the center of P_3, with position vector $\mathbf{R}_3(T_3)$.

In Fig. 8, the short solid line represents a small portion of P_2's orbit about the Sun when the vehicle is nearby. The points D, E, and G are the planet's positions at T_1^*, T_2, and T_2^*, respectively. The longer solid line represents a small portion of the vehicle's trajectory near P_2. The point A is the position of the vehicle at time T_1^* as it enters τ, the point B is its position at time T_2 when it is closest to P_2, and the point C is the position of the vehicle at time T_2^* as it leaves the moving region τ. The trajectory of the vehicle bounded by A and C is not conic since the Figure is drawn with respect to Σ. When viewed from Σ', this portion of the trajectory is hyperbolic (see Fig. 9). The vehicle's elliptic trajectory outside τ is represented by straight line segments because of the scale of the Figure. Since the Sun is so far away, the vectors $\mathbf{R}(T_1^*)$, $\mathbf{R}_2(T_2)$, and $\mathbf{R}(T_2^*)$ appear as parallel vectors. The dotted lines are continuations of $\overset{\frown}{P_1 P_2}$ and

$\overset{\frown}{P_2 P_3}$. The points B' and B'' correspond to the positions of the vehicle moving on the orbits of $\overset{\frown}{P_1 P_2}$ and $\overset{\frown}{P_2 P_3}$ at time T_2 as though P_2 did not exist.

Figure 8 displays some very important facts. It is easy to see that the position vectors of B' and B'' are almost identical with $\mathbf{R}_2\ (T_2)$. Thus, by employing Lambert's theorem, using the appropriate formula from Eq. (24) to (29) with $T = T_2 - T_1$, $\mathbf{R}_1 = \mathbf{R}_1\ (T_1)$, and $\mathbf{R}_2 = \mathbf{R}_2\ (T_2)$, the semimajor axis a_1 of $\overset{\frown}{P_1 P_2}$ can be calculated. Then by using either Eq. (32) or (33), depending upon which formula was used to calculate a_1, the eccentricity e_1 can be found. Consequently, the vectors $\mathbf{e}_1$ and $\mathbf{h}_1$ corresponding to $\overset{\frown}{P_1 P_2}$ can be calculated from Eq. (8) to (12), where $l_1 = a_1\ (1 - e_1^2\ )$.

Similarly, by setting $T = T_3 - T_2$, $\mathbf{R}_1 = \mathbf{R}_2\ (T_2)$, and $\mathbf{R}_2 = \mathbf{R}_3\ (T_3)$, application of Lambert's theorem yields $a_3 = a_3\ (T_3)$. Since T_3 is unknown, a_3 is written as $a_3\ (T_3)$, meaning that a_3 is a function of T_3. In theory, by following the above procedure, the functions $e_3\ (T_3)$, $l_3\ (T_3)$, $\mathbf{e}_3\ (T_3)$, and $\mathbf{h}_3\ (T_3)$ can be obtained. In practice, these functions are not actually determined, since use of a high-speed digital computer makes it possible to give T_3 an actual trial numerical value. Thus, $a_3\ (T_3)$, $e_3\ (T_3)$, $l_3\ (T_3)$, $\mathbf{e}_3\ (T_3)$, and $\mathbf{h}_3\ (T_3)$ all take on actual numerical values corresponding to the trial value given to T_3.

The actual value of T_3 can be obtained by noticing a second important fact suggested from Fig. 8. It is evident that the vehicle's velocity vectors at A and C are almost identical with the hypothetical velocity vectors at B' and B''. Consequently, in view of our first observation, these velocities can easily be found from Eq. (13) to be

$$\mathbf{V}\ (T_1{}^*) = \frac{1}{l_1}\ \mathbf{h}_1 \times [\hat{\mathbf{R}}_2\ (T_2) + \mathbf{e}_1]$$

and

$$\mathbf{V}\ (T_2{}^*) = \frac{1}{l_3\ (T_3)}\ \mathbf{h}_3\ (T_3) \times [\hat{\mathbf{R}}_2\ (T_2) + \mathbf{e}_3\ (T_3)]$$

The actual value of T_3 is that value yielding a solution to Eq. (40). In general, there is an infinite set of values of T_3 generating vectors $\mathbf{V}\ (T_2{}^*)$ that satisfy Eq. (40), but we shall choose that solution which gives $T_3 - T_2$ the smallest value.

A systematic search for T_3 can be initiated which, when completed, determines the values of a_3, e_3, l_3, $\mathbf{e}_3$, and $\mathbf{h}_3$, along with $\mathbf{V}\ (T_2{}^*)$. Hence the elliptic orbits associated with $\overset{\frown}{P_1 P_2}$ and $\overset{\frown}{P_2 P_3}$ can be completely determined. We emphasize at this point that, even though $\mathbf{V}\ (T_1{}^*)$ and $\mathbf{V}\ (T_2{}^*)$ are known, $T_1{}^*$, $T_2{}^*$, $\mathbf{R}\ (T_1{}^*)$, and $\mathbf{R}\ (T_2{}^*)$ remain to be calculated.

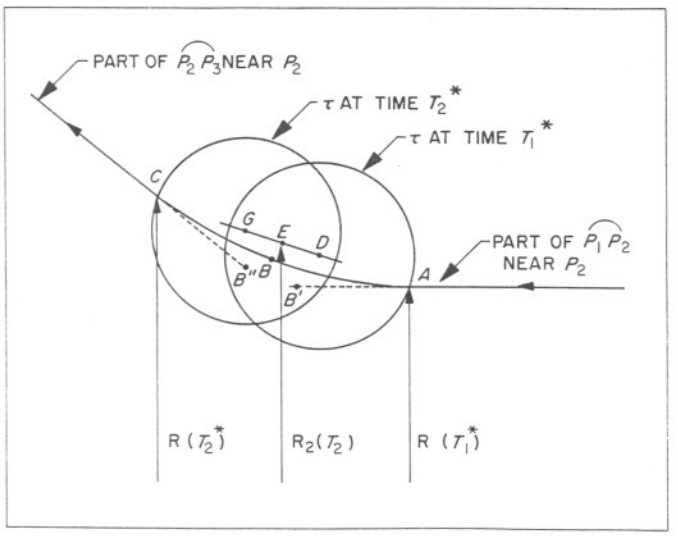

Fig. 8. Trajectory in the vicinity of P_2 with respect to the Sun

C. The Determination of the Hyperbolic Trajectory

We now consider the part of the vehicle's trajectory that is in τ. The seemingly difficult task of finding this trajectory turns out to be surprisingly easy.

Figure 9 is drawn with respect to Σ'; thus the vehicle's trajectory appears as hyperbolic. The points A, B, and C correspond to the points A, B, and C of Fig. 8. From Eq. (36) we calculate the vehicle's velocity vectors at A and C:

$$\mathbf{V}'\ (T_i{}^*) = \mathbf{V}\ (T_i{}^*) - \mathbf{V}_2 \qquad (i = 1, 2)$$

The quantities $V'^2\ (T_1{}^*)$ and $V'^2\ (T_2)$ are now calculated, and, in view of Eq. (38), we calculate their average V'^2:

$$V'^2 = \frac{1}{2}\ [V'^2\ (T_1{}^*) + V'^2\ (T_2{}^*)]$$

By applying Eq. (14), the energy equation, we find the semimajor axis a_2 of the hyperbolic trajectory:

$$a_2 = \frac{\mu_2 \rho^*}{V'^2 \rho^* - 2\mu_2} \tag{41}$$

where

$$\rho^* = \left(\frac{m}{M}\right)^{2/5} R_2 (T_2)$$

The term $2\mu_2$ is negligible compared to $V'^2 \rho^*$ since, with respect to the hyperbolic trajectory, the sphere of influence lies at infinity; hence, this term may be omitted from Eq. (41) with little or no effect.

If we denote the length of the conjugate axis of the hyperbolic path by b_2, as shown in Fig. 9, we observe that

$$\tan \phi = \frac{b_2}{a_2}$$

where ϕ is one-half of the angle between the asymptotes. Since the eccentricity e_2 is related to a_2 and b_2 by

$$e_2 = \left[1 + \left(\frac{b_2}{a_2}\right)^2 \right]^{1/2}$$

we find

$$\cos \phi = \frac{1}{e_2} \tag{42}$$

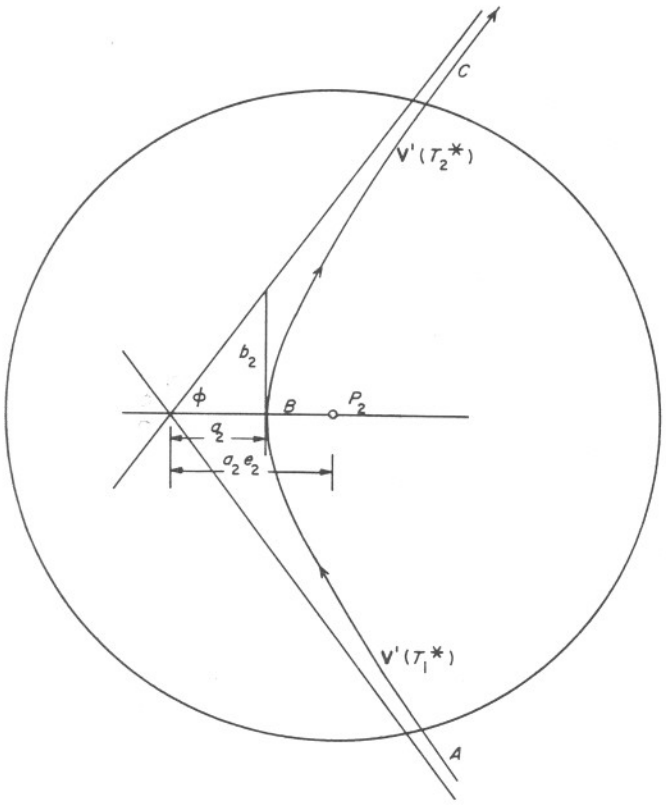

Fig. 9. Hyperbolic trajectory relative to the planet P_2

and, by studying the Figure, we find

$$\mathbf{V}'(T_1^*) \cdot \mathbf{V}'(T_2^*) = V'(T_1^*)\, V'(T_2^*) \cos 2\left(\frac{\pi}{2} - \phi\right)$$

This is expressible as

$$\mathbf{V}'(T_1^*) \cdot \mathbf{V}'(T_2^*) = V'(T_1^*)\, V'(T_2^*)\,(1 - 2\cos^2 \phi)$$

By making use of Eq. (42), the eccentricity of the hyperbolic path can be calculated by

$$e_2 = \left[\frac{2\, V'(T_1^*)\, V'(T_2^*)}{V'(T_1^*)\, V'(T_2^*) - \mathbf{V}'(T_1^*) \cdot \mathbf{V}'(T_2^*)} \right]^{1/2} \tag{43}$$

The distance of closest approach to the surface of P_2 can now be easily calculated by

$$d = a_2 (e_2 - 1) - \text{Radius of } P_2 \tag{44}$$

If this quantity turns out to be negative, the trajectory is obviously physically unrealizable. The value of T_3 is then progressively increased by appropriate amounts until the next smallest value of T_3 is found. Figure 10 is an example of some possible values of T_3 in some interval of time after T_2. Suppose the values of T_3' and T_3'' satisfy Eq. (40) but give a negative value for the distance of closest approach. The smallest possible value of T_3 yielding a positive distance of closest approach is T_3''' This is the value we choose. T_3'''' is the next possible T_3 value yielding a positive value for d.

After T_3 has been determined, the velocity at closest approach V'_{CA} with respect to P_2 can be obtained by again making use of the energy equation. We find

$$V'_{CA} = \left[\frac{\mu_2}{a_2} \left(\frac{e_2 + 1}{e_2 - 1} \right) \right]^{1/2} \tag{45}$$

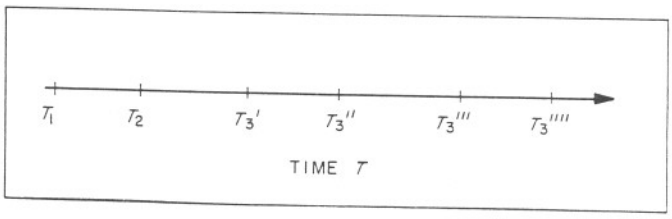

Fig. 10. Possible values for the P_3 intercept date

The magnitude of the **h** vector can be calculated by

$$h_2 = \left[\mu_2 a_2 (e_2^2 - 1)\right]^{1/2} \tag{46}$$

By observing Fig. 9, which shows the trajectory of the vehicle in τ with respect to Σ', the **e** and **h** vectors can readily be obtained by

$$\mathbf{e}_2 = \frac{\mathbf{V}'(T_1^*) - \mathbf{V}'(T_2^*)}{|\mathbf{V}'(T_1^*) - \mathbf{V}'(T_2^*)|} e_2 \tag{47}$$

and by

$$\mathbf{h}_2 = \frac{\mathbf{V}'(T_1^*) \times \mathbf{V}'(T_2^*)}{|\mathbf{V}'(T_1^*) \times \mathbf{V}'(T_2^*)|} h_2 \tag{48}$$

These vectors determine the required approach trajectory.

Let $\Delta T = 1/2\,(T_2^* - T_1^*)$. Then by making use of Eq. (35), setting $R_0 = a_2\,(e_2 - 1)$ and $R = \rho^*$, we obtain

$$\Delta T = \left[\frac{a_2}{\mu_2}\right]^{1/2} (\alpha - \beta) \tag{49}$$

where

$$\alpha = \left[\rho^{*2} + 2\,a_2\,\rho^* - a_2^2\,(e_2^2 - 1)\right]^{1/2}$$

and

$$\beta = a_2 \log\left[\frac{1}{a_2\,e_2}\,(\alpha + \rho^* + a_2)\right]$$

Thus we may calculate T_1^* and T_2^* by

$$T_1^* = T_2 - \Delta T$$

and

$$T_2^* = T_2 + \Delta T$$

Consequently, the position vectors of A and C can be calculated with respect to Σ by

$$\mathbf{R}(T_i^*) = \mathbf{R}_2(T_i^*) + \boldsymbol{\rho}(T_i^*) \qquad (i = 1, 2) \tag{50}$$

We have now completely determined both the approach and departure elliptic transfer trajectories and the trajectory of the vehicle near the planet P_2 that will take the vehicle to P_3. Of course, in view of the above approximations, the trajectory is not exact. However, one may now, by an obvious iteration process, proceed to obtain a trajectory that is arbitrarily close to the desired elliptic and hyperbolic parts of the total trajectory. In practice, it turns out that these approximations introduce very little error, so that it is impractical to try to obtain greater accuracy.

We conclude this Section with a very important observation. Recalling the method of solution, we first determined $\overset{\frown}{P_1 P_2}$ from the given initial conditions. We then proceeded to find $\overset{\frown}{P_2 P_3}$ by solving Eq. (40) such that $d > 0$. Finally, the trajectory in τ was calculated. Now, instead of terminating the mission at P_3, suppose we wish to use P_3 to go on to some other planet, say P_4. Since the initial conditions specifying T_1, T_2, P_1, and P_2 are equivalent (on an interplanetary scale) to specifying $\overset{\frown}{P_1 P_2}$, we simply take $\overset{\frown}{P_2 P_3}$ as an initial condition for proceeding to P_4. Thus $\overset{\frown}{P_3 P_4}$ and the hyperbolic trajectory in the vicinity of P_3 can be determined in a completely analogous manner; hence, the method permits one to determine far more advanced and complex space trajectories. The numerical results that we take up in the next Part clearly display the feasibility of such advanced missions.

IV. NUMERICAL RESULTS[2]

In Part III we were able to determine very general and complicated interplanetary free-fall trajectories. This was accomplished by employing the vector techniques developed in Part II and by assuming that, at any given time, only one body of the solar system influences the vehicle's motion. The following examples depict the typical multiple planetary free-fall interplanetary trajectories that we will consider:

1. Trajectories of a vehicle that is launched from Earth at a given time T_1 and that makes a closest approach to Venus at a given time T_2 (we shall call T_2 the P_2 intercept date) such that the gravitational influence of Venus sends the vehicle back to Earth (Earth–Venus–Earth).

2. Trajectories of a vehicle that is launched from Earth at a given time T_1 and that intercepts Mars at a given time T_2 such that the gravitational influence of Mars sends the vehicle back to Earth (Earth–Mars–Earth).

3. Trajectories of a vehicle that is launched from Earth at time T_1 and that makes a closest approach to Venus at time T_2 such that the gravitational influence of Venus sends the vehicle on an intercept course with Mercury (Earth–Venus–Mercury).

4. Trajectories of a vehicle that is launched from Earth at time T_1 and that at time T_2 makes a closest approach to Venus where the gravitational influence of Venus causes the vehicle to intercept Mars such that the gravitational influence of Mars sends the vehicle back to Earth (Earth–Venus–Mars–Earth).

5. Trajectories of a vehicle that is launched from Earth at time T_1 and that at time T_2 makes a closest approach to Venus which causes the vehicle to intercept Mars; the gravitational influence of Mars causes the vehicle to return to Earth where the Earth's gravitational influence causes the vehicle to repeat the same flight; the vehicle is sent to Venus such that the Venusian influence sends it to Mars whereupon the Martian gravitational influence causes the vehicle to return to Earth (Earth–Venus–Mars–Earth–Venus–Mars–Earth).

These examples represent only a small fraction of the total number of possible different types of multiple planetary free-fall trajectories having $n-1$ planetary encounters. For example, the total number of different types of advanced trajectories having only two planetary encounters of the form P_1–P_2–P_3, where P_1 = Earth, is 9^{3-1} or 81! In general, the total number of different trajectories of the form P_1–P_2–$\cdots$–P_n having $n-1$ planetary encounters is 9^n. Thus the trajectory given by example 4 is only one of the 729 different types possible of the form P_1–P_2–P_3–P_4, where P_1 = Earth.

Exact numerical calculations of even the most simple types of these trajectories having only two planetary encounters have (so far as the author knows) never been carried out. A few round-trip trajectories to Mars of the type given in example 2 have been calculated at the Massachusetts Institute of Technology by R. Battin (see Ref. 3).

Battin reported on six different trajectories; the shortest associated flight time was about 1,050 days. This minimum total flight time is obviously very long. Consequently, as the program for the digital computer was being written, corresponding to Part III, many important questions remained unanswered. For example, since Battin calculated flight times in excess of 1,000 days for relatively simple trajectories, such as the one in example 2, how much time would a trajectory like example 4 require? Moreover, it was not even known whether an example 3 trajectory would be possible, to say nothing of an example 5 trajectory.

When the early numerical calculations were confirmed by elaborate integrating programs at the Jet Propulsion Laboratory, the Computing Facility at the University of California at Los Angeles, where the program was written, was used to begin the first extensive numerical analysis of these trajectories. These early calculations at UCLA not only proved the feasibility of using such trajectories for missions but also showed that in some cases such trajectories could provide significant savings in launch energy and lifetime.

As the numerical calculations were enlarged by also utilizing the computing complex at the Jet Propulsion Laboratory, three distinct types of advanced missions became apparent. These missions follow in a natural chronological order:

[2]See appendix B for the constants of the solar system used in the calculations.

A. Unmanned exploration of the inner planets by instrumented space vehicles on advanced trajectories

B. Initial interplanetary missions by manned vehicles

C. Interplanetary transportation networks to support manned bases on Venus and Mars

We now consider each of the three types of missions separately.

A. Unmanned Exploration of the Inner Planets by Instrumented Space Vehicles on Advanced Trajectories

This category of missions utilizing advanced trajectories must simultaneously satisfy the following three important requirements:

1. Short flight times
2. Low launch energies
3. Safe distances of closest approach

In view of the first desired characteristic property, these missions employing multiple planetary trajectories must be of the form

$$P_1\text{–}P_2\text{–}P_3$$

where P_1 = Earth, and where $P_2 \neq P_3$ and must be either Mercury, Venus, or Mars. Consequently, the six possibilities are

1. Earth–Mercury–Venus
2. Earth–Mercury–Mars
3. Earth–Venus–Mercury
4. Earth–Venus–Mars
5. Earth–Mars–Mercury
6. Earth–Mars–Venus

The first two possibilities can be eliminated immediately because launch energies for Earth–Mercury transfers are very high. The last two possibilities were found to require long flight times and hence shall not be considered at this time; however, these trajectories shall be studied, and the results will be given at a later date. Thus only two of the six possible mission types will be considered in this Report:

1. Earth–Venus–Mercury
2. Earth–Venus–Mars

The analysis proceeded by first noting that any favorable launch period requiring low launch energies and relatively short flight times for multiple planetary trajectories will also be a favorable launch period for simple direct-flight trajectories to Venus. In general, any favorable launch period for any multiple planetary trajectory of the form $P_1\text{–}P_2\text{–}\cdots\text{–}P_n$, where P_1 = Earth and P_2 = Venus, will necessarily be a favorable launch period for simple Earth–Venus trajectories. The converse, of course, is obviously false. In view of this simple but important observation, a great number of multiple planetary trajectories were not calculated because if a launch date did not fall in some favorable Earth–Venus launch period, the trajectory would automatically require a high launch energy. These favorable Earth–Venus launch periods were all found by preliminary calculations utilizing Lambert's theorem and from Ref. 4.

For each launch date (differing by 2-day increments and running continuously through the entire decade), a large set of simple Earth–Venus transfer trajectories was calculated corresponding to various flight times differing by 2-day increments. Letting θ_{12} denote the heliocentric center angle associated with each trajectory, one may calculate three subsets of trajectories characterized by

$$0 \text{ deg} < \theta_{12} < 180 \text{ deg}$$

$$180 \text{ deg} < \theta_{12} < 360 \text{ deg}$$

and

$$360 \text{ deg} < \theta_{12} < 540 \text{ deg}$$

The trajectories of each subset are called Type I, Type II, and Type III, respectively. By the optimum Type I, Type II, and Type III trajectories for a particular launch date T_1, we shall mean the trajectories having the lowest launch energies from among those trajectories in each of the three subsets of the set corresponding to the launch date T_1. For some launch dates these optimum trajectories have relatively low launch energies. These periods of relatively low launch energies are the favorable launch periods. The favorable periods for Type I and Type II

Table 1. Some important properties of optimum Earth–Venus transfer trajectories

Launch period	Min. HEV_1 km/sec	Max. HEV_1 km/sec	Min. T_{12} days	Max. T_{12} days	Min. HEV_2 km/sec	Max. HEV_2 km/sec
	Type I					
10/17/65–12/4/65	3.65	4.25	104	122	2.90	6.23
5/10/67– 7/11/67	2.52	4.22	118	144	2.86	5.81
12/10/68– 2/6/69	2.77	3.59	106	154	3.78	4.58
7/13/70– 9/11/70	2.91	3.64	96	144	5.04	5.75
2/21/72– 4/21/72	3.50	4.42	94	136	5.02	7.21
10/13/73–12/6/73	3.65	4.40	102	122	2.91	6.44
	Type II					
6/21/65– 8/26/65	2.69	3.66	134	184	4.12	4.46
4/24/67– 6/15/67	2.41	3.28	148	184	2.86	4.43
1/9/69 – 3/10/69	3.54	3.74	168	178	4.43	7.82
8/14/70–10/11/70	3.00	3.57	160	178	5.28	7.25
3/6/72 – 5/5/72	2.86	3.44	164	186	4.86	6.59
10/5/73 –12/4/73	2.71	3.54	136	178	4.15	5.14

HEV_1 Hyperbolic excess velocity relative to launch planet P_1 (Earth)
HEV_2 Hyperbolic excess velocity relative to second planet P_2 (Venus)
T_{12} Flight time from P_1 to P_2

trajectories almost always coincide with each other, but the favorable periods for Type III trajectories are quite distinct from the other two. Type III trajectories require longer flight times than those of Type I or Type II. Consequently, we have restricted the P_1–P_2 transfer trajectories to be either Type I or Type II.

Table 1 contains all the favorable Type I and Type II Earth–Venus launch periods occurring in the 10-year time interval beginning with 1965 and running through 1974. We observe that there are only six such periods for the decade. Each period was chosen to be approximately two months long. Notice that the midpoints of successive periods are separated by about 19.2 mo, which is approximately the synodic period of Venus. The Table also gives some important properties of the optimum trajectories associated with each period. The symbols HEV_1 and HEV_2 denote the vehicle's hyperbolic excess velocity (in kilometers per second) as it leaves the first planet (Earth) and as it arrives at the second planet (Venus), respectively. A vehicle's hyperbolic excess velocity at a planet is the amount by which the vehicle's velocity exceeds the planet's escape velocity. The flight time (in days) is denoted by T_{12}. In describing the launch or approach energies we shall refer to the vis-viva energies, which are the squares of the hyperbolic excess velocities; however, these are not tabulated. For example, from Table 1 we observe that the lowest launch energy required for Type I trajectories of the 1965 period is 1.84 times greater than the lowest launch energy for Type II trajectories of the same launch period.

In order that the full potentialities of multiple planetary trajectories corresponding to the two mission types given above may be clearly understood, let us examine the optimum Earth–Mercury and Earth–Mars trajectories for their respective favorable launch periods during the 1965–1974 time interval. Calculations of optimum Earth–Mercury and Earth–Mars transfer trajectories were carried out like those for the Earth–Venus trajectories. Tables 2 and 3 give their respective periods, along with some important facts similar to Table 1. Since Mercury's synodic period is approximately one-fifth that of Venus, there are about five times as many minimum launch energy periods. Unlike the Earth–Venus periods, the minimum launch energy for each period of the Earth–Mercury trajectories sometimes varies by more than 200%. This is due to Mercury's high eccentricity and inclination to the ecliptic. Consequently, only eleven Earth–Mercury launch periods appear in Table 2. These are the eleven most favorable periods.

Table 2. Some important properties of optimum Earth–Mercury transfer trajectories

Launch period	Min. HEV_1 km/sec	Max. HEV_1 km/sec	Min. T_{12} days	Max. T_{12} days	Min. HEV_2 km/sec	Max. HEV_2 km/sec
	Type I					
1/1/65 – 2/3/65	7.20	7.88	86	114	15.42	18.32
12/6/65 – 1/17/66	6.84	7.82	86	122	15.57	18.04
11/15/66–12/31/66	6.59	7.91	86	126	15.50	17.05
11/10/67–12/12/67	6.46	7.78	88	116	14.19	15.35
11/6/68 –11/24/68	6.85	7.92	92	104	12.48	16.24
2/15/70– 3/1/70	8.01	8.14	88	100	14.65	15.78
1/19/71– 2/14/71	7.50	7.94	86	108	16.00	17.07
12/21/71– 1/28/72	7.04	7.93	84	116	16.14	18.96
11/25/72– 1/10/73	6.72	7.88	84	126	16.13	17.59
11/12/73–12/22/73	6.49	7.73	88	124	14.85	15.99
11/9/74 –12/5/74	6.43	7.87	90	110	12.15	15.36
	Type II					
8/28/65– 9/19/65	7.50	7.87	108	124	12.98	14.40
8/17/66– 9/4/66	7.98	8.20	108	120	13.05	15.06
11/3/66 –11/13/66	8.09	8.26	134	142	12.15	14.61
10/19/67–11/22/67	6.94	7.94	120	142	11.94	14.64
10/3/68 –11/18/68	6.44	7.95	108	142	12.00	16.25
9/22/69–11/5/69	6.56	7.84	98	138	12.21	13.15
9/11/70–10/21/70	6.85	7.89	104	134	12.96	14.70
9/2/71 –10/2/71	7.23	7.86	106	128	12.95	14.63
8/25/72– 9/12/72	7.70	7.93	108	122	13.35	14.57
10/29/73–11/18/73	7.57	7.94	130	140	12.02	13.47
10/12/74–11/21/74	6.62	7.94	116	144	11.82	14.67

HEV_1 Hyperbolic excess velocity relative to launch planet P_1 (Earth)
HEV_2 Hyperbolic excess velocity relative to second planet P_2 (Mercury)
T_{12} Flight time from P_1 to P_2

The synodic period of Venus is approximately three-quarters as long as the synodic period of Mars. Thus, since there are six Earth–Venus periods for the decade, there should be only four and one-half Earth–Mars periods. The beginning of the decade falls almost in the middle of an Earth–Mars period, thus accounting for the expected half period. Table 3 displays the four complete Earth–Mars launch periods.

It is important to keep in mind that the trajectories described in the three tables are optimum trajectories. Thus, from Table 1, we notice that the lowest hyperbolic excess velocity required to reach Venus on a Type I trajectory for the entire decade is 2.52 km/sec; this trajectory occurs during the 1967 launch period. Only 2.41 km/sec is required for a Venus Type II trajectory, which also occurs during the 1967 period. From Table 2 we find that the lowest hyperbolic excess velocity required to reach Mercury during the decade is 6.43 km/sec. The required trajectory is Type I and occurs during the 1974 launch period. This minimum energy is 267% greater than the lowest launch energy required to reach Venus.

Table 3. Some important properties of optimum Earth–Mars transfer trajectories

Launch period	Min. HEV_1 km/sec	Max. HEV_1 km/sec	Min. T_{12} days	Max. T_{12} days	Min. HEV_2 km/sec	Max. HEV_2 km/sec
	Type I					
12/5/66 –2/3/67	3.00	4.23	190	208	4.05	6.89
2/2/69 –4/3/69	2.96	3.84	176	214	3.60	6.52
4/23/71–6/22/71	2.81	3.52	188	228	2.80	3.61
7/7/73 –8/16/73	3.80	4.25	194	198	2.55	3.44
	Type II					
12/21/66–2/19/67	2.94	3.00	308	348	3.63	6.35
2/26/69–3/27/69	2.82	3.02	288	302	4.53	5.41
4/9/71 –5/31/71	3.09	4.00	244	296	3.10	3.76
8/4/73 –9/11/73	4.00	4.20	364	442	3.13	4.22

HEV_1 Hyperbolic excess velocity relative to launch planet P_1 (Earth)
HEV_2 Hyperbolic excess velocity relative to second planet P_2 (Mars)
T_{12} Flight time from P_1 to P_2

The lowest hyperbolic excess velocity required to reach Mars during the decade is 2.81 km/sec, which is a Type I occurring in 1971.

The information given in the tables clearly displays the following facts:

1. Launch energies for direct Earth–Mercury trajectories are very high.

2. There are relatively few launch opportunities for direct Earth–Mars missions; each is separated by approximately 780 days.

If the Earth–Mercury trajectories are replaced by Earth–Venus–Mercury trajectories, the energy barrier obstructing trips to Mercury can be circumvented. Similarly, by employing advanced trajectories of the type Earth–Venus–Mars in addition to the simple Earth–Mars trajectories, the number of launch opportunities for missions to Mars can be more than doubled.

1. Earth–Venus–Mercury Trajectories

We recall that any multiple planetary trajectory where P_1 = Earth and P_2 = Venus will necessarily require a high launch energy if the launch date does not fall in one of the favorable Earth–Venus launch periods. Consequently, the numerical analysis of the Earth–Venus–Mercury trajectories proceeded by first carrying out a rough analysis for each of the six Earth–Venus launch periods given in Table 1. These calculations were aimed at finding the approximate values of the pairs (T_1, T_2) that yielded the most promising trajectories for each period. (We recall that T_1 and T_2 are the launch and the P_2 closest approach dates, respectively, where in this case, P_2 = Venus.) This method involved determining many trajectories with initial conditions (T_1, T_2) represented by the intersections in a net about each launch period. We shall refer to these nets as the coarse nets. For example, the coarse net about the 1965 launch period is shown in Fig. 11. Notice that this launch interval and its range of flight times completely covers the 1965 Earth–Venus launch period given in Table 1.

The calculation of this net was performed by first setting T_1 = September 15, 1965, and $T_2 - T_1 = 70$ days. After this trajectory was calculated (or rejected because its total flight time was too long, or because it was physically unrealizable), the next trajectory having the same launch date, but with $T_2 - T_1 = 76$ days, was calculated (or rejected). This process continued until the Earth–Venus flight time $(T_2 - T_1)$ reached 226 days whereupon the launch date was advanced 6 days to September 21 and $T_2 - T_1$ dropped back to 70 days. This was done until all nineteen different launch dates had been examined. The calculation involved $27 \times 19 = 513$ trajectories for each of the two types of missions. The grid of this net will be referred to as 6×6 days, where the first number

means that the Venus intercept date was advanced by 6-day increments for each fixed launch date and the second number means that the launch dates were advanced by 6-day increments. This grid was used for all coarse nets except for the 1967 period, where a 1 × 4 day grid was employed.

These coarse-net results revealed that all six Earth–Venus launch periods were also periods for possible Earth–Venus–Mercury missions. Thus, it was discovered that these trajectories were not only possible but even occurred during each Earth–Venus period throughout the entire decade.

Guided by the results of the coarse nets, a much more localized study was begun. For each period, this involved calculating a much finer net covering the most attractive trajectories found by the coarse net. These fine nets employed a grid of 0.2 × 2 days. Thus, corresponding to each launch date of the fine net, as many as 250 different trajectories were sometimes determined. Consequently, in some fine nets, almost 5,000 multiple planetary trajectories were calculated (of which many were rejected). It was observed that advancing the Venus intercept date by only 0.2-day increments sometimes produced a 200 to 500 km change in the distance of closest approach. Thus, when the distance of closest approach became small for some launch periods, a third extra-fine net employing a 0.01 × 2 day grid was calculated. From the results of all these calculations, trajectories having near-minimum launch energies or near-maximum distances of closest approach for each launch date of a net were found.

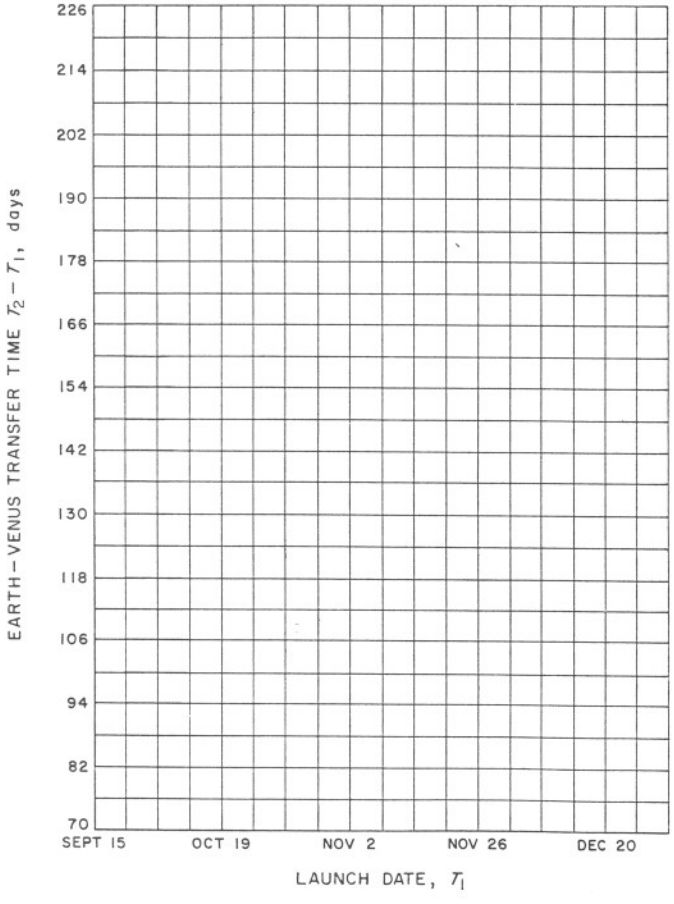

Fig. 11. Illustration of coarse net for Earth–Venus–Mercury 1965 trajectories

All the tables appearing in this Report shall adhere to the following notation:

HEV_k = hyperbolic excess velocity at P_k, km/sec

$T_{k,\,k+1}$ = time taken by vehicle to pass from P_k to P_{k+1} (i.e., $T_{k+1} - T_k$), days

$\theta_{k,\,k+1}$ = heliocentric angle swept out by the vehicle passing from P_k to P_{k+1}, deg

TISI_k = amount of time vehicle spends in P_k's sphere of gravitational influence, days

DOCA_k = distance of closest approach to P_k's surface, km

VACA_k = velocity at closest approach to P_k, km/sec

DA_k = angular difference between the vehicle's velocity vectors as it enters and leaves P_k's sphere of influence, deg

TFT = total flight time, days

The quantities labeled $(\mathbf{B} \cdot \hat{\mathbf{T}})_k$ and $(\mathbf{B} \cdot \hat{\mathbf{R}})_k$ are used by an integrating program at the Jet Propulsion Laboratory; with this program, the *actual trajectory can be precisely determined.* The vectors $\mathbf{B}$, $\hat{\mathbf{T}}$, and $\hat{\mathbf{R}}$ are defined at P_k with respect to Σ', which is taken to be an ecliptic coordinate system (epoch 1950.0). The $\mathbf{B}$ vector, measured in kilometers, is the vector originating at P_k which meets the vehicle's incoming hyperbolic asymptote at right angles. The unit vectors $\hat{\mathbf{T}}$ and $\hat{\mathbf{R}}$ are defined by

$$\mathbf{T} = \frac{\mathbf{V}'(T^*_{k-1}) \times \hat{\mathbf{k}}}{|\mathbf{V}'(T^*_{k-1}) \times \hat{\mathbf{k}}|}$$

and

$$\hat{\mathbf{R}} = \frac{\mathbf{V}'(T^*_{k-1}) \times \hat{\mathbf{T}}}{\mathbf{V}'(T^*_{k-1})}$$

where, according to the notation of Part III, T^*_{k-1} is the time at which the vehicle enters the gravitational sphere of influence of P_k.

The following comments, which are applicable to all the tables given in this Report, should be carefully noted:

1. If some symbols do not have any subscripts, the subscript k is assumed to be 2; for example, DOCA means $DOCA_2$.

2. The times corresponding to all given calendar dates that appear without reference to a particular hour are always taken to be 1200 hours GMT.

3. The radius of the planet Venus, which is taken to be 6,100 km, was determined optically (see Ref. 5). Consequently, the distances of closest approach to Venus appearing in some of the tables should be understood as meaning the distances of closest approach to the Venusian visible cloud layer as viewed from the Earth.

a. Earth–Venus–Mercury, 1965–1966. The first Earth–Venus launch period for the decade under consideration occurs during the winter of 1965. Although accurate planetary approach guidance may not be available for this launch period, it may be possible to place a vehicle on an Earth–Venus–Mercury trajectory by employing advanced techniques of midcourse corrections. Even if the midcourse corrections were only partially successful, the vehicle could perhaps obtain very useful information about regions close to the Sun.

Since detailed properties of the Venusian atmosphere are unknown at this time, the trajectories appearing in Table 4 were chosen so that their distances of closest approach to the surface of Venus would exceed 800 km, and so that at the same time their launch energies would be nearly minimum for each launch date of the period satisfying this restriction. These trajectories were found from the fine-net results. Comparing these trajectories with the general properties of optimum Earth–Mercury trajectories, we find some very significant characteristics. These trajectories require less than one-third of the launch energies required for the *optimum* Earth–Mercury trajectories for the periods occurring in 1965 and 1966. We also notice that the Mercury approach energies are less than one-half of those resulting from the simple direct-flight trajectories. Planetary approach energies will become increasingly important when orbiting or landing on the planet becomes necessary.

The flight times required for these advanced missions are considerably longer than those required for the direct-flight trajectories, but they are quite within reason. In Table 3 we notice that these flight times are in the same range of flight times required for direct Earth–Mars missions.

It is interesting to observe the strong influence that the gravitational field of Venus exerts on the vehicle's trajectory. During the 2 days when the vehicle's motion is dominated by the Venusian gravitational field, the direction of the vehicle's velocity vector is altered by as much as 55 deg.

Before considering these trajectories for the next launch period, it is desirable to have some general idea of the configuration of the planets during the critical phases of the missions when the vehicle encounters Venus and Mercury. This configuration is shown in Fig. 12. From the geometry of the situation, we find that the communication distances to Earth during the Venus and Mercury encounters will be approximately 1.6 and 1.3 astronomical units (au), respectively. The Figure reveals

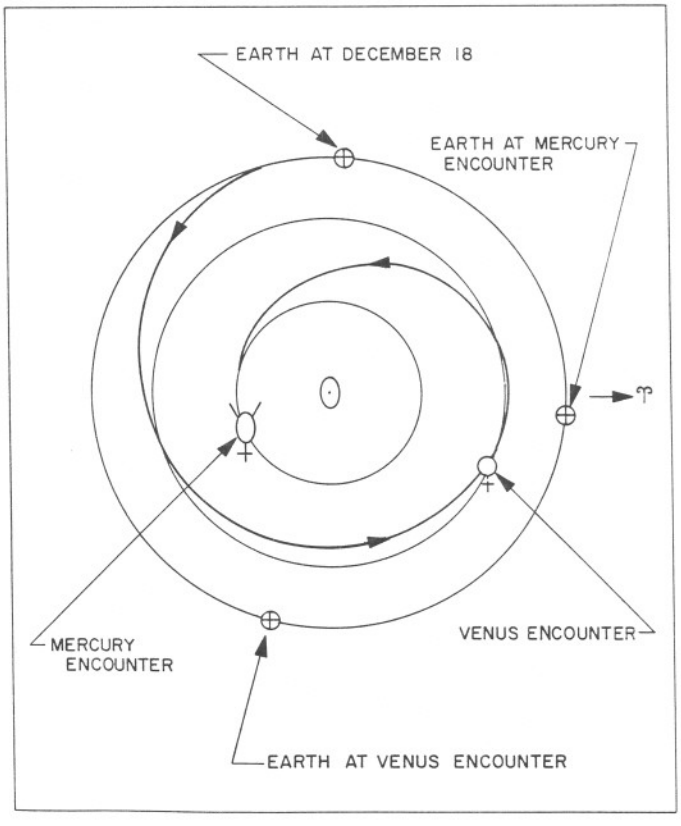

Fig. 12. Planetary configuration for Earth–Venus–Mercury, 1965-6 (December 18 trajectory)

Table 4. Some important properties of Earth–Venus–Mercury trajectories, 1965-6

Launch date	HEV_1 km/sec	T_{12} days	θ_{12} deg	$B \cdot \hat{T}$ km	$B \cdot \hat{R}$ km	HEV_2 km/sec	TISI days	DOCA km	VACA km/sec	DA deg	T_{23} days	θ_{23} deg	HEV_3 km/sec	TFT days
Nov. 28	4.39	186.9	264.93	−12,810.	123.	7.15	1.94	1,849.	11.53	52.72	110.98	241.11	9.13	297.92
30	4.32	185.3	263.55	−12,845.	124.	7.10	1.95	1,832.	11.50	53.22	110.25	239.41	9.18	295.59
Dec. 2	4.25	183.75	262.16	−12,863.	158.	7.06	1.96	1,805.	11.49	53.71	109.60	238.12	9.18	293.35
4	4.19	182.15	260.77	−12,869.	108.	7.02	1.97	1,772.	11.48	54.18	108.82	236.05	9.28	290.91
6	4.13	180.55	259.38	−12,862.	50.	6.99	1.98	1,733.	11.48	54.63	107.92	233.98	9.40	288.47
8	4.09	178.96	257.99	−12,842.	−15.	6.97	1.99	1,688.	11.49	55.06	107.09	231.93	9.55	286.05
10	4.05	177.36	256.60	−12,807.	−91.	6.95	1.99	1,637.	11.50	55.45	106.26	229.86	9.71	283.62
12	4.01	175.56	254.89	−12,843.	36.	6.91	2.00	1,635.	11.48	55.76	106.15	229.83	9.69	281.71
14	3.99	173.76	253.18	−12,857.	132.	6.89	2.01	1,622.	11.47	56.05	105.95	229.53	9.70	279.71
16	3.97	171.97	251.47	−12,848.	186.	6.87	2.01	1,596.	11.47	56.32	105.65	228.87	9.75	277.61
18	3.97	170.17	249.76	−12,820.	205.	6.86	2.01	1,560.	11.48	56.57	105.62	227.95	9.83	275.43
20	3.97	168.17	247.73	−12,833.	397.	6.84	2.02	1,557.	11.47	56.76	105.47	228.66	9.75	273.65
22	4.00	166.17	245.70	−12,817.	547.	6.83	2.02	1,538.	11.48	56.92	105.59	229.04	9.71	271.76
24	4.03	165.38	245.57	−12,443.	−358.	6.91	2.00	1,288.	11.65	57.25	102.31	220.06	10.76	267.69
26	4.07	164.78	245.75	−11,927.	−1,204.	7.01	1.97	979.	11.87	57.75	99.49	212.80	11.86	264.27
28	4.12	162.98	244.04	−11,830.	−1,256.	7.03	1.97	920.	11.91	57.83	99.10	211.78	12.03	262.08
30	4.19	160.98	242.01	−11,787.	−1,203.	7.05	1.96	893.	11.94	57.80	99.02	211.51	12.09	260.00
Jan. 1	4.27	158.98	239.98	−11,718.	−1,173.	7.07	1.96	855.	11.98	57.74	98.91	211.10	12.18	257.89
3	4.37	156.79	237.64	−11,686.	−1,047.	7.10	1.95	840.	12.00	57.58	99.08	211.32	12.18	255.87
5	4.49	154.59	235.29	−11,621.	−945.	7.13	1.94	810.	12.04	57.39	99.20	211.37	12.21	253.79

that special consideration must be given to radio disturbance caused by solar radiation during the Mercury encounter. This problem could be alleviated by utilizing large radio antennas with high resolution, such as the new 210-ft dish planned for the Goldstone site. Figure 13 gives part of the December 18 trajectory in the sphere of influence of Venus. The trajectory is drawn with respect to Venus and, hence, is hyperbolic. According to the scale of the Figure, the sphere of influence has a radius of approximately 13 ft. The circle depicting Venus represents the top of its cloud layer and not its surface.

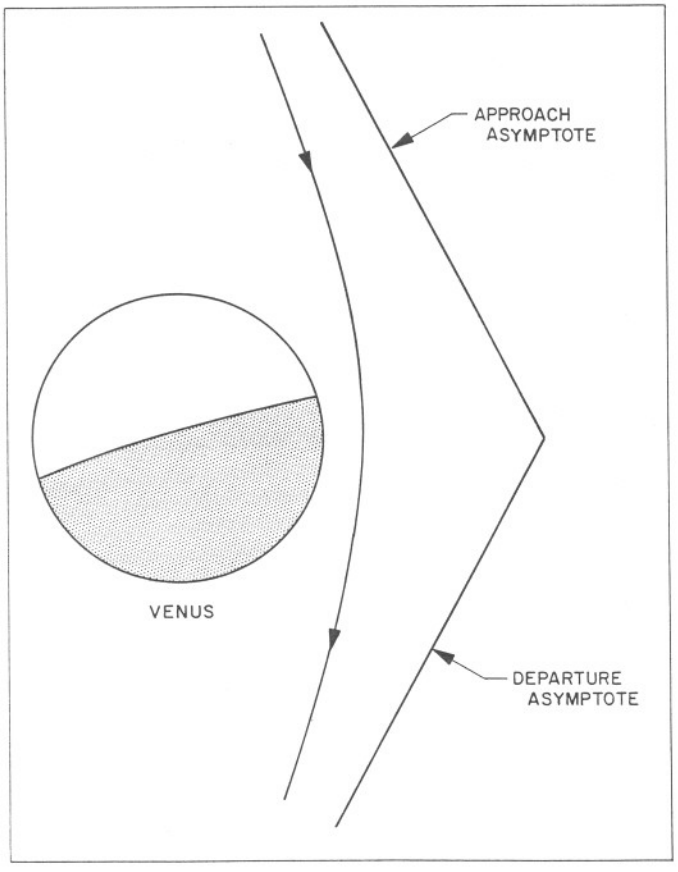

Fig. 13. December 18, 1965, Earth–Venus–Mercury trajectory at Venus intrecept

We have noticed that these multiple planetary trajectories use only a fraction of the launch energies and arrival energies characteristic of the optimum Earth–Mercury trajectories. Besides this great saving of energy, these trajectories can be used not only to reach Mercury, but *also to enable the vehicle to perform various tasks as it passes Venus*. For example, the launch vehicle could carry two scientific payloads, one of which could be "dropped off" as it passes Venus on its way to Mercury. Of course, vehicles capable of carrying out these sophisticated missions will weigh more than those required for direct Earth–Mercury flights, but the proportional difference in weight should be more than offset by the lower launch energies required for the multiple planetary trajectories.

b. Earth–Venus–Mercury, 1967. From Table 1 we notice that the second Earth–Venus launch period occurs during the summer of 1967. The multiple planetary trajectories for this period come very close to Venus. Consequently, an extra-fine net was calculated to find those trajectories corresponding to the different launch dates that maximized the distances of closest approach. Table 5 is an example of the method by which these greatest passing distance trajectories were found; in particular, it contains a set of trajectories for the June 7 launch date. Each trajectory was obtained by advancing the Venus intercept date T_2 by only 0.01-day increments. Of course, trajectories for this launch date passing much farther from Venus probably exist, but they will have flight times or launch energies several times greater. Thus, it shall always be assumed that trajectories will be referred to as maximum passing distance trajectories or minimum launch energy trajectories only if they have short flight times *and* the lowest possible launch energies.

The maximum passing distance trajectories for the various launch dates of the 1967 launch period appear in Table 6. If measurements of the Venusian atmosphere show that the densities at various altitudes are approximately twice as great as the densities for the Earth, these trajectories would be very questionable. On the other hand, if the densities at various altitudes are approximately equal for both planets, these trajectories may, in fact, be ideal. A vehicle passing just outside the Venusian atmosphere on its way to Mercury could easily obtain excellent observations and measurements.

Unlike the trajectories for the 1965–1966 launch period, these trajectories take the vehicle less than halfway around the Sun for the Earth–Venus portions of the mission. The transfers to Mercury are also shorter. Thus, these trajectories have flight times approximately 100 days shorter than those of the previous launch interval. Notice that the launch energies are lower than those of the 1965–1966 launch period. The Mercury–approach energies are also lower. One observes that a vehicle moving on these trajectories spends slightly more time under the gravitational influence of Venus than in the previous launch period. This characteristic, together with the fact that these trajectories take the vehicle very close

Table 5. Some important properties of Earth–Venus–Mercury trajectories (June 7, 1967, launch)

HEV_1 km/sec	T_{12} days	θ_{12} deg	$B \cdot \hat{T}$ km	$B \cdot \hat{R}$ km	HEV_2 km/sec	TISI days	DOCA km	VACA km/sec	DA deg	T_{23} days	θ_{23} deg	HEV_3 km/sec	TFT days
3.56	107.32	117.77	11,429.	−1,524.	6.44	2.13	6.7	12.16	68.37	71.70	189.38	9.82	179.02
3.56	107.33	117.79	11,448.	−1,482.	6.44	2.13	15.8	12.15	68.34	71.71	189.44	9.80	179.04
3.56	107.34	117.80	11,468.	−1,437.	6.44	2.13	25.2	12.14	68.31	71.72	189.51	9.78	179.07
3.56	107.35	117.82	11,487.	−1,390.	6.43	2.13	34.5	12.14	68.28	71.74	189.58	9.75	179.09
3.56	107.36	117.83	11,507.	−1,343.	6.43	2.13	43.9	12.13	68.25	71.76	189.65	9.73	179.12
3.56	107.37	117.85	11,526.	−1,294.	6.43	2.13	53.1	12.12	68.21	71.77	189.73	9.70	179.15
3.56	107.38	117.87	11,546.	−1,243.	6.43	2.13	62.4	12.11	68.18	71.79	189.81	9.67	179.17
3.56	107.39	117.88	11,565.	−1,189.	6.43	2.13	71.8	12.11	68.15	71.81	189.89	9.65	179.21
3.56	107.40	117.90	11,585.	−1,134.	6.42	2.13	81.3	12.10	68.12	71.83	189.99	9.62	179.24
3.56	107.41	117.91	11,604.	−1,075.	6.42	2.13	90.9	12.09	68.09	71.86	190.09	9.59	179.27
3.56	107.42	117.93	11,623.	−1,015.	6.42	2.13	100.2	12.08	68.05	71.89	190.19	9.56	179.31
3.56	107.43	117.94	11,643.	−951.	6.42	2.13	109.7	12.07	68.02	71.91	190.30	9.53	179.35
3.56	107.44	117.96	11,662.	−883.	6.42	2.13	119.2	12.07	67.99	71.95	190.43	9.49	179.39
3.56	107.45	117.97	11,681.	−812.	6.42	2.13	128.6	12.06	67.96	71.98	190.56	9.46	179.43
3.56	107.46	117.99	11,694.	−766.	6.41	2.13	135.4	12.05	67.93	72.00	190.64	9.44	179.46
3.56	107.47	118.01	11,717.	−644.	6.41	2.14	146.5	12.05	67.90	72.06	190.85	9.39	179.53
3.55	107.48	118.02	11,733.	−588.	6.41	2.14	155.1	12.04	67.87	72.10	191.00	9.35	179.58
3.55	107.49	118.04	11,754.	−477.	6.41	2.14	165.8	12.03	67.83	72.16	191.24	9.30	179.65
3.55	107.50	118.05	11,770.	−380.	6.41	2.14	174.4	12.02	67.80	72.23	191.46	9.25	179.72
3.55	107.51	118.07	11,787.	−261.	6.40	2.14	183.4	12.02	67.77	72.30	191.74	9.20	179.81
3.55	107.52	118.08	11,802.	−111.	6.40	2.14	192.5	12.01	67.75	72.41	192.11	9.13	179.93
3.55	107.53	118.10	11,815.	86.	6.40	2.14	200.9	12.00	67.72	72.57	192.65	9.05	180.10
3.55	107.54	118.11	11,762.	967.	6.40	2.14	187.5	12.01	67.81	73.53	195.83	8.69	181.07
3.55	107.56	118.15	11,618.	1,546.	6.39	2.14	115.6	12.06	68.25	74.52	198.97	8.50	182.08
3.55	107.57	118.16	11,541.	1,761.	6.39	2.14	76.7	12.08	68.47	75.00	200.51	8.46	182.57
3.55	107.58	118.18	11,457.	1,949.	6.39	2.14	31.0	12.17	68.74	75.50	202.10	8.45	183.08

Table 6. Some important properties of Earth–Venus–Mercury trajectories, 1967

Launch date	HEV_1 km/sec	T_{12} days	θ_{12} deg	$B \cdot \hat{T}$ km	$B \cdot \hat{R}$ km	HEV_2 km/sec	TISI days	DOCA km	VACA km/sec	DA deg	T_{23} days	θ_{23} deg	HEV_3 km/sec	TFT days
June 5	3.56	109.40	119.81	11,812.	212.	6.37	2.15	170.	12.01	68.18	72.87	193.42	8.96	182.27
7	3.55	107.53	118.10	11,815.	86.	6.40	2.14	201.	12.00	67.72	72.57	192.65	9.05	180.10
9	3.55	105.67	116.41	11,816.	453.	6.42	2.13	234.	11.99	67.29	72.71	193.35	8.92	178.38
11	3.56	103.80	114.71	11,816.	361.	6.45	2.12	260.	11.99	66.88	72.43	192.65	8.99	176.23
13	3.58	101.92	112.99	11,808.	49.	6.48	2.12	280.	11.99	66.47	72.00	191.44	9.15	173.92
15	3.61	100.05	111.29	11,793.	278.	6.50	2.11	296.	11.99	66.14	72.00	191.66	9.08	172.05
17	3.65	98.16	109.57	11,774.	158.	6.53	2.10	307.	12.00	65.80	71.74	191.02	9.16	169.91
19	3.70	96.28	107.84	11,745.	10.	6.56	2.09	311.	12.01	65.49	71.49	190.36	9.25	167.77
21	3.77	94.39	106.12	11,709.	−22.	6.58	2.08	309.	12.03	65.22	71.32	189.99	9.30	165.71
23	3.84	92.52	104.41	11,668.	4.	6.61	2.08	301.	12.05	65.00	71.18	189.74	9.31	163.69
25	3.93	90.63	102.69	11,617.	−45.	6.64	2.07	286.	12.07	64.80	71.00	189.35	9.36	161.63
27	4.04	88.73	100.95	11,552.	−147.	6.67	2.06	262.	12.11	64.64	70.81	188.91	9.44	159.55
29	4.16	86.85	99.22	11,480.	−189.	6.69	2.05	230.	12.14	64.52	70.66	188.58	9.48	157.50
July 1	4.29	84.96	97.51	11,399.	−195.	6.72	2.04	189.	12.18	64.46	70.52	188.31	9.51	155.48
3	4.44	83.08	95.78	11,304.	−245.	6.75	2.04	139.	12.23	64.44	70.36	187.99	9.56	153.44

to the Venusian surface, indicates that the vehicle's direction of motion will be changed by an amount greater than that for the previous launch period. This is indeed true, for Table 6 shows that the vehicle's velocity vector will be deflected approximately 10 deg more than it will be for the 1965–1966 period.

Figure 14 displays the planetary configuration for the 1967 launch period. It shows that excellent communication with the vehicle should be possible (except, of course, when it passes behind Venus) throughout the entire mission. At the Venus and Mercury encounters the Earth's distance should be approximately 0.29 and 1.3 au, respectively.

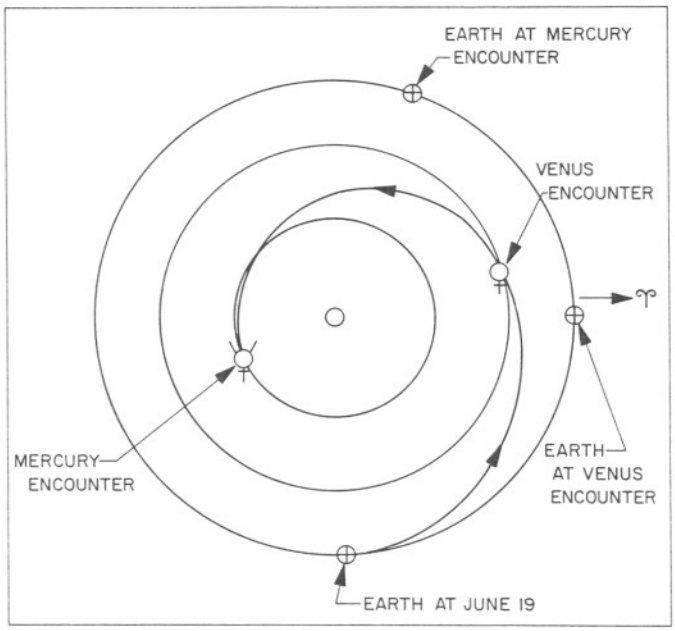

Fig. 14. Planetary configuration for Earth–Venus–Mercury, 1967 (June 19 trajectory)

Figure 15 displays part of the hyperbolic trajectory in the vicinity of Venus corresponding to the June 19 launch date.

c. Earth–Venus–Mercury, 1969. The third favorable launch period for these advanced trajectories occurs during January of 1969. A fine-net calculation was found to be sufficient for determining the trajectories having the lowest launch energies for each launch date. These minimum launch energy trajectories appear in Table 7.

These multiple planetary trajectories for the 1969 launch period, as for the 1965–1966 period, all have Type II Earth–Venus transfers and Type II Venus–Mercury transfers, whereas the trajectories for the 1967 period have Type I Earth–Venus and Type II Venus–Mercury transfers. The Type I Earth–Venus transfers cause the flight times for the 1967 trajectories to be much shorter than those required for the 1965–1966 trajectories. In Table 7 we notice that the 1969 trajectories are very similar to those occurring for the 1965–1966 period: both Earth–Venus and Venus–Mercury transfers are Type II. It is important to point out that the minimum launch energy trajectories appearing in Table 4 for the 1965–1966 period were obtained only from those trajectories of the fine net having distances of closest approach greater than 800 km. This constraint was not applied to the multiple planetary trajectories of the 1969 period. If this constraint were removed, the minimum launch energies would not continually decrease as do those of the 1969 period. In addition to continually decreasing launch energies, we notice that the 1969 opportunity has continually decreasing distances of closest approach with increasing launch date. Except for one or two cases, these minimum launch energy trajectories also maximize the distances of closest approach. This property also

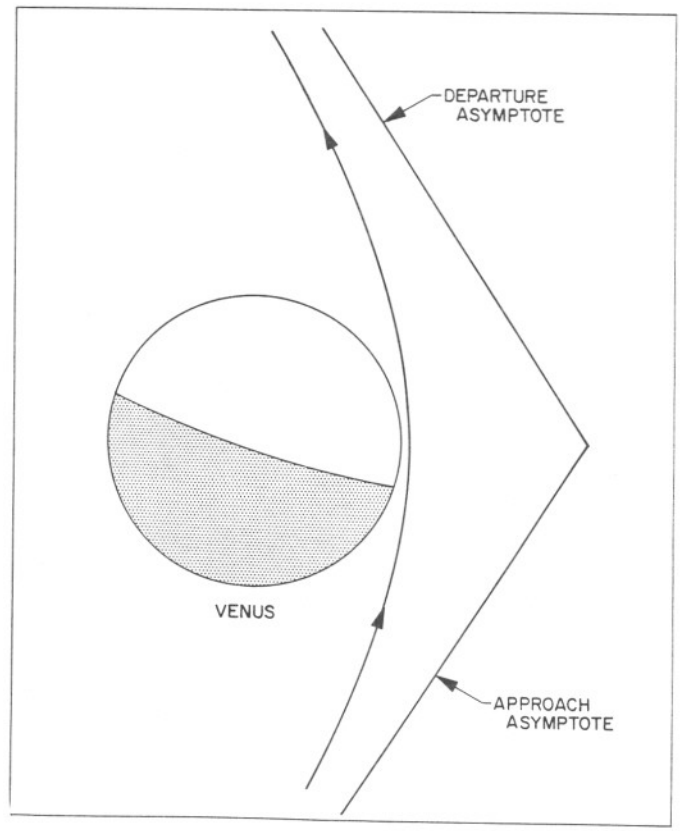

Fig. 15. June 19, 1967, Earth–Venus–Mercury trajectory at Venus intercept

Table 7. Some important properties of Earth–Venus–Mercury trajectories, 1969

Launch date	HEV_1 km/sec	T_{12} days	θ_{12} deg	$B \cdot \hat{T}$ km	$B \cdot \hat{R}$ km	HEV_2 km/sec	TISI days	DOCA km	VACA km/sec	DA deg	T_{23} days	θ_{23} deg	HEV_3 km/sec	TFT days
Jan. 3	4.89	204.76	269.87	−12,088.	4,899.	6.75	2.04	1,634.	11.38	57.34	115.01	229.67	9.55	319.76
5	4.77	203.16	268.47	−12,254.	4,637.	6.68	2.06	1,612.	11.35	58.07	111.50	220.23	9.82	314.66
7	4.68	201.76	267.39	−12,170.	4,655.	6.65	2.07	1,510.	11.38	58.85	110.42	217.91	9.94	312.18
9	4.59	200.36	266.32	−12,069.	4,678.	6.62	2.08	1,401.	11.42	59.63	109.42	215.79	10.07	309.78
11	4.48	198.76	264.92	−11,941.	4,872.	6.57	2.09	1,302.	11.44	60.58	109.83	217.51	9.86	308.60
13	4.40	197.37	263.85	−11,835.	4,850.	6.54	2.10	1,186.	11.49	61.33	108.57	214.62	10.05	305.93
15	4.30	195.77	262.45	−11,533.	5,294.	6.50	2.11	1,053.	11.54	62.37	112.00	224.89	9.48	307.77
17	4.22	194.37	261.38	−11,581.	4,947.	6.49	2.11	954.	11.58	62.99	107.36	212.45	10.13	301.73
19	4.13	192.77	259.99	−11,455.	5,024.	6.46	2.12	845.	11.63	63.84	107.15	212.37	10.08	299.94
21	4.05	191.18	258.59	−11,324.	5,081.	6.43	2.13	732.	11.68	64.68	106.85	212.02	10.06	298.03
23	3.96	189.38	256.88	−11,209.	5,226.	6.39	2.14	645.	11.71	65.57	107.67	214.64	9.79	279.05
25	3.89	187.78	255.49	−11,079.	5,228.	6.37	2.15	529.	11.77	66.33	107.01	213.26	9.86	294.79
27	3.82	185.98	253.79	−10,960.	5,328.	6.34	2.16	439.	11.81	67.13	107.71	215.52	9.66	293.69
29	3.76	184.39	252.40	−10,829.	5,277.	6.33	2.16	316.	11.89	67.85	106.55	212.71	9.83	290.94
31	3.70	182.59	250.69	−10,713.	5,314.	6.31	2.16	221.	11.94	68.56	106.70	213.38	9.75	289.28
Feb. 2	3.65	180.79	248.99	−10,596.	5,325.	6.30	2.17	124.	12.00	69.24	106.61	213.40	9.73	287.40

occurred for many of the launch dates of the 1965–1966 trajectories. Strictly speaking, this property does not show up for the 1967 period; however, since the Venus intercept dates are so sensitive for this period, their launch energies differ from the lowest value for each launch date by an extremely small amount.

Figure 16 gives the planetary configuration during the critical phases of these missions. One observes that, at the Mercury encounter, the Sun is almost directly between the Earth and Mercury, but this is a false representation caused by the fact that the Figure is only a rough two-dimensional approximation of the real situation. However, there should be very serious difficulties with radio communication since Mercury will be near its superior conjunction and the Earth–Sun–Mercury angle will be about 168 to 172 deg. Only the largest radio antennas could perhaps cope with this situation. At the Venus encounters, the communication distances should be approximately 1.0 au, and during the Mercury encounters, they should be about 1.4 au.

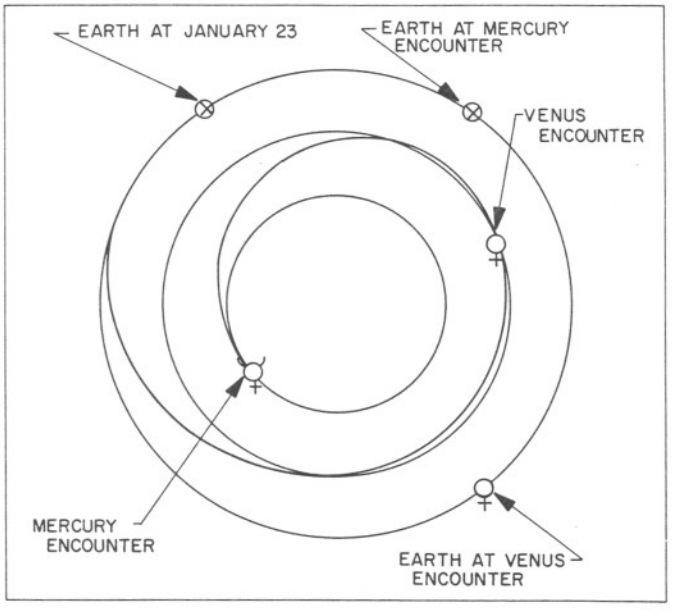

Fig. 16. Planetary configuration for Earth–Venus–Mercury, 1969 (January 23 trajectory)

The January 23 trajectory in the immediate vicinity of Venus appears in Fig. 17.

d. Earth–Venus–Mercury, 1970. The summer of 1970 finds us in the next Earth–Venus launch period. This period is unusually favorable for this particular type of multiple planetary trajectory. We shall discover later

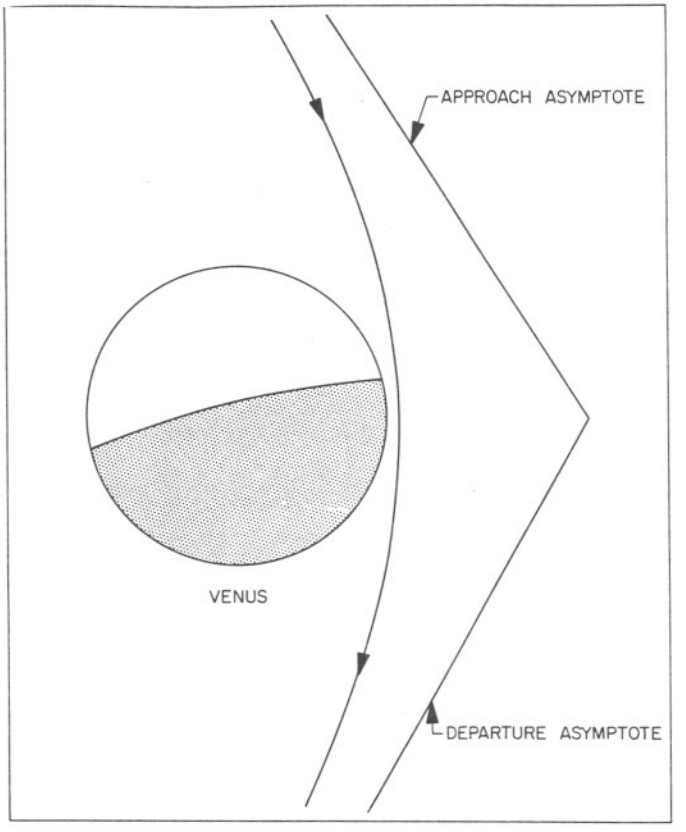

Fig. 17. January 23, 1969, Earth–Venus–Mercury trajectory at Venus intercept

that this launch period is also very favorable for other types of multiple planetary trajectories.

An extra-fine net was calculated over this period to find the minimum launch energy trajectories. These trajectories, appearing in Table 8, cover a 50-day launch interval. From this Table we immediately observe that these trajectories have lower launch energies and shorter flight times than those trajectories of the previous periods. The Earth–Venus–Mercury transfers require only about 35% more launch energy than the optimum Earth–Venus trajectories. The flight times are short since both the Earth–Venus and Venus–Mercury transfers are Type I. It must be pointed out that these trajectories have higher Mercury approach energies; however, by observing the optimum Earth–Mercury trajectories in Table 2, we find that the approach energies are still much lower than those resulting from the direct-flight 1970 trajectories.

The planetary configuration for this launch period is given in Fig. 18. Notice that the trajectories allow the vehicle to remain relatively near the Earth: at the Venus encounter, the Earth is approximately 0.35 au away;

Table 8. Some important properties of Earth–Venus–Mercury trajectories, 1970

Launch date	HEV_1 km/sec	T_{12} days	θ_{12} deg	$B \cdot \hat{T}$ km	$B \cdot \hat{R}$ km	HEV_2 km/sec	TISI days	DOCA km	VACA km/sec	DA deg	T_{23} days	θ_{23} deg	HEV_3 km/sec	TFT days
July 25	3.78	123.23	130.18	13,213.	894.	7.07	1.94	2,156.	11.34	52.25	58.95	142.67	12.79	182.23
27	3.74	121.46	128.56	13,278.	946.	7.12	1.93	2,265.	11.33	51.42	58.85	142.62	12.75	180.30
29	3.71	119.64	126.94	13,406.	936.	7.16	1.92	2,425.	11.29	50.44	58.87	142.97	12.64	178.51
31	3.68	117.82	125.31	13,579.	866.	7.21	1.91	2,622.	11.24	49.35	59.00	143.63	12.48	176.82
Aug. 2	3.65	115.98	123.67	13,607.	949.	7.25	1.90	2,698.	11.24	48.71	58.83	143.36	12.49	174.81
4	3.62	114.15	122.02	13,727.	924.	7.30	1.88	2,850.	11.22	47.83	58.86	143.69	12.39	173.01
6	3.59	112.31	120.37	13,895.	829.	7.34	1.87	3,040.	11.18	46.84	59.00	144.36	12.25	171.31
8	3.56	110.48	118.72	13,996.	808.	7.38	1.86	3,173.	11.16	46.06	59.00	144.60	12.18	169.48
10	3.54	108.63	117.04	14,090.	785.	7.42	1.85	3,300.	11.14	45.33	59.00	144.82	12.12	167.63
12	3.53	106.78	115.37	14,181.	758.	7.47	1.85	3,423.	11.13	44.62	59.00	145.03	12.06	165.78
14	3.51	104.92	113.68	14,163.	893.	7.51	1.84	3,454.	11.15	44.20	58.75	144.49	12.10	163.68
16	3.50	103.07	111.99	14,112.	1,061.	7.55	1.83	3,456.	11.18	43.88	58.45	143.77	12.17	161.52
18	3.50	101.22	110.31	14,432.	649.	7.59	1.82	3,768.	11.11	42.66	59.00	145.66	11.91	160.22
20	3.50	99.35	108.60	14,256.	1,028.	7.63	1.81	3,662.	11.17	42.66	58.41	144.07	12.07	157.76
22	3.51	97.49	106.89	14,281.	1,064.	7.67	1.80	3,725.	11.18	42.19	58.31	143.94	12.06	155.79
24	3.53	95.63	105.19	14,630.	504.	7.70	1.79	4,056.	11.10	40.99	59.00	146.23	11.78	154.63
26	3.56	93.69	103.36	13,413.	2,002.	7.76	1.78	3,099.	11.44	43.41	56.40	138.33	12.90	150.09
28	3.59	91.89	101.75	14,480.	900.	7.78	1.77	4,004.	11.17	40.58	58.36	144.67	11.90	150.25
30	3.63	90.02	100.03	14,755.	320.	7.82	1.77	4,272.	11.12	39.60	59.00	146.77	11.68	149.02
Sept. 1	3.68	88.14	98.30	14,777.	250.	7.85	1.76	4,325.	11.14	39.21	59.00	146.95	11.65	147.14
3	3.75	86.27	96.56	14,501.	867.	7.89	1.75	4,121.	11.22	39.49	58.18	144.67	11.83	144.45
5	3.82	84.39	94.81	14,428.	958.	7.93	1.74	4,089.	11.25	39.31	57.98	144.22	11.86	142.37
7	3.91	82.52	93.08	14,484.	777.	7.97	1.74	4,163.	11.26	38.87	58.13	144.84	11.78	140.64
9	4.02	80.64	91.33	14,384.	866.	8.00	1.73	4,106.	11.30	38.77	57.91	144.38	11.80	138.55
11	4.14	78.76	89.59	14,400.	683.	8.04	1.72	4,142.	11.32	38.43	58.05	144.95	11.73	136.81
13	4.27	76.89	87.84	14,254.	799.	8.08	1.71	4,042.	11.37	38.44	57.79	144.34	11.77	134.67

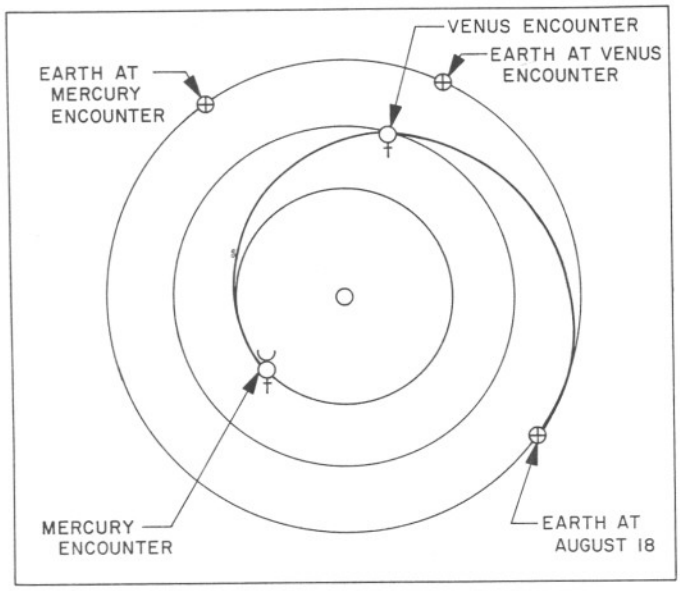

Fig. 18. Planetary configuration for Earth–Venus–Mercury, 1970 (August 18 trajectory)

during the Mercury encounter, the Earth is approximately 1.2 au away. The Figure shows that these encounters occur when Mercury is near greatest elongation. Thus, ideal radio communication with the vehicle should be available during these encounters.

Figure 19 displays the August 18 trajectory when the vehicle is well within the gravitational sphere of influence of Venus. We recall that the radius of this sphere of influence (according to the scale of the Figure) would be approximately 13 ft.

e. Earth–Venus–Mercury, 1972. The fifth Earth–Venus launch period occurs during the spring of 1972. The multiple planetary trajectories of this period will take a vehicle fairly close to the Venusian cloud layer. An extra-fine net was calculated so that the trajectories having maximum closest approach distances could be found. These trajectories, which are given in Table 9, also minimize the launch energy. This property, which appeared in the first three launch periods, was absent from the 1970 trajectories.

The Earth–Venus and Venus–Mercury transfers are Type II and Type I, respectively, and hence are very similar to those corresponding to the 1969 period. Both periods have continually decreasing launch energies with increasing launch date.

From Table 2 we observe that this is the first period in which Mercury approach energies are higher than

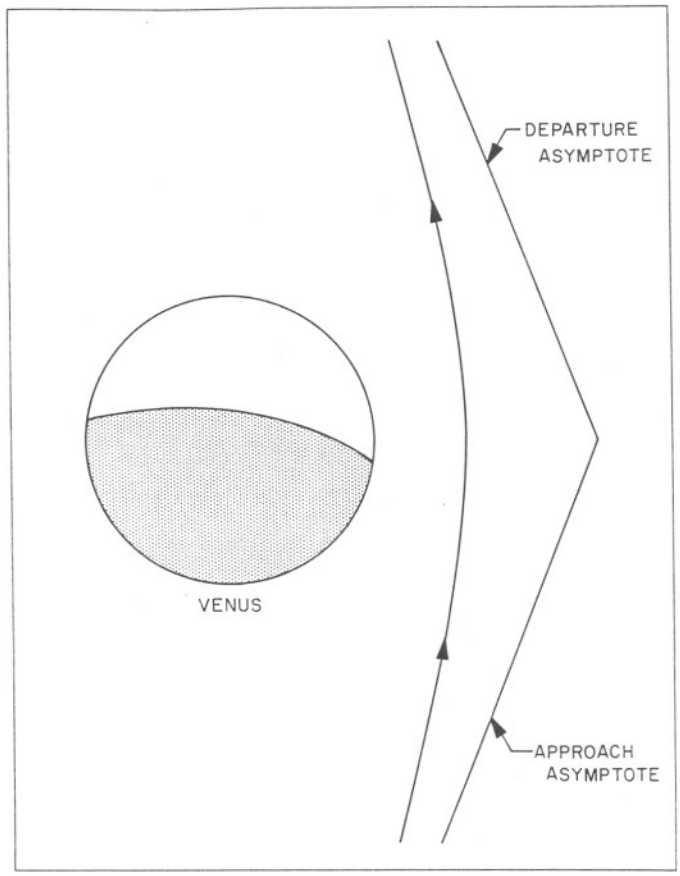

Fig. 19. August 18, 1970, Earth–Venus–Mercury trajectory at Venus intercept

those resulting from the optimum direct Earth–Mercury trajectories. This undesirable property cannot be removed by sacrificing a little launch energy because any change would require a closer distance of closest approach.

Figure 20 shows the planetary configuration for this launch period. The Venus and Mercury encounters occur approximately 1.2 and 1.4 au from the Earth, respectively.

The trajectory close to Venus having the April 1 launch date appears in Fig. 21.

f. Earth–Venus–Mercury, 1973. The last launch period for the decade occurs during the winter of 1973. The multiple planetary trajectories of this period do not require very close approaches, although the launch energies are found to be fairly high. Consequently, an extra-fine net was calculated; the resulting minimum launch energy trajectories appear in Table 10. The Earth–Venus and Venus–Mercury transfers for these trajectories are Type I, which yield very short total flight times. These trajectories, then, closely resemble those of the 1970 period.

Table 9. Some important properties of Earth–Venus–Mercury trajectories, 1972

Launch date	HEV_1 km/sec	T_{12} days	θ_{12} deg	$B \cdot \hat{T}$ km	$B \cdot \hat{R}$ km	HEV_2 km/sec	TISI days	DOCA km	VACA km/sec	DA deg	T_{23} days	θ_{23} deg	HEV_3 km/sec	TFT days
Mar. 18	4.62	206.70	272.60	−10,283.	−3,956.	7.61	1.81	654.	12.41	53.97	87.28	153.53	15.22	293.98
20	4.52	205.15	271.34	−10,685.	−2,830.	7.54	1.82	630.	12.38	54.66	85.51	149.16	15.86	290.66
22	4.43	203.72	270.27	−10,716.	−2,797.	7.49	1.83	610.	12.37	55.15	85.00	148.40	15.84	288.72
24	4.33	202.21	269.08	−10,717.	−3,105.	7.44	1.85	637.	12.32	55.50	85.00	148.97	15.56	287.21
26	4.25	200.80	268.06	−10,495.	−3,914.	7.40	1.85	643.	12.29	55.81	85.58	151.25	14.97	286.38
28	4.19	199.60	267.37	−10,142.	−4,506.	7.39	1.86	545.	12.34	56.36	85.76	152.66	14.55	285.36
30	4.10	198.00	266.05	−10,272.	−4,401.	7.33	1.87	563.	12.30	56.78	85.29	151.82	14.55	283.29
Apr. 1	4.03	196.58	265.01	−10,211.	−4,501.	7.30	1.88	521.	12.30	57.27	85.00	151.67	14.40	281.58
3	3.94	194.97	263.67	−10,789.	−2,648.	7.25	1.89	432.	12.33	58.18	82.00	143.85	15.78	276.97
5	3.86	193.32	262.27	−10,818.	−2,864.	7.20	1.90	458.	12.28	58.52	82.00	144.27	15.56	275.32
7	3.78	191.70	260.91	−10,827.	−3,082.	7.15	1.91	474.	12.25	58.87	81.99	144.67	15.34	273.69
9	3.71	190.05	259.51	−10,821.	−3,302.	7.11	1.92	483.	12.21	59.23	82.00	145.10	15.13	272.05
11	3.65	188.41	258.13	−10,794.	−3,521.	7.07	1.93	481.	12.19	59.61	82.00	145.52	14.93	270.41
13	3.59	186.77	256.77	−10,747.	−3,738.	7.03	1.94	470.	12.18	59.98	82.00	145.93	14.73	268.77
15	3.54	185.13	255.39	−10,681.	−3,950.	7.00	1.95	449.	12.17	60.39	82.00	146.34	14.54	267.13
17	3.50	183.50	254.02	−10,595.	−4,157.	6.97	1.96	417.	12.18	60.81	82.00	146.75	14.35	265.50
19	3.46	181.94	252.80	−10,447.	−4,384.	6.96	1.96	359.	12.21	61.26	82.00	147.24	14.12	263.94
21	3.44	180.34	251.49	−10,298.	−4,593.	6.94	1.97	296.	12.24	61.74	82.00	147.69	13.94	262.34

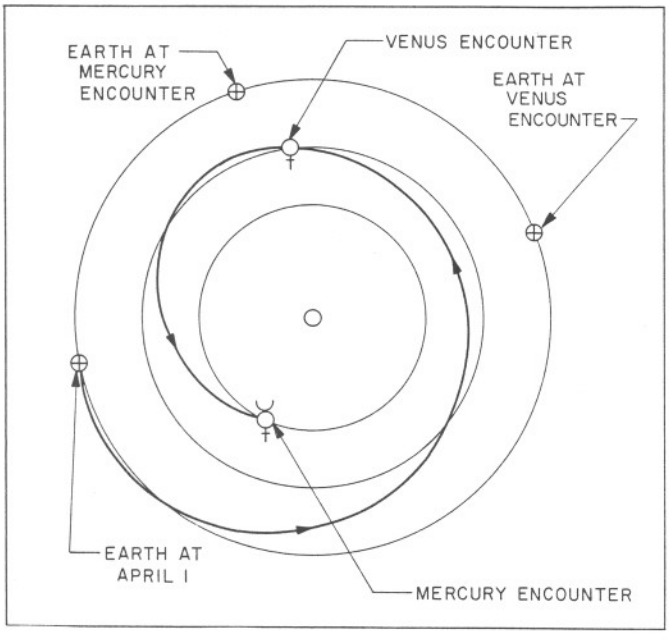

Fig. 20. Planetary configuration for Earth–Venus–Mercury, 1972 (April 1 trajectory)

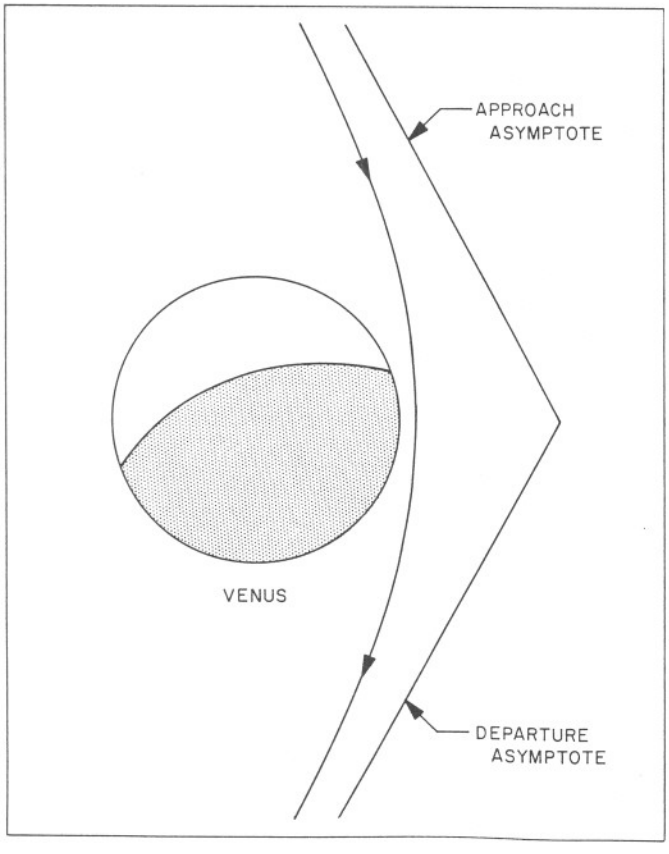

Fig. 21. April 1, 1972, Earth–Venus–Mercury trajectory at Venus intercept

It is interesting to note, however, that for the 1970 period we find low launch energies but high Mercury-approach energies, while for the 1973 trajectories these characteristics are reversed. The distances of closest approach are neither maximum nor minimum.

The planetary configuration for this launch period appears in Fig. 22. The Earth's distance from the Venus and Mercury encounters is approximately 0.32 and 1.2 au, respectively.

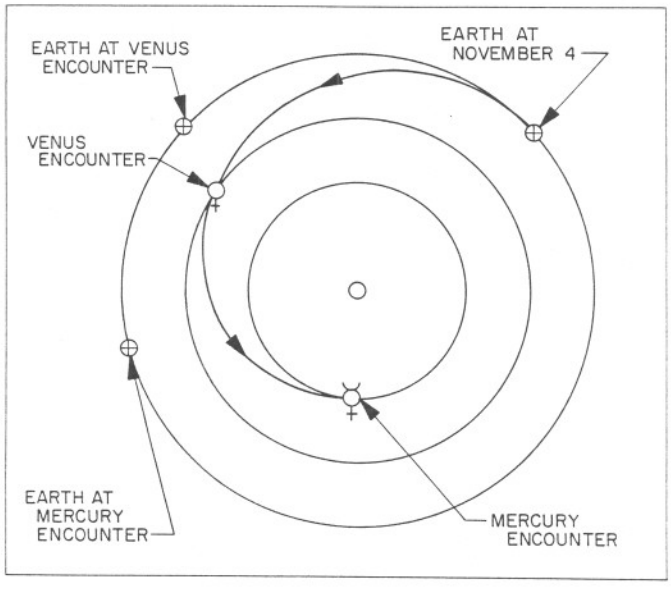

Fig. 22. Planetary configuration for Earth–Venus–Mercury, 1973 (November 4 trajectory)

The Venus intercept trajectory corresponding to the November 4 launch date appears in Fig. 23.

2. Earth–Venus–Mars Trajectories

The same method employed to calculate nets for the numerical analysis of the Earth–Venus–Mercury trajectories was used for all the multiple planetary trajectories considered in this Report. Thus, for the Earth–Venus–Mars trajectories that we now consider, six coarse nets with 6 × 6 day grids were calculated about the six Earth–Venus launch periods appearing in Table 1. Three of these periods, as shown by the preliminary calculations, require relatively long flight times and therefore have been discarded. The three remaining are the 1968–1969, the 1970, and the 1972 periods. Since the sophisticated vehicles required for multiple planetary trajectories will probably not be available before 1968, these three periods should be favorable for the most effective use of the space vehicles.

Table 10. Some important properties of Earth–Venus–Mercury trajectories, 1973

Launch date	HEV_1 km/sec	T_{12} days	θ_{12} deg	$B \cdot \hat{T}$ km	$B \cdot \hat{R}$ km	HEV_2 km/sec	TISI days	DOCA km	VACA km/sec	DA deg	T_{23} days	θ_{23} deg	HEV_3 km/sec	TFT days
Oct. 21	4.39	106.56	115.30	12,558.	−5,758.	7.86	1.75	3,423.	11.40	41.68	58.00	136.29	10.86	164.56
23	4.36	104.73	113.58	12,706.	−5,800.	7.89	1.75	3,596.	11.37	40.92	57.59	135.32	10.81	162.32
25	4.33	102.91	111.88	12,342.	−6,008.	7.93	1.74	3,400.	11.46	41.26	57.87	136.35	10.90	160.78
27	4.30	101.09	110.19	12,078.	−6,160.	7.96	1.73	3,271.	11.52	41.40	58.00	136.94	10.97	159.09
29	4.28	99.26	108.47	11,997.	−6,259.	8.00	1.72	3,275.	11.54	41.14	57.88	136.83	10.99	157.15
31	4.26	97.44	106.76	11,733.	−6,383.	8.03	1.72	3,139.	11.61	41.31	58.00	137.38	11.06	155.44
Nov. 2	4.25	95.61	105.04	11,610.	−6,474.	8.07	1.71	3,107.	11.65	41.17	57.93	137.39	11.08	153.54
4	4.25	93.79	103.34	11,370.	−6,567.	8.10	1.70	2,983.	11.71	41.31	58.00	137.83	11.14	151.79
6	4.25	91.97	101.61	11,228.	−6,643.	8.13	1.70	2,931.	11.75	41.23	57.94	137.88	11.17	149.91
8	4.25	90.14	99.89	10,992.	−6,712.	8.17	1.69	2,802.	11.82	41.40	58.00	138.27	11.23	148.14
10	4.27	88.31	98.16	10,933.	−6,770.	8.20	1.68	2,810.	11.84	41.13	57.82	137.98	11.23	146.14
12	4.29	86.49	96.45	10,601.	−6,814.	8.24	1.68	2,594.	11.94	41.59	58.00	138.72	11.33	144.49
14	4.33	84.66	94.71	10,450.	−6,852.	8.27	1.67	2,521.	11.99	41.59	57.94	138.76	11.36	142.60
16	4.37	82.83	92.98	10,365.	−6,887.	8.31	1.66	2,499.	12.02	41.42	57.78	138.52	11.36	140.61

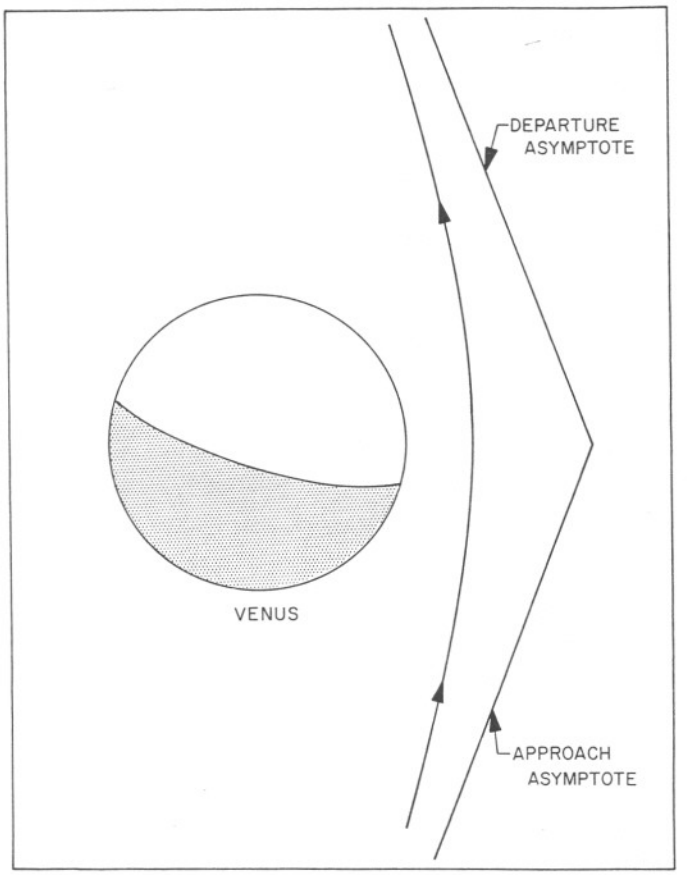

Fig. 23. November 4, 1973, Earth–Venus–Mercury trajectory at Venus intercept

a. Earth–Venus–Mars, 1968–1969. The multiple planetary Earth–Venus–Mars trajectories of this period require relatively close approaches to Venus. Thus, the calculations were aimed at determining the maximum distances of closest approach. It has been found that these trajectories can be determined reasonably well from the fine-net calculation. The results appear in Table 11. These maximum Venus passing-distance trajectories require approximately 6 to 12% greater launch energies than does the minimum, which occurs when the Venus closest approach distances are all zero. It is interesting to note that the distances of closest approach, together with the required launch energies, decrease monotonically as one proceeds through the launch period. We also notice that the Earth–Venus transfers are Type I, requiring only about 100 days, whereas the Venus–Mars transfers are Type II, requiring about 400 days. The resulting total mission flight times are approximately 500 days.

Let us now refer back to Table 3. We find that the launch dates for our multiple planetary trajectories occur approximately 2 mo before the launch dates for direct Earth–Mars 1969 Type I trajectories and occur about 2-1/2 mo before the Type II trajectories. The Mars intercept dates for the multiple planetary missions occur 8 to 9 mo after the Type I direct-flight intercept dates and about 3-1/4 to 5 mo after the Type II trajectories. We are forced to conclude that, if the primary objective is to reach Mars during the time interval under consideration, the direct-flight trajectories of 1969 should be employed. This is also evident from the fact that vehicles approaching Mars on these multiple planetary trajectories would have approximately nine times as much energy relative to Mars as the minimum approach energy of the direct-flight trajectories. However, we present these trajectories with the opinion that their use will probably be valuable for perfecting the extremely accurate planetary-approach guidance system necessary to perform these advanced missions.

The planetary configuration for this period appears in Fig. 24. The Earth's distance at the Venus and Mars encounters is approximately 0.34 au and 2.5 au, respectively.

Figure 25 describes the January 1 trajectory in the immediate vicinity of Venus.

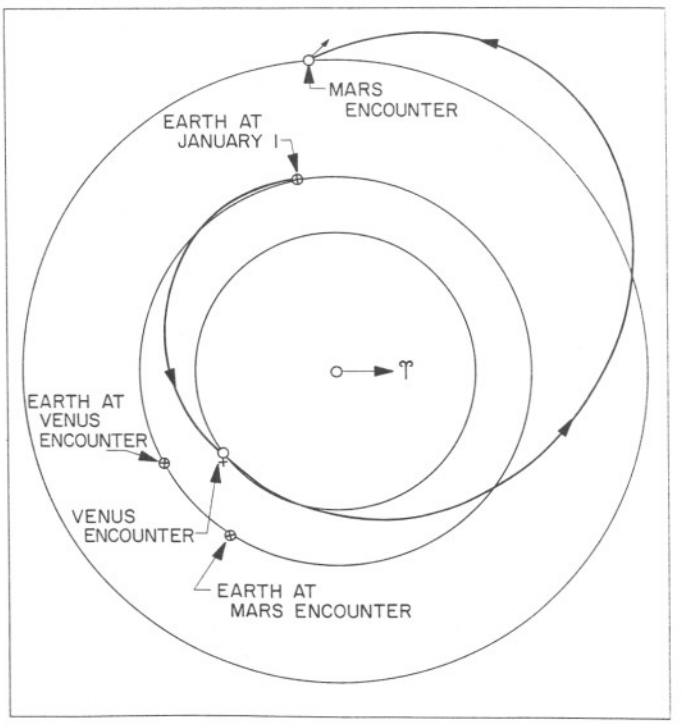

Fig. 24. Planetary configuration for Earth–Venus–Mars, 1968-9 (January 1 trajectory)

Table 11. Some important properties of Earth–Venus–Mars trajectories, 1968-9

Launch date	HEV_1 km/sec	T_{12} days	θ_{12} deg	$B \cdot \hat{T}$ km	$B \cdot \hat{R}$ km	HEV_2 km/sec	TISI days	DOCA km	VACA km/sec	DA deg	T_{23} days	θ_{23} deg	HEV_3 km/sec	TFT days
Dec. 22	5.00	114.35	119.46	−10,551.	−1,676.	8.49	1.64	989.	12.80	45.72	390.25	240.91	10.98	504.60
24	4.94	112.75	118.08	−10,435.	−1,707.	8.52	1.63	908.	12.86	45.86	391.52	241.08	10.99	504.28
26	4.86	111.35	117.01	−10,356.	−1,743.	8.50	1.63	830.	12.89	46.31	392.51	240.89	10.98	503.87
28	4.77	109.96	115.94	−10,280.	−1,775.	8.49	1.64	756.	12.91	46.75	393.48	240.69	10.98	503.43
30	4.71	108.36	114.55	−10,181.	−1,797.	8.51	1.63	685.	12.97	46.90	394.69	240.83	10.98	503.05
Jan. 1	4.63	106.96	113.48	−10,116.	−1,824.	8.49	1.64	617.	12.99	47.35	395.60	240.59	10.98	502.56
3	4.57	105.36	112.08	−10,028.	−1,841.	8.51	1.63	553.	13.04	47.50	396.77	240.70	10.98	502.13
5	4.52	103.77	110.69	−9,944.	−1,857.	8.53	1.63	492.	13.09	47.64	397.91	240.80	10.99	501.67
7	4.44	102.37	109.62	−9,896.	−1,878.	8.50	1.63	435.	13.10	48.11	398.73	240.51	10.98	501.09
9	4.41	100.57	107.91	−9,793.	−1,886.	8.56	1.62	381.	13.17	47.94	400.11	240.95	10.99	500.68
11	4.34	99.17	106.84	−9,757.	−1,904.	8.53	1.63	331.	13.18	48.40	400.86	240.63	10.98	500.03
13	4.30	97.57	105.45	−9,696.	−1,917.	8.54	1.63	285.	13.21	48.55	401.89	240.67	10.98	499.46
15	4.26	95.98	104.06	−9,640.	−1,929.	8.54	1.63	243.	13.24	48.69	402.88	240.69	10.98	498.85
17	4.21	94.58	102.98	−9,622.	−1,945.	8.50	1.63	205.	13.24	49.16	403.51	240.31	10.97	498.09
19	4.19	92.98	101.59	−9,579.	−1,958.	8.51	1.63	171.	13.27	49.30	404.44	240.30	10.97	492.42
21	4.18	91.38	100.20	−9,543.	−1,971.	8.51	1.63	141.	13.28	49.44	405.33	240.27	10.97	496.71

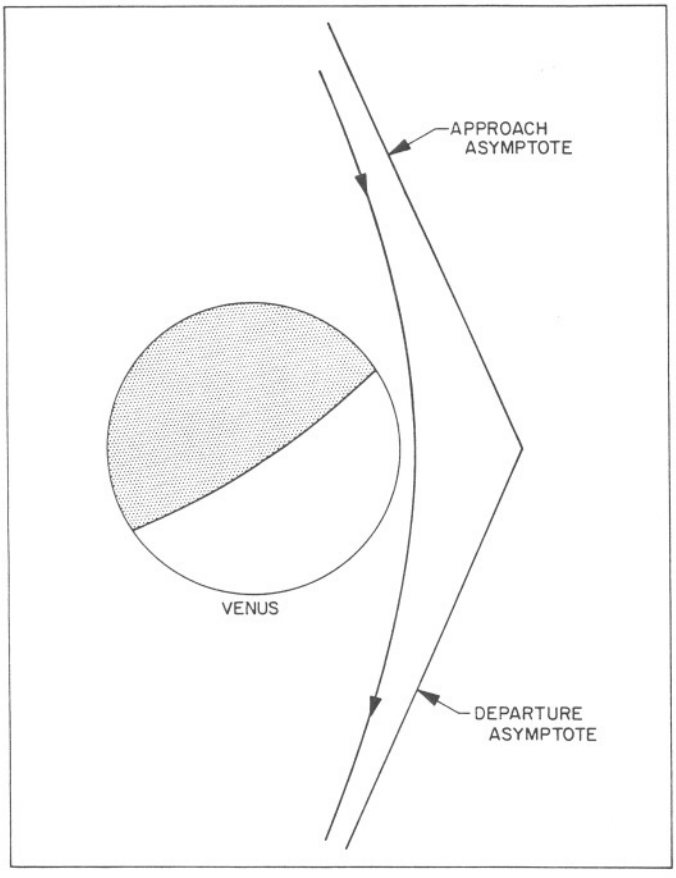

Fig. 25. January 1, 1969, Earth–Venus–Mars trajectory at Venus intercept

b. Earth–Venus–Mars, 1970. The 1970 Earth–Venus–Mars trajectories were found to be much more attractive than those of the previous period. An extra-fine net was calculated so that an accurate determination of the minimum launch energy trajectories could be made. These minimum energy trajectories are given in Table 12. One immediately finds that the Earth–Venus transfers are almost optimum trajectories, as described in Table 1. The distances of closest approach are well outside the Venusian atmosphere. From Table 3 we notice that these trajectories have flight times that are only about 20 to 40 days longer than those required for optimum Type II Earth–Mars trajectories in the 1971 launch period. We also notice that the launch and Mars intercept dates for these multiple planetary trajectories are almost halfway between those of the optimum Earth–Mars 1969 and 1971 trajectories.

The planetary configuration for this launch period appears in Fig. 26. The Earth is approximately 0.5 au distant at the Venus encounter and approximately 0.62 au distant during the Mars encounter.

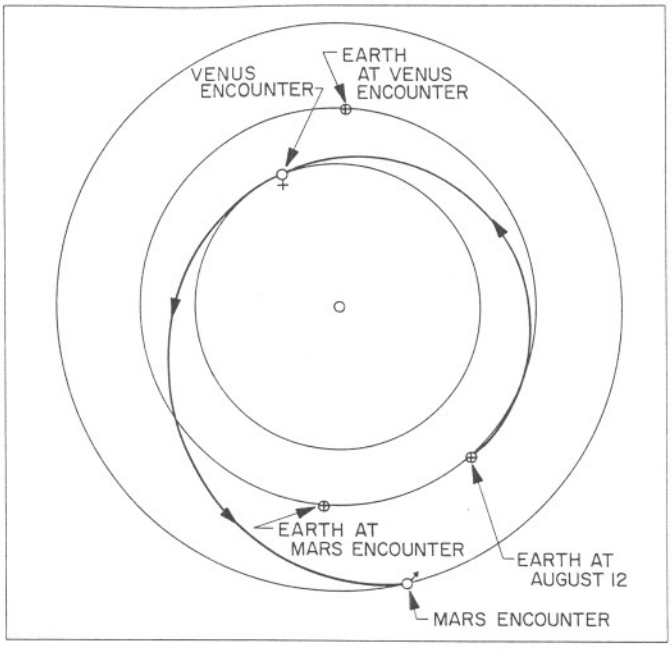

Fig. 26. Planetary configuration for Earth–Venus–Mars, 1970 (August 12 trajectory)

The near-Venus geometry for the August 12 trajectory is shown in Fig. 27.

c. Earth–Venus–Mars, 1972. The multiple planetary trajectories for this period are given in Table 13. It has been found that the May 11 to May 25 trajectories yield minimum launch energies when the Venus closest approaches are zero. Thus, the trajectories appearing in Table 13 were chosen on the basis of low launch energies together with safe distances of closest approach. The May 27 to June 6 trajectories were found to have minimum energies when the distances of closest approach are not zero. Thus, these trajectories are minimum launch energy trajectories. The trajectories appearing in Table 13 were found from a net with a 0.5 × 2 day grid.

Referring to Table 3, we find that this launch opportunity very conveniently falls right between the 1971 and 1973 Earth–Mars trajectories. Indeed, we notice that these trajectories are even better than the Type II trajectories for 1973. Figure 28 shows the over-all flight path of these trajectories while Fig. 29 describes the May 21 trajectory in the immediate vicinity of Venus.

The numerical results given in Tables 4 to 13 definitely indicate that space vehicles equipped with highly accurate planetary-approach guidance systems can play an important role in the unmanned exploration of Mercury, Venus, and Mars.

Table 12. Some important properties of Earth–Venus–Mars trajectories, 1970

Launch date	HEV_1 km/sec	T_{12} days	θ_{12} deg	$B \cdot \hat{T}$ km	$B \cdot \hat{R}$ km	HEV_2 km/sec	TISI days	DOCA km	VACA km/sec	DA deg	T_{23} days	θ_{23} deg	HEV_3 km/sec	TFT days
July 23	3.52	142.17	159.33	−12,927.	19,125.	5.91	2.30	9,490.	8.75	43.87	196.21	189.98	6.05	338.39
25	3.48	140.80	158.43	−14,121.	19,323.	5.87	2.31	10,191.	8.62	43.03	196.99	189.82	5.98	337.79
27	3.44	139.45	157.57	−15,407.	19,537.	5.82	2.33	10,986.	8.48	42.09	198.97	190.36	5.87	338.43
29	3.40	138.13	156.77	−16,592.	19,722.	5.78	2.34	11,733.	8.36	41.28	201.95	191.47	5.74	340.09
31	3.37	136.88	156.06	−17,556.	19,880.	5.75	2.36	12,355.	8.26	40.67	205.45	192.85	5.62	342.33
Aug. 2	3.35	135.69	155.45	−10,574.	15,577.	5.72	2.36	5,252.	9.48	55.64	180.00	176.71	6.94	315.69
4	3.32	134.34	154.57	−10,496.	15,240.	5.66	2.38	4,869.	9.55	57.36	180.00	176.05	6.91	314.32
6	3.29	133.00	153.75	−10,496.	14,956.	5.61	2.40	4,571.	9.61	58.86	180.00	175.36	6.87	313.00
8	3.28	131.71	152.98	−10,538.	14,705.	5.56	2.42	4,321.	9.66	60.22	180.00	174.63	6.84	311.71
10	3.27	130.47	152.29	−10,584.	14,455.	5.52	2.43	4,082.	9.71	61.55	180.00	173.85	6.79	310.47
12	3.26	129.28	151.68	−10,630.	14,206.	5.47	2.45	3,850.	9.76	62.87	180.00	173.01	6.75	309.28
14	3.28	128.15	151.18	−10,651.	13,939.	5.43	2.47	3,603.	9.82	64.21	180.00	172.11	6.70	308.15
16	3.30	127.11	150.80	−10,639.	13,650.	5.40	2.48	3,335.	9.90	65.61	180.00	171.13	6.65	307.11
18	3.34	126.14	150.56	−10,577.	13,328.	5.37	2.49	3,036.	9.99	67.06	180.00	170.07	6.59	306.14
20	3.39	125.29	150.48	−10,447.	12,963.	5.35	2.50	2,698.	10.12	68.59	180.00	168.89	6.53	305.29
22	3.47	124.55	150.61	−10,226.	12,540.	5.34	2.50	2,305.	10.29	70.20	180.00	167.59	6.46	304.55
24	3.57	123.95	150.94	−9,898.	12,059.	5.36	2.49	1,862.	10.50	71.85	180.00	166.16	6.39	303.95
26	3.70	123.50	151.51	−9,445.	11,518.	5.40	2.47	1,367.	10.78	73.50	180.00	164.58	6.32	303.50
28	3.86	123.18	152.29	−8,864.	10,931.	5.48	2.44	835.	11.12	75.06	180.00	162.86	6.24	303.18

Table 13. Some important properties of Earth–Venus–Mars trajectories, 1972

Launch date		HEV_1 km/sec	T_{12} days	θ_{12} deg	$B \cdot \hat{T}$ km	$B \cdot \hat{R}$ km	TISI days	DOCA km	VACA km/sec	DA deg	T_{23} days	θ_{23} deg	HEV_3 km/sec	TFT days
May	11	4.33	183.50	269.68	9,991.	−75.	1.59	490.	13.21	46.36	113.31	108.78	13.24	296.81
	13	4.22	181.00	266.94	10,176.	−150.	1.61	581.	13.07	46.86	114.45	109.94	13.09	295.45
	15	4.10	178.00	263.39	10,041.	−261.	1.64	354.	13.09	49.10	114.87	111.25	13.18	292.87
	17	4.04	175.50	260.65	10,076.	−340.	1.66	325.	13.05	49.96	155.50	112.13	13.14	291.00
	19	4.02	173.50	258.73	10,302.	−402.	1.67	507.	12.92	49.39	116.34	112.58	12.97	289.84
	21	4.03	172.00	257.62	10,794.	−454.	1.66	966.	12.67	47.26	117.70	112.77	12.61	289.70
	23	4.04	170.00	255.70	10,958.	−533.	1.67	1,103.	12.59	46.86	118.31	113.10	12.49	288.31
	25	4.07	168.00	253.78	11,069.	−621.	1.67	1,198.	12.53	46.58	118.71	113.32	12.41	286.71
	27	4.11	165.50	251.05	10,757.	−710.	1.68	887.	12.66	48.21	117.98	113.47	12.64	283.48
	29	4.16	165.50	252.38	12,590.	−817.	1.65	2,691.	11.98	40.52	123.47	114.29	11.29	288.97
	31	4.22	165.00	252.91	14,802.	−875.	1.64	4,869.	11.44	34.04	132.56	117.70	9.66	297.56
June	2	4.27	165.00	254.24	18,083.	−220.	1.61	8,123.	10.94	27.27	152.76	127.05	7.25	317.76
	4	4.32	165.00	255.57	19,229.	1,138.	1.59	9,383.	10.89	24.83	170.13	135.17	6.19	335.13
	6	4.37	165.00	256.91	19,022.	2,470.	1.56	9,413.	11.00	24.14	182.72	140.69	5.96	347.72

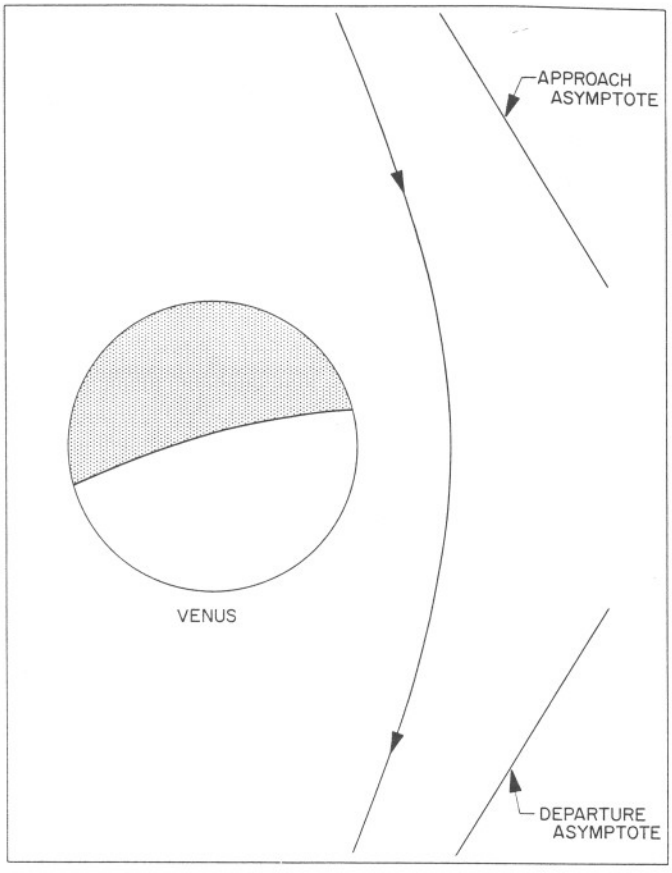

Fig. 27. August 12, 1970, Earth–Venus–Mars trajectory at Venus intercept

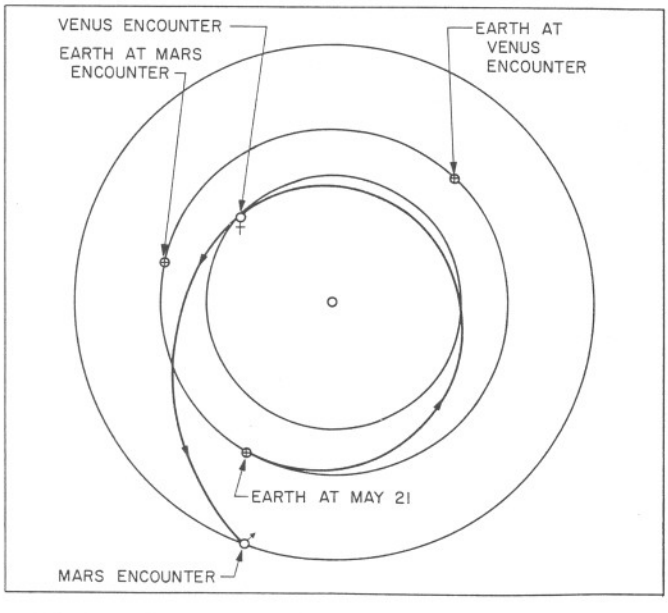

Fig. 28. Planetary configuration for Earth–Venus–Mars, 1972 (May 21 trajectory)

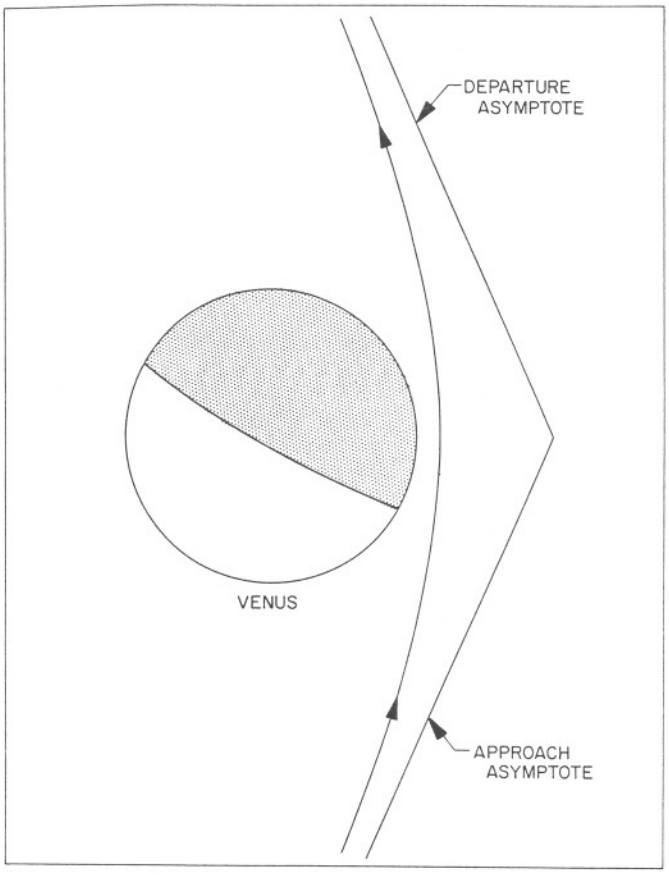

Fig. 29. May 21, 1972, Earth–Venus–Mars trajectory at Venus intercept

B. Initial Interplanetary Missions by Manned Vehicles

We now consider possible applications of multiple planetary trajectories to manned interplanetary space flights. Perhaps the first manned interplanetary voyages will be simple reconnaissance missions of Venus and Mars where the spacecraft will not actually land or go into orbit about these planets. Since our study is confined to the decade beginning in 1965, we shall confine ourselves to the period of 1970 to 1975. Let us now turn to the first of these two types of reconnaissance missions.

1. Earth–Venus–Earth (Reconnaissance), 1970–1974

The Earth–Venus–Earth missions were found to be much more feasible than the Earth–Mars–Earth missions. It has been found that the former missions have launch periods (for the favorable trajectories) that almost span the entire launch periods for the one-way Earth–Venus trajectories given in Table 1. Thus, relatively coarse nets have been found to be sufficient for obtaining a general idea of the characteristics of the most favorable trajec-

tories for each period. Table 14 is a selection of three trajectories from the three launch periods in 1970–1975. These trajectories were chosen on the basis of short flight times, low launch energies, and, of course, safe distances of closest approach. The first trajectory was obtained from a 2 × 2 day net, while the second and third came from 6 × 6 day nets.

The trajectories given in Table 14 show that it may be possible to carry out these manned Venus reconnaissance missions with non-nuclear launch vehicles. This possibility will be considered later.

We turn now to manned Earth–Mars–Earth reconnaissance missions.

2. Earth–Mars–Earth (Reconnaissance), 1970–1974

There are only two Earth–Mars launch periods in 1970–1974: the first in 1971 and the second in 1973 (see Table 3). Both were analyzed for possible Earth–Mars–Earth trajectories by calculating coarse nets with 4 × 4 and 6 × 6 day grids, respectively. The results indicated that a more detailed study was not necessary. All of the trajectories have been found to require high launch energies and to have flight times in excess of 1,000 days. The best trajectories found from each net appear in Table 15. The long flight times result from Type III Mars–Earth transfers. It is interesting to note that the 1973 trajectory permits the vehicle to remain under the influence of Mars for almost 5.5 days. This situation occurs since the vehicle's hyperbolic excess velocity as it approaches Mars is only 2.53 km/sec. The long flight times required for these trajectories make these missions unattractive. It is possible to obtain shorter flight time trajectories, but these require increases in launch energies of more than 200%.

Thus, with respect to the manned planetary reconnaissance missions, we find ourselves faced with another very difficult situation. A non-nuclear launch vehicle could probably be used for manned Venus reconnaissance missions but not for manned Mars reconnaissance missions during the time period 1970–1974.

During the early part of June 1962, while the author was checking some newly calculated multiple planetary trajectories of the form Earth–Venus–Mars–Earth, a very remarkable fact was discovered. It was already known at that time that the Earth–Mars–Earth trajectories had very long flight times. Thus, it was believed that the most favorable Earth–Venus–Mars–Earth trajectories would have flight times much longer than 1,000 days; however, this is not always true. It was discovered that in some cases this assumption was false by a very wide margin. These cases very conveniently turned out to be the 1970 and the 1972 Earth–Venus launch periods.

3. Earth–Venus–Mars–Earth (Reconnaissance), 1970

The manned Venus–Mars reconnaissance trajectories were studied very carefully. Three nets were calculated. The first net had a 3 × 3 day grid while the second and third were fine and extra-fine nets with 0.2 × 2 and 0.01 × 2 day grids, respectively. It has been found that the minimum launch energy trajectories have ideal distances of closest approach and almost minimum flight times. These trajectories are given in Table 16. Recalling the near-optimum Earth–Mars–Earth trajectories in Table 15, we notice the remarkable fact that these multiple encounter trajectories require only about one-half of the launch energies and flight times required by the best Earth–Mars–Earth reconnaissance trajectories of the 1971 and 1973 periods. It should be noted, however, that these trajectories will bring a space vehicle back to Earth with a great deal of energy. If this high return-energy problem can be solved without employing massive retro rockets, such missions can probably be accomplished with a non-nuclear *Saturn* 5-type launch vehicle. These Venus–Mars reconnaissance missions offer a very attractive first step in manned interplanetary space flights. They could be extremely useful in paving the way for actual manned landings on Venus and Mars.

The flight path for these manned reconnaissance missions appears in Fig. 30. We notice that the vehicle is never very far from the Earth throughout the entire flight. Thus, continuous radio communication should be quite feasible. It is also important to notice that the entire trajectory is confined to the region between the orbits of Venus and Mars. The Venus and Mars encounters take place when the vehicle is approximately 0.35 and 0.6 au from the Earth. Figures 31 and 32 show the August 12 trajectory in the vicinity of Venus and Mars, respectively. These Figures are drawn to the same scale. According to this scale, the radius of the gravitational sphere of influence of Venus is 12.8 ft, while the radius of the Martian sphere of influence is 11.2 ft.

4. Earth–Venus–Mars–Earth (Reconnaissance), 1972

The multiple planetary Venus–Mars reconnaissance trajectories for this period are even more surprising than those of the previous period. It is observed that trajectories exist that have much shorter flight times than those of the 1970 period. These short flight time trajectories

Table 14. Some important properties of Earth–Venus–Earth trajectories

Launch date	HEV_1 km/sec	T_{12} days	θ_{12} deg	$B \cdot \hat{T}$ km	$B \cdot \hat{R}$ km	TISI days	DOCA km	VACA km/sec	DA deg	T_{23} days	θ_{23} deg	HEV_3 km/sec	TFT days
8/20/70	2.92	114.00	132.23	−13,653.	−3,187.	2.46	725.5	11.39	76.16	250.96	227.48	7.13	364.96
4/3/72	3.69	114.00	134.07	−18,362.	4,964.	2.69	3,983.	9.47	68.29	260.95	235.43	8.18	374.95
11/4/73	3.76	110.00	139.29	−22,410.	219.	2.94	5,343.5	8.76	71.80	269.46	241.00	7.90	385.46

Table 15. Some important properties of Earth–Mars–Earth trajectories

Launch date	HEV_1 km/sec	T_{12} days	θ_{12} deg	$B \cdot \hat{T}$ km	$B \cdot \hat{R}$ km	TISI days	DOCA km	VACA km/sec	DA deg	T_{23} days	θ_{23} deg	HEV_3 km/sec	TFT days
6/8/71	3.97	316.00	204.84	1,017.	7,652.	3.23	2,251.1	5.74	34.88	795.83	530.43	5.85	1,111.83
8/20/73	4.60	236.00	151.68	2,222.	15,623.	5.46	7,024.	3.83	46.06	790.72	502.25	6.56	1,027.7

Table 16. Some important properties of Earth–Venus–Mars–Earth trajectories, 1970

Launch date		HEV_1 km/sec	T_{12} days	θ_{12} deg	$(B \cdot \hat{T})_2$ km	$(B \cdot \hat{R})_2$ km	HEV_2 km/sec	TISI days	$DOCA_2$ km	$VACA_2$ km/sec	DA_2 deg	T_{23} days	θ_{23} deg
July	15	3.74	147.86	163.23	−9,238.	18,335.	6.11	2.23	7,495.	9.22	45.95	196.99	192.81
	17	3.68	146.42	162.22	−10,626.	19,898.	6.06	2.25	9,278.	8.88	42.87	210.00	200.13
	19	3.63	144.99	161.24	−11,499.	20,089.	6.01	2.26	9,732.	8.78	42.52	210.00	199.55
	21	3.57	143.58	160.28	−11,806.	18,872.	5.96	2.28	8,819.	8.89	44.68	195.56	190.20
	23	3.52	142.18	159.34	−12,883.	19,081.	5.91	2.30	9,435.	8.76	43.96	195.81	189.74
	25	3.48	140.80	158.44	−14,114.	19,312.	5.87	2.31	10,179.	8.62	43.05	196.88	189.75
	27	3.44	139.45	157.57	−15,406.	19,531.	5.82	2.33	10,981.	8.48	42.10	198.92	190.32
	29	3.40	138.14	156.77	−16,592.	19,718.	5.78	2.34	11,731.	8.36	41.28	210.85	191.40
	31	3.37	136.88	156.06	−17,570.	19,867.	5.75	2.36	12,335.	8.26	40.67	205.30	192.75
Aug.	2	3.35	135.69	155.46	−10,571.	15,575.	5.72	2.26	5,250.	9.48	55.65	180.00	176.71
	4	3.32	134.33	154.58	−10,493.	15,237.	5.66	2.38	4,867.	9.56	57.37	180.00	176.05
	6	3.29	133.00	153.75	−10,494.	14,955.	5.61	2.40	4,569.	9.61	58.86	180.00	175.36
	8	3.28	131.71	152.98	−10,536.	14,703.	5.56	2.42	4,320.	9.66	60.22	180.00	174.63
	10	3.27	130.47	152.29	−10,583.	14,453.	5.52	2.43	4,080.	9.71	61.56	180.00	173.84
	12	3.26	129.28	151.68	−10,628.	14,205.	5.47	2.45	3,848.	9.76	62.87	180.00	173.01
	14	3.28	128.16	151.18	−10,649.	13,937.	5.43	2.47	3,601.	9.82	64.22	180.00	172.11
	16	3.30	127.11	150.80	−10,637.	13,649.	5.40	2.48	3,334.	9.90	65.61	180.00	171.13
	18	3.34	126.15	150.56	−10,575.	13,327.	5.37	2.49	3,035.	10.00	67.07	180.00	170.06
	20	3.39	125.29	150.48	−10,446.	12,962.	5.35	2.50	2,696	10.12	68.59	180.00	168.89
	22	3.47	124.56	150.61	−10,224.	12,539.	5.34	2.50	2,304.	10.29	70.20	180.00	167.59
	24	3.57	123.96	150.95	−9,897.	12,057.	5.36	2.49	1,861.	10.50	71.85	180.00	166.16
	26	3.70	123.50	151.51	−9,446.	11,518.	5.40	2.47	1,368.	10.78	73.50	180.00	164.58
	28	3.86	123.18	152.29	−8,865.	10,932.	5.48	2.44	836.	11.12	75.06	180.00	162.86

Launch date		$(B \cdot \hat{T})_3$ km	$(B \cdot \hat{R})_3$ km	HEV_3 km/sec	$TISI_3$ days	$DOCA_3$ km	$VACA_3$ km/sec	DA_3 deg	T_{34} days	θ_{34} deg	HEV_4 km/sec	TFT days
July	15	11,551.	5,981.	6.11	2.02	8,494.	6.68	10.10	303.50	285.09	8.77	648.35
	17	9,407.	1,642.	5.63	2.18	4,873.	6.48	16.18	294.24	281.05	8.42	650.65
	19	9,474.	1,468.	5.61	2.18	4,904.	6.47	16.20	293.91	280.93	8.41	648.90
	21	13,120.	5,747.	6.11	2.03	9,802.	6.62	9.20	303.35	285.05	8.77	642.50
	23	13,724.	5,037.	6.07	2.04	10,083.	6.57	9.13	302.67	284.71	8.73	640.67
	25	14,027.	3,777.	5.99	2.06	9,962.	6.50	9.43	301.33	287.02	8.67	639.01
	27	13,659.	2,225.	5.87	2.10	9,235.	6.43	10.29	299.28	283.02	8.58	637.65
	29	12,609.	880.	5.74	2.14	7,988.	6.37	11.77	296.76	281.89	8.49	636.75
	31	11,214.	−23.	5.62	2.18	6,521.	6.35	13.82	294.21	280.93	8.42	636.38
Aug.	2	5,574.	12,065.	6.94	1.80	9,012.	7.42	7.68	312.08	292.15	9.51	630.77
	4	5,103.	11,317.	6.91	1.81	8,132.	7.43	8.30	314.63	291.95	9.48	628.96
	6	4,844.	10,806.	6.87	1.82	7,552.	7.42	8.79	314.13	291.72	9.45	627.13
	8	4,704.	10,430.	6.84	1.82	7,143.	7.41	9.19	313.58	291.46	9.42	625.29
	10	4,649.	10,121.	6.79	1.83	6,830.	7.39	9.56	313.00	291.18	9.38	623.47
	12	4,644.	9,870.	6.75	1.85	6,590.	7.36	9.89	312.36	290.86	9.34	621.63
	14	4,684.	9,646.	6.70	1.86	6,393.	7.32	10.20	311.66	290.51	9.30	619.81
	16	4,762.	9,437.	6.65	1.87	6,227.	7.29	10.52	310.89	290.13	9.26	618.00
	18	4,877.	9,227.	6.59	1.89	6,079.	7.24	10.83	310.06	289.71	9.21	616.21
	20	5,026.	9,006.	6.53	1.90	5,939.	7.20	11.17	309.15	289.25	9.16	614.44
	22	5,211.	8,756.	6.46	1.92	5,797.	7.15	11.53	308.15	288.75	9.10	612.70
	24	5,427.	8,465.	6.39	1.94	5,643.	7.09	11.95	307.05	288.21	9.04	611.01
	26	5,670.	8,115.	6.32	1.96	5,466.	7.04	12.42	305.87	287.63	8.98	609.37
	28	5,926.	7,682.	6.24	1.98	5,246.	6.99	12.98	304.65	287.06	8.92	607.82

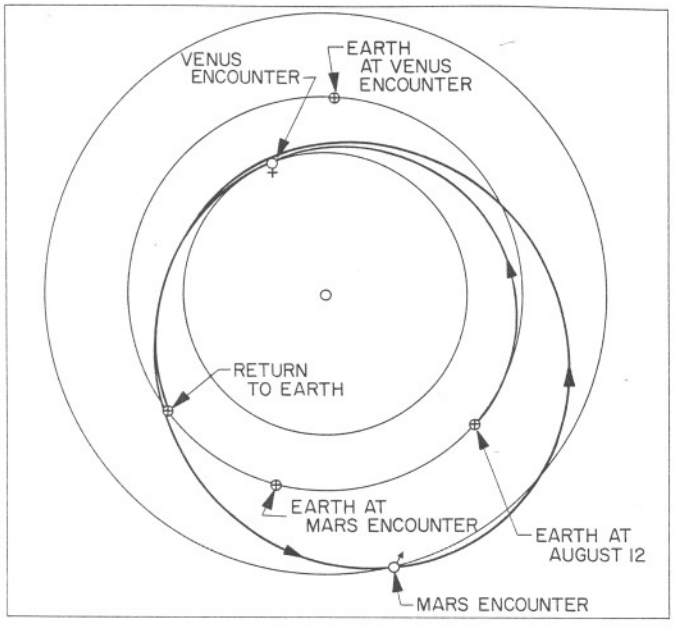

Fig. 30. Planetary configuration for Earth–Venus–Mars–Earth, 1970 (August 12 trajectory)

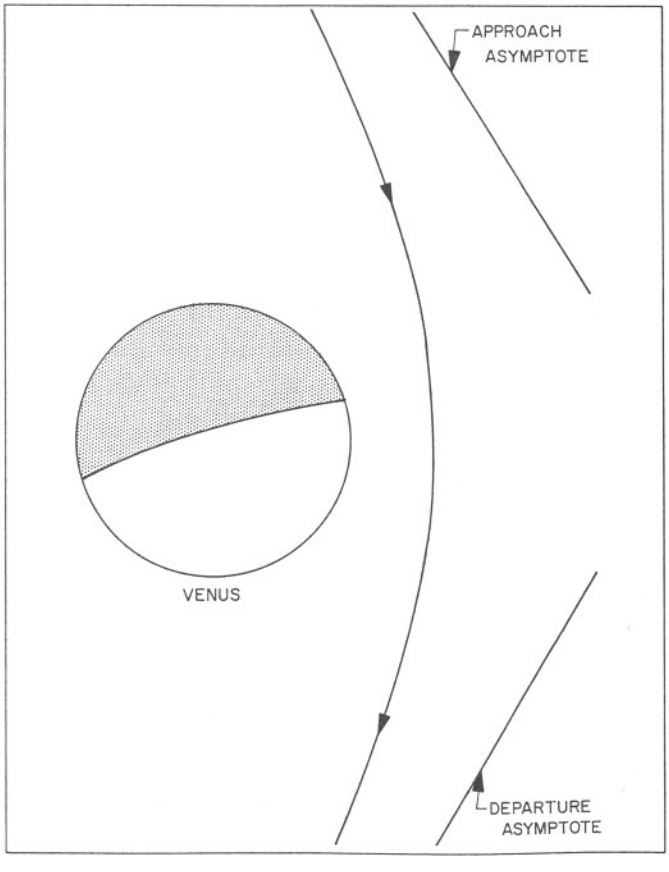

Fig. 31. August 12, 1970, Earth–Venus–Mars–Earth trajectory at Venus intercept

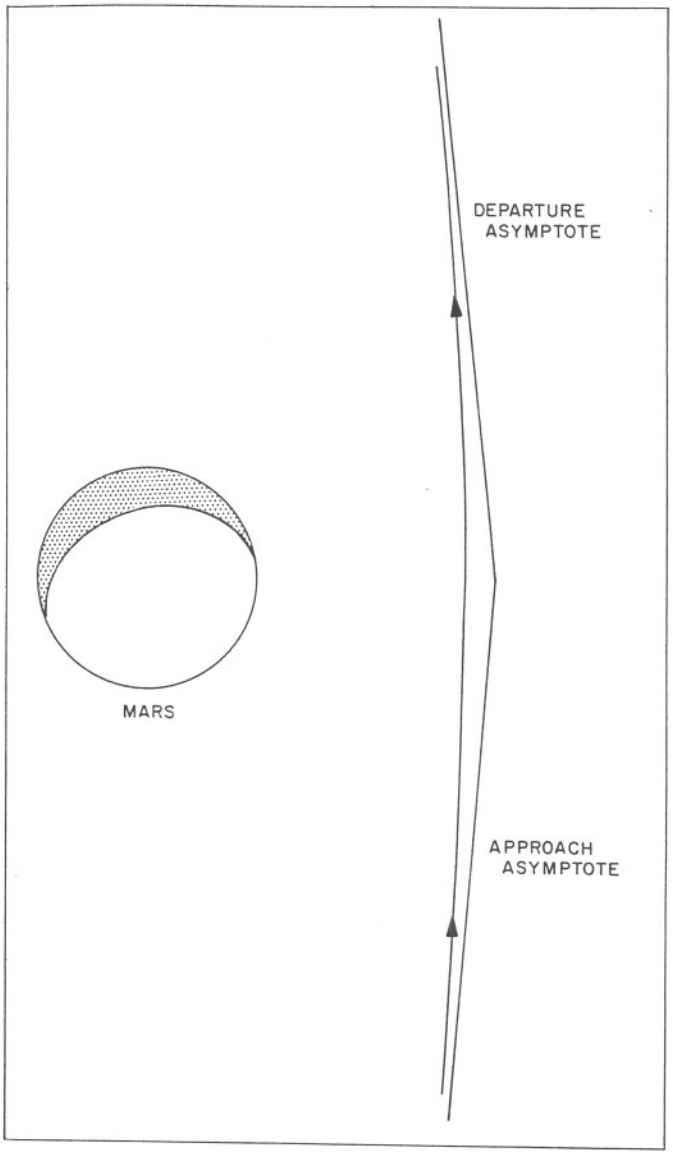

Fig. 32. August 12, 1970, Earth–Venus–Mars–Earth trajectory at Mars intercept

also occur when the launch energies are nearly minimum. It has been found that the flight times are minimum when the Mars distances of closest approach are zero. Thus our search has been directed toward finding trajectories that have near-minimum flight times but do not pass too close to the surface of Mars. The fine-net calculation has proved to be sufficient for this purpose. The trajectories of this net that were selected are given in Table 17. Comparing these trajectories with those of the 1970 period, we find that the flight times are about 150 days shorter, the launch energies are about 60% greater, and the return energies are about 200% greater. By increasing the launch energies and flight times by small

Table 17. Some important properties of Earth–Venus–Mars–Earth trajectories, 1972

Launch date		HEV_1 km/sec	T_{12} days	θ_{12} deg	$(B \cdot \hat{T})_2$ km	$(B \cdot \hat{R})_2$ km	HEV_2 km/sec	$TISI_2$ days	$DOCA_2$ km	$VACA_2$ km/sec	DA_2 deg	T_{23} days	θ_{23} deg
May	13	4.73	186.93	276.57	15,319.	1,435.	9.31	1.49	5,988.	11.85	27.38	137.98	116.57
	15	4.56	184.34	273.67	15,674.	1,278.	9.13	1.52	6,207.	11.67	27.82	139.62	118.12
	17	4.42	181.74	270.78	15,876.	1,046.	8.97	1.55	6,282.	11.53	28.44	140.22	119.09
	19	4.32	179.35	268.22	16,156.	876.	8.86	1.57	6,462.	11.41	28.70	141.50	120.24
	21	4.24	176.95	265.65	16,303.	646.	8.76	1.58	6,521.	11.32	29.10	141.91	120.89
	23	4.19	174.55	263.09	16,308.	364.	8.67	1.60	6,455.	11.27	29.67	141.45	121.05
	25	4.17	172.35	260.85	16,457.	156.	8.62	1.61	6,553.	11.21	29.78	142.04	121.59
	27	4.16	170.16	258.61	16,491.	−93.	8.57	1.62	6,552.	11.17	30.01	141.94	121.74
	29	4.18	168.16	256.70	16,732.	−272.	8.55	1.62	6,766.	11.12	29.73	143.16	122.43
	31	4.22	165.96	254.47	16,523.	−588.	8.53	1.62	6,561.	11.14	30.22	141.68	121.80
June	2	4.27	163.97	252.56	16,543.	−834.	8.53	1.62	6,592.	11.13	30.15	141.65	121.78
	4	4.34	161.97	250.65	16,457.	−1,103.	8.54	1.62	6,532.	11.15	30.21	141.04	121.43
	6	4.42	160.17	249.07	16,648.	−1,327.	8.57	1.62	6,756.	11.14	29.65	142.10	121.82
	8	4.51	158.37	247.49	16,753.	−1,578.	8.61	1.61	6,907.	11.14	29.19	142.70	121.95

Launch date		$(B \cdot \hat{T})_3$ km	$(B \cdot \hat{R})_3$ km	HEV_3 km/sec	$TISI_3$ km/sec	$DOCA_3$ km	$VACA_3$ km/sec	DA_3 deg	T_{34} days	θ_{34} deg	HEV_4 km/sec	TFT days
May	13	−4,092.	2,841.	8.53	1.50	1,011.	9.60	13.52	156.56	78.25	13.36	481.47
	15	−4,283.	3,188.	8.40	1.52	1,350.	9.42	13.01	157.15	79.24	13.13	481.11
	17	−4,275.	3,124.	8.39	1.52	1,305.	9.42	13.14	157.26	79.35	13.12	479.21
	19	−4,437.	3,459.	8.29	1.54	1,620.	9.26	12.69	157.73	80.16	12.93	478.57
	21	−4,437.	3,422.	8.28	1.54	1,596.	9.26	12.76	157.80	80.24	12.91	476.66
	23	−4,270.	3,028.	8.37	1.53	1,242.	9.41	13.37	157.48	79.58	13.07	473.49
	25	−4,344.	3,163.	8.32	1.53	1,374.	9.34	13.17	157.69	79.95	12.99	472.09
	27	−4,283.	3,026.	8.35	1.53	1,249.	9.39	13.40	157.59	79.72	13.04	469.68
	29	−4,516.	3,540.	8.22	1.55	1,722.	9.18	12.65	158.14	80.75	12.80	469.45
	31	−4,191.	2,841.	8.40	1.52	1,075.	9.47	13.72	157.41	79.37	13.12	465.06
June	2	−4,185.	2,831.	8.40	1.52	1,066.	9.48	13.74	157.40	79.35	13.13	463.02
	4	−4,059.	2,618.	8.47	1.51	854.	9.59	14.13	157.10	78.81	13.25	460.11
	6	−4,317.	3,095.	8.33	1.53	1,314.	9.36	13.29	157.67	79.87	13.01	459.93
	8	−4,473.	3,455.	8.25	1.55	1,640.	9.22	12.76	157.99	80.51	12.86	459.07

amounts, it is possible to reduce these high return energies. The flight times are short because the Venus–Mars and Mars–Earth transfers are both Type I, while the Earth–Venus transfers are Type II. For the 1970 trajectories this situation is reversed.

Although the energy requirements for these trajectories are somewhat higher than those of the previous period, these missions would be ideally suited for manned vehicles. The planetary configuration for these manned reconnaissance missions appears in Fig. 33. Figures 34 and 35 describe the May 27 trajectory as it passes Venus and Mars.

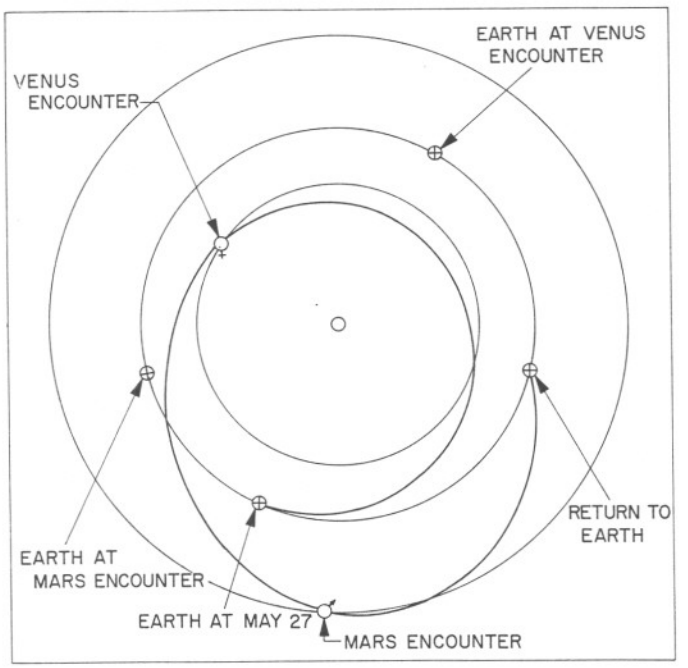

Fig. 33. Planetary configuration for Earth–Venus–Mars–Earth, 1972 (May 27 trajectory)

When more attention is directed toward manned interplanetary flights of the near future, the above reconnaissance trajectories of the 1970 and 1972 launch periods should warrant serious consideration.

5. Manned Landings on Venus and Mars Utilizing Multiple Planetary Trajectories (The *Saturn 5* Possibility)

We shall now give another example of how multiple planetary trajectories can be applied to early manned interplanetary missions. In particular, let us consider the trajectories for manned landings on Venus and Mars. Tables 18 and 19 describe the optimum Venus–Earth and Mars–Earth transfer trajectories, respectively. If we compare these Tables with Tables 1 and 3, we find that the

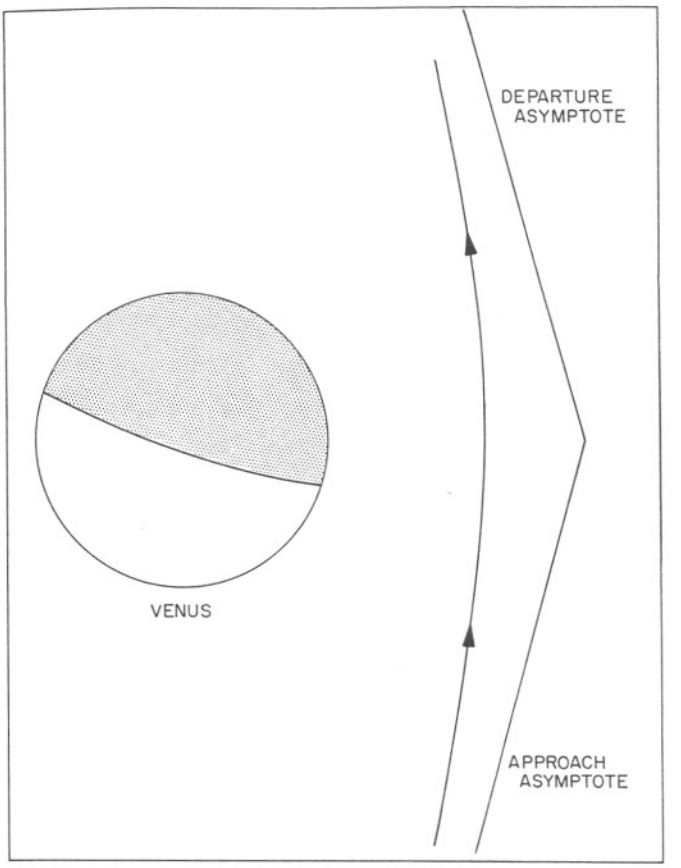

Fig. 34. May 27, 1972, Earth–Venus–Mars–Earth trajectory at Venus intercept

optimum Venus–Earth return trajectories occur 20 to 40 days after the optimum Earth–Venus departure trajectories. The optimum Mars–Earth return trajectories occur 40 to 60 days *before* the optimum Earth–Mars departure trajectories!

A brief study of manned missions to Venus and Mars during 1970–1975 was carried out to obtain some characteristic properties of the most favorable trajectory profiles. The results appear in Tables 20 and 21. The symbol ΔT represents the number of days spent on Venus or Mars. One immediately notices the unusually high hyperbolic excess velocities associated with the return Mars missions. This is a characteristic property of all missions to Mars of this type where only one vehicle is involved. These high velocities occur because the Mars launch date will always fall much later than the optimum launch dates for the Mars–Earth transfers. Thus, in general, only a relatively small amount of time can be devoted to the exploration of Mars. These properties are also generally true for the mission to Venus. It is important to note, however, that it is not always advantageous, from an

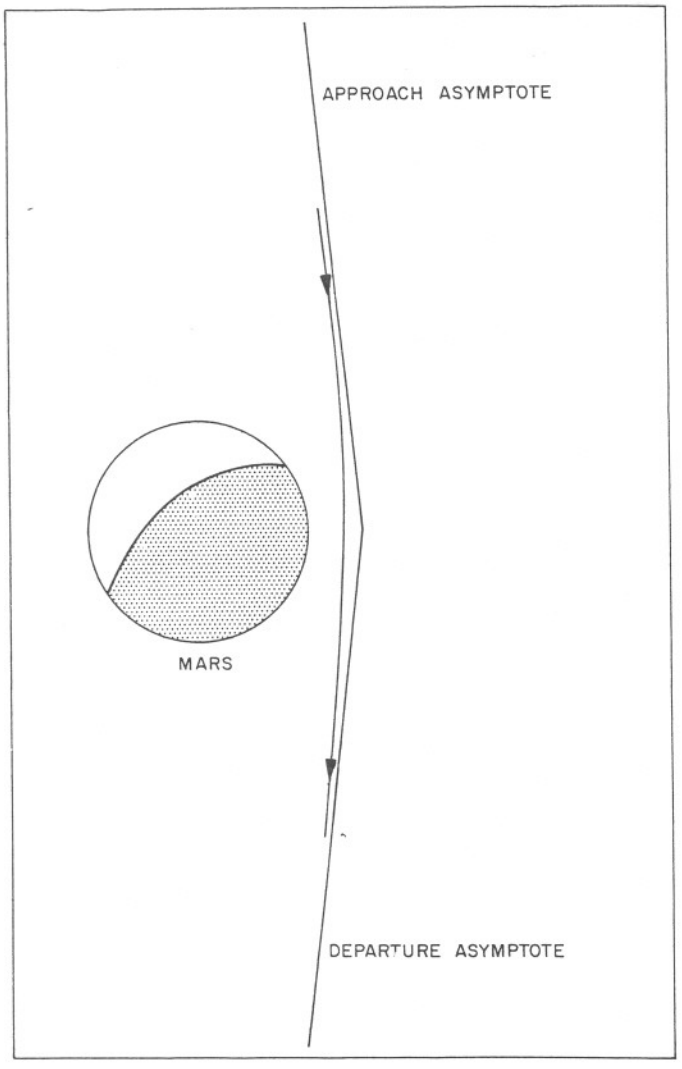

Fig. 35. May 27, 1972, Earth–Venus–Mars–Earth trajectory at Mars intercept

energy point of view, to start the return trip as soon as possible. For example, the Venus launch energies for Type II Venus–Earth trajectories actually decrease from December 22, 1970, to January 15, 1971, although the optimum launch date is October 21, 1970. This situation does not appear in the Mars missions. Type I Venus–Earth and Mars–Earth transfers require much higher launch energies than the Type II return trajectories and hence are of little interest.

Now it may appear that the manned exploration of Mars will require more powerful launch vehicles than those required for the Venus missions; however, since the escape velocities of Venus and Mars are 10.40 and 5.03 km/sec, respectively, the missions to Venus will actually require the more powerful rockets. In view of the low Mars escape velocity, it appears that, if we can find low Earth launch-energy trajectories that will take a vehicle to Mars such that the Mars arrival date is sufficiently close to the favorable Mars–Earth launch dates, it may be possible to conduct manned missions to Mars before nuclear rockets become available. *Such trajectories do indeed exist.* As a matter of fact, we have already calculated some – the Earth–Venus–Mars trajectories. By utilizing these trajectories as our Earth-to-Mars transfer trajectories, it may be possible to save a great deal of energy. Table 22 contains trajectory profiles of the 1971 and 1973 manned missions to Mars using Earth–Venus–Mars trajectories as the Earth-to-Mars transfers. These trajectories clearly require far less weight-lifting capability of the primary Earth launch vehicle. Unfortunately, the Earth–Venus–Mars trajectories of 1973 and of 1975 require much longer flight times and, hence, are unattractive Earth-to-Mars transfer trajectories.

Although the alternative trajectory profiles given in Table 22 represent a considerable improvement over the conventional trajectory profiles given in Table 21, large *Nova*-type launch vehicles, along with advanced nuclear propulsion systems, will still be necessary. These large launch vehicles will probably not be available before 1973. *There is, however, a way that would permit a manned exploration of Mars using a conventional non-nuclear Saturn 5 launch vehicle.*

Recent studies regarding manned interplanetary missions to Mars show that a Mars landing can be carried out with almost total atmospheric braking (see Ref. 6 and 7). These studies show that the dry weight of the smallest possible vehicle of this type (including the heat shield) would be approximately 13,000 lb. This vehicle, called a Mars Excursion Module, could accommodate a crew of four men. It has also been calculated that the weight of an interplanetary mission module carrying all the life-support equipment and related supplies to last a crew of five for a 1-yr period would be in the neighborhood of 40,000 lb. It was also determined that an *Apollo*-type (six-man) Earth re-entry vehicle re-entering at 13.3 km/sec and employing total atmospheric braking would weigh approximately 13,180 lb.

Before attempting an actual manned landing mission, it would probably be desirable first to carry out a manned Mars fly-by mission. This mission could provide an ideal means of testing man's endurance under prolonged interplanetary space flights. For this reason, the August 12, 1970 Earth–Venus–Mars–Earth trajectory appearing in Table 16 may be highly suited for this purpose. Let us

Table 18. Some important properties of optimum Venus–Earth transfer trajectories

Launch period	Min. HEV_1 km/sec	Max. HEV_1 km/sec	Min. T_{12} days	Max. T_{12} days	Min. HEV_2 km/sec	Max. HEV_2 km/sec
	Type I					
8/6/70 –10/17/70	3.21	6.15	94	122	3.65	5.87
3/24/72– 5/21/72	4.04	6.32	92	128	3.27	7.91
11/6/73 – 1/15/74	4.12	6.38	96	162	2.71	7.60
	Type II					
7/15/70– 3/22/71	3.47	5.93	152	348	2.85	10.48
3/8/72 –10/20/72	3.13	5.78	174	348	3.04	9.77
10/17/73– 5/9/74	2.96	5.58	166	330	3.59	10.04

Table 19. Some important properties of optimum Mars–Earth transfer trajectories

Launch period	Min. HEV_1 km/sec	Max. HEV_1 km/sec	Min. T_{12} days	Max. T_{12} days	Min. HEV_2 km/sec	Max. HEV_2 km/sec
	Type I					
7/7/70 – 7/8/71	2.55	5.57	172	360	3.05	9.02
12/21/72– 8/14/73	3.53	5.55	168	296	2.93	4.93
	Type II					
3/3/70 – 9/22/71	2.75	5.48	242	508	3.45	9.00
3/22/72–11/20/73	3.71	5.61	260	516	3.00	11.56

now perform for this trajectory some rough calculations based on the before-mentioned vehicle design parameters.

We recall the well-known formula

$$\frac{M_1}{M_2} = \exp\left(\frac{\Delta V}{c}\right)$$

where M_1 and M_2 are the masses of the vehicle before and after obtaining a velocity change of ΔV km/sec, using a rocket engine with an exhaust velocity of c km/sec. In carrying out our calculations we shall assume simple single-stage burning with an exhaust velocity of 3.6 km/sec (i.e., I_{sp} = 367 sec). Now, assuming a crew of three or four, the weight of the primary interplanetary mission module could be taken to be 43,000 lb. Since our trajectory's Earth approach hyperbolic excess velocity is 9.34 km/sec and since the Earth's escape velocity is about 11.0 km/sec, the re-entry module would re-enter the Earth's atmosphere at about

$$\left(9.34^2 + 11.00^2\right)^{1/2} \text{ km/sec} = 14.43 \text{ km/sec}$$

Thus, we shall employ partial rocket braking to permit our 13,000-lb module to re-enter the Earth's atmosphere at 13.3 km/sec. Consequently, the mass of the module before retro will be

$$13{,}500 \exp\,(1.13/3.6)\text{ lb} = 18{,}400 \text{ lb}$$

where we assume the weight of the retro engine is 500 lb. Hence the total weight at the beginning of the fly-by mission will be about 62,000 lb. The *Saturn* 5 launch vehicle will have the capacity of sending 90,000 lb on an

Table 20. Some important properties of near-optimum trajectory profiles for manned exploration of Venus

Launch date	HEV_1 km/sec	T_{12} days	HEV_2 km/sec	ΔT days	Venus launch date	HEV_2 km/sec	T_{23} days	HEV_3 km/sec	Arrival date	Total time
Aug. 18, 1970	2.91	116	5.43	32	Jan. 13, 1971	4.81	302	8.65	Nov. 11, 1971	450
Mar. 26, 1972	3.50	112	6.16	20	Aug. 5, 1972	4.59	284	8.51	May 16, 1973	416
Nov. 10, 1973	3.66	106	4.89	14	Mar. 10, 1974	4.49	284	8.34	Dec. 19, 1974	404

Table 21. Some important properties of near-optimum trajectory profiles for manned exploration of Mars

Launch date	HEV_1 km/sec	T_{12} days	HEV_2 km/sec	ΔT days	Mars launch date	HEV_2 km/sec	T_{23} days	HEV_3 km/sec	Arrival date	Total time
May 19, 1971	3.53	135	5.52	9	Oct. 10, 1971	5.78	264	9.86	June 30, 1972	408
July 27, 1973	3.90	175	3.62	9	Jan. 27, 1974	6.81	258	15.77	Oct. 12, 1974	442

Table 22. Some important properties of alternative trajectory profiles for manned exploration of Mars

Launch date	HEV_1 km/sec	T_{12} days	HEV_2 km/sec	ΔT days	Mars launch date	HEV_2 km/sec	T_{23} days	HEV_3 km/sec	Arrival date	Total time
Aug. 12, 1970	3.26	309	6.75	19	July 6, 1971	4.19	246	6.44	Mar. 8, 1972	574
June 4, 1972	4.32	335	6.19	61	June 19, 1973	3.54	190	3.42	Dec. 26, 1973	586

escape trajectory (parabolic); thus this rocket will be able to send approximately

$$90{,}000 \exp\left[\frac{11.00 - \left(11.00^2 + 3.26^2\right)^{1/2}}{3.6}\right] \text{lb} = 78{,}300 \text{ lb}$$

on the required trajectory! The *Saturn 5* should be a highly reliable standard launch vehicle by 1970.

We shall now describe the method by which a Mars-landing mission can be carried out using only the standard non-nuclear *Saturn 5* launch vehicle. To carry out this mission, two vehicles will be used. The first, which we shall denote by A, shall be a simple Earth–Venus–Mars–Earth fly-by vehicle. The second vehicle, denoted by B, shall be launched on an Earth–Venus–Mars trajectory, and, in place of an Earth re-entry module, it shall carry a small Mars excursion module. The mission profile consists of launching A and B on particular trajectories that will bring B to Mars several days before A makes its Mars closest approach. During this time the crew of B can be exploring the surface of Mars. Then, as A begins to make its closest approach, the crew of B launches their small Mars excursion vehicle to rendezvous with A whereupon they abandon the excursion module to complete the journey back to Earth in A.

As in the case of the 1970 fly-by mission, we shall consider a definite trajectory profile. The particular trajectories that we shall choose do not appear in any of the tables given in this Report. They have, however, been carefully calculated. The Earth–Venus–Mars trajectory that we select for B has the following important characteristics:

T_1 = May 31, 1972

T_2 = November 17, 1972

T_3 = May 12, 1973

HEV_1 = 4.27 km/sec

$DOCA_2$ = 9,223 km

HEV_3 = 6.03 km/sec

T_{12} = 170.00 days

T_{23} = 175.65 days

TFT = 345.64 days

The Earth–Venus–Mars–Earth fly-by trajectory that we select for A is described by the following characteristics:

T_1 = June 4, 1972

T_2 = November 19, 1972

T_3 = May 23, 1973

T_4 = October 17, 1973

HEV_1 = 4.33 km/sec

$DOCA_2$ = 9,164 km

HEV_3 = 5.97 km/sec

$DOCA_3$ = 609 km

HEV_4 = 9.51 km/sec

T_{12} = 167.56 days

T_{23} = 185.44 days

T_{34} = 146.67 days

TFT = 499.67 days

For the re-entry profile associated with this trajectory, a retro thrust must be applied, as in the previous case, to dissipate about 1.23 km/sec to enable the re-entry to take place at 13.3 km/sec. Consequently, before retro, the module will weigh approximately 19,000 lb. Since the interplanetary mission module of A will be occupied by a crew of only one or two persons during the first 353 days, which represents about 70% of the total flight time, we can take its weight to be about 41,000 lb. The *Saturn 5* will be able to send about 71,700 lb on this trajectory. This is 11,700 lb more than required.

Now just before the Mars excursion module is launched from the surface of Mars to rendezvous with A, it is literally stripped of all equipment (heat shield, etc.) that is not absolutely necessary to effect a successful rendezvous. Thus, at the moment it joins A, we may assume that it weighs 12,000 lb. Consequently, prior to launch it would weigh

$$12{,}000 \exp\left[\frac{(5.03^2 + 5.97^2)^{1/2}}{3.6}\right] \text{lb} = 106{,}500 \text{ lb}$$

Assuming that 1.5 tons of supplies and equipment are left on Mars, we find that B's weight at the beginning of its flight will be approximately 145,000 lb. The *Saturn 5* will be able to send about one-half of this weight on B's trajectory. This means that only two *Saturn 5*'s would be necessary to send B on its required trajectory.

It should be stressed at this point that the trajectories which we have chosen for A and B are not the best ones available; more desirable ones do exist. It should also be pointed out that we have taken only the *minimum* launch capabilities of the *Saturn 5* as seen at the present time. This vehicle may develop a high growth potential: by 1972 it may be capable of sending payloads weighing considerably more than 90,000 lb on an escape trajectory. On the other hand, these calculations are optimistic in that many small items, which may have a significant cumulative effect, were omitted. Our main purpose for making these calculations is to show that the *Saturn 5* could be used as the launch vehicle for the first manned landing mission to Mars. No *Nova* launch vehicle or advanced propulsion system would be required.

The unusual mission profiles described for the above manned mission to Mars lead us to the last major topic of this Report.

C. *Interplanetary Transportation Networks to Support Manned Bases on Venus and Mars*

After the first flights to the inner planets, man will naturally construct bases on them. These bases, no matter when they are constructed, will naturally require means by which men and equipment can be taken to and from these bases. In the distant future when propulsion systems far more advanced than those currently being studied are developed, it will probably be possible to make interplanetary voyages, such as Earth–Mars transfers, with flight times as short as one or two weeks. But for the near future all interplanetary transfers will have to be made on near-optimum transfer trajectories with low departure and arrival hyperbolic excess velocities. Consequently, a great deal of life-support equipment will be necessary to transport a few persons from one planet to another. In short, cargo vehicles shall probably be robot-type vehicles carrying no equipment necessary for manned flight, while the manned vehicles will probably carry very limited amounts of cargo. In addition to carrying all the extra equipment for manned flight, these vehicles will also probably be required to be able to induce some artificial gravity. Hence, the transportation of just 10 men, for example, from Mars to Earth should ordinarily require a large and very expensive rocket. Methods of recovery will become a necessity. This problem of economics can be conveniently solved by constructing a long-lasting interplanetary transportation network designed for the sole purpose of transporting personnel from one planet to another.

Preliminary calculations have shown that if the planets P_i are restricted to Mercury, Venus, Earth, and Mars, where P_1 = Earth and $P_i \neq P_{i+1}$ for $i = 1, 2, \cdots, n$, it is possible to find sequences $P_1 - P_2 - \cdots - P_n$ such that the flight times $T_{i+1} - T_i$ are comparable to those required for optimum $P_i - P_{i+1}$ transfers. Moreover, many of these multiplanet trajectories were found to have very low launch energies.

The network can be established by first constructing the many large space vehicles that are to be used in the transportation system. This can be done by methods of prefabrication and orbital assembly. These vehicles can be designed to accommodate 20 to 60 persons, and, since artificial gravity will be highly desirable, the geometry of such a vehicle could resemble a torus with an outside diameter of perhaps 200 to 300 ft. When each individual vehicle is completed, one simply awaits its launch date T_1, when the vehicle (i.e., space bus) is injected into its prescribed interplanetary trajectory. This could be accomplished by convenient strap-on solid-propellant rocket engines. Each vehicle will carry extra provisions and life-support equipment to last until it makes its first Earth rendezvous, whereupon its supply can be replenished to last until it makes its second Earth rendezvous, etc. When such a vehicle approaches a planet P_i, a small excursion module orbiting P_i and containing a few men wishing to go to P_{i+1} can be injected onto an intercept trajectory with the space bus. Upon making rendezvous, the excursion module containing very accurate, automatic planetary approach guidance equipment could be left a few miles behind the space bus on an almost identical interplanetary trajectory to be used to transport the men from the space bus onto an orbit about P_{i+1}. A tanker vehicle, also equipped with accurate automatic planetary approach guidance and also following the space bus, could be used to refuel the planetary excursion modules. Other transportation systems could be established on each separate planet to provide a means for bringing the men from the orbiting excursion modules down to a planet's surface. The modules, however, could be left in respective circular orbits about the planets for future use. Tanker vehicles orbiting the planets could provide a means for refueling the excursion modules, which never actually land on a planet.

The transportation network outlined above seems attractive for several reasons. One notices that all the vehicles involved in the network (which could be made up of several dozen space buses all on their own different interplanetary trajectories) can be used as often as desired. These interplanetary transfer vehicles could be very large and hence could be designed so that these necessarily long planetary transfers could become quite acceptable. The relatively large number of transfer vehicles in the network would greatly preclude the possibility of a crew's running out of supplies and becoming isolated on a planet. Table 23 contains an example of one such trajectory that a space bus might fly and that has the form

Earth–Venus–Mars–Earth–Mars–Earth–Venus–Earth

Table 23. An example of a possible trajectory for an interplanetary transportation network

	$i=1$ Earth	$i=2$ Venus	$i=3$ Mars	$i=4$ Earth	$i=5$ Mars	$i=6$ Earth	$i=7$ Venus	$i=8$ Earth
T_i	8/14/70	12/20/70	6/17/71	4/25/72	12/11/73	5/31/74	3/26/75	7/30/75
HEV_i, km/sec	3.28	5.44	6.74	9.34	13.46	11.81	10.83	7.91
$T_{i,\ i+1}$, days	—	128.20	179.30	312.22	595.03	171.58	298.37	126.26
$\theta_{i,\ i+1}$, deg	—	151.25	171.65	290.81	203.10	191.74	196.13	220.57
$DOCA_i$, km/sec	—	3,817.	6,838.	8,089.	592.	6,249.	9,455.	—
$VACA_i$, km/sec	—	9.75	7.34	11.93	14.23	14.23	12.61	—
$TISI_i$, days	—	2.47	1.85	2.26	0.97	1.82	1.29	—
DA_i, deg	—	63.44	9.69	27.79	6.41	21.27	17.39	—

V. CONCLUDING REMARKS

The numerical results described in Part IV show that multiple planetary free-fall interplanetary trajectories involving more than two planets of the form

$$P_1 - P_2 - P_3 - \cdots - P_n$$

can be of great value in both the unmanned and manned exploration of the inner planets. The results definitely indicate that these trajectories may be of significant value for future missions. Let us take another look at the difficulties that we are forced to contend with if we are restricted to the use of conventional direct-flight transfer trajectories. We have found that the four principal time–energy barriers are as follows:

1. The lowest possible launch energies for Earth–Mercury missions are exceptionally high.

2. Direct-flight Earth–Mars missions have their favorable launch periods separated by long intervals of time lasting approximately 780 days.

3. Minimum-energy manned Mars reconnaissance trajectories of the form Earth–Mars–Earth require flight times in excess of 1,000 days.

4. The favorable Mars–Earth launch periods occur 40 to 60 days *before* the favorable Earth–Mars launch periods, resulting in very high hyperbolic excess velocities for all trajectories of manned round-trip Mars missions.

The most important mission affected by the application of multiple planetary trajectories is, of course, the manned mission to Mars. We have seen that the *Saturn* 5 launch vehicle currently being developed for the *Apollo* Moon mission could possibly be utilized as the primary launch vehicle not only for a manned Venus–Mars fly-by mission but also for an actual manned Mars landing mission. This 1970 and 1972 *Saturn* 5 possibility is also attractive because of high solar activity during the period from 1977 to 1981. Manned interplanetary flights during this period may require a relatively large amount of radiation shielding.

Now there remains one very important aspect of multiple planetary trajectories calculated in this Report that must be considered. This involves the question of accuracy. Just how good is the assumption that one, and only one, body influences the vehicle's motion at any given time? The Jet Propulsion Laboratory has a precision trajectory computer program such that, if the geometry of the trajectory near P_i is sufficiently close to the exact trajectory required for the vehicle to intercept P_{i+1}, an iteration process is begun by integrating the original trajectory to determine the miss vector at P_{i+1} and then using this information to modify the trajectory near P_i to reduce this miss vector. The iteration continues until the miss vector becomes smaller than some specified amount. The program is highly unstable in the sense that, if the initial trajectory in the vicinity of P_i is not extremely close to the real one required to permit the vehicle to rendezvous with P_{i+1}, the iteration process will not converge. It has been observed that each time this program was employed to check the trajectories resulting from the solution given in this Report, very rapid convergence resulted. This could only mean that our fundamental assumption must not give trajectories very far from those that would actually occur in the real situation.

NOMENCLATURE

A Earth–Venus–Mars–Earth manned reconnaissance vehicle carrying a standard Earth-landing module

A position of space vehicle at time $T_1{}^*$ as it enters the sphere of influence τ of the planet P_i

a semimajor axis

a_1 semimajor axis of $\overset{\frown}{P_1 P_2}$

a_2 semimajor axis of hyperbolic trajectory in τ with respect to Σ'

a_3 semimajor axis of $\overset{\frown}{P_2 P_3}$

a_{ii} defined by Eq. (11)

a_{ij} defined by Eq. (12)

B Earth–Venus–Mars–Earth manned vehicle carrying a Mars-landing module

B position of space vehicle at time T_2 when closest to P_2

B' position of vehicle moving on the orbit $\overset{\frown}{P_1 P_2}$ at time T_2 as though P_2 did not exist

B'' position of vehicle moving on the orbit $\overset{\frown}{P_2 P_3}$ at time T_2 as though P_2 did not exist

b_i defined by Eq. (11)

b_2 length of the conjugate axis

C the boundary of S

C position of space vehicle at time $T_2{}^*$ as it leaves the moving region τ

$\mathbf{c}$ constant vector of integration

c the distance between P and Q

$\mathbf{c}$ exhaust velocity

DA_k angular difference between the vehicle's velocity vectors as it enters and leaves P_k's sphere of influence, deg

$DOCA_k$ distance of closest approach to P_k's surface, km

D position of planet P_2 at time $T_1{}^*$

d distance of closest approach to the surface of P_2

E position of planet P_2 at time T_2

$\mathbf{e}$ one of the two vectors that describe conic motion; this vector has magnitude equal to the conic's eccentricity, and it points in the direction of perihelion passage

e eccentricity of a conic and equal to the magnitude of $\mathbf{e}$

e_1 component of $\mathbf{e}$ in the X direction, defined by Eq. (18)

e_2 component of $\mathbf{e}$ in the Y direction, defined by Eq. (19)

e_3 component of $\mathbf{e}$ in the Z direction, defined by Eq. (20)

F the primary focus

F^* the vacant focus

$\mathbf{f}$ vector function having continuous gradient $\nabla \mathbf{f}$ over S

G (1) position of planet P_2 at time $T_2{}^*$
(2) universal gravitational constant

HEV_k hyperbolic excess velocity at P_k, km/sec

$\mathbf{h}$ angular momentum vector for conic motion

h magnitude of angular momentum

h_1 component of $\mathbf{h}$ in the X direction, defined by Eq. (21)

h_2 component of $\mathbf{h}$ in the Y direction, defined by Eq. (22)

h_3 component of $\mathbf{h}$ in the Z direction, defined by Eq. (23)

$\hat{\mathbf{i}}$ unit vector in the X direction

$\mathbf{I}$ idemfactor

i inclination of orbit plane to equatorial or ecliptic plane

$\hat{\mathbf{j}}$ unit vector in the Y direction

$\hat{\mathbf{k}}$ unit vector in the Z direction

k integer equal to the kth planet of the solar system

l semilatus rectum $= h^2/\mu$

l_1 semilatus rectum of $\overset{\frown}{P_1 P_2}$

l_3 semilatus rectum of $\overset{\frown}{P_2 P_3}$

M (1) point at which the vehicle arises above the ecliptic
(2) mass of the Sun

m mass of a planet

m_2 mass of P_2

$\hat{\mathbf{n}}$ unit vector directed toward M

n number of planetary encounters

P (1) point on an interplanetary trajectory with position vector $\mathbf{R}_1$
(2) period of a trajectory

P_1 launch planet, usually Earth

P_2 first intercept planet

P_3 second intercept planet

$\overset{\frown}{P_1 P_2}$ the elliptical transfer trajectory from P_1 to P_2

$\overset{\frown}{P_2 P_3}$ the elliptical transfer trajectory from P_2 to P_3

Q point on interplanetary trajectory with position vector $\mathbf{R}_2$

$\mathbf{R}(t)$ position vector of vehicle with respect to Σ at time t

$\mathbf{R}_i(t)$ position vector of P_i with respect to Σ at time t ($i = 1, 2, \cdots n$)

$\hat{\mathbf{R}}$ unit vector directed from the center of a body to a vehicle separated by a distance $R = \mathbf{R}/R$

R distance from center of gravitating body to vehicle

S area of π bounded by the arc of the trajectory and the radius vectors $\mathbf{R}(T_1)$ and $\mathbf{R}(T_2)$

S sign of $\sin \theta_i$

s semiperimeter of triangle FPQ

TFT total flight time, days

TISI_k amount of time vehicle spends in P_k's sphere of gravitational influence, days

T_1 time at which vehicle leaves planet P_1

T_1^* time at which vehicle enters τ of P_2

T_2 time of vehicle's closest approach to P_2

T_2^* time at which vehicle leaves τ of P_2

T_3 time of vehicle's closest approach to planet P_3

$T_{k,k+1}$ time taken by vehicle to pass from P_k to P_{k+1} (i.e., $T_{k+1} - T_k$), days

T_P time of perihelion passage

VACA_k velocity at closest approach to P_k, km/sec

$\mathbf{V}(t)$ velocity vector of vehicle with respect to Σ at time t

$\mathbf{V}'(t)$ velocity vector of vehicle with respect to Σ' at time t

$\mathbf{V}_i(t)$ velocity vector of P_i with respect to Σ at time t ($i = 1, 2, 3$)

V characteristic velocity for a mission using a single-stage rocket with exhaust velocity = c

V'_{cA} velocity of closest approach with respect to P_2

α scalar defined by Eq. (10)

β scalar defined by Eq. (11)

$\boldsymbol{\zeta}$ arbitrary constant vector

θ the angle measured from **e** in the positive direction (i.e., counterclockwise) to **R**, i.e., the true anomaly

$\theta_{k,k+1}$ heliocentric angle swept out by vehicle passing from P_k to P_{k+1}, deg

μ constant scalar = GM

μ_2 m_2G

π plane of motion of a body moving under the influence of one, and only one, other body

ρ^* radius of τ

$\boldsymbol{\rho}(t)$ position vector of vehicle with respect to Σ' at time t

Σ any Cartesian inertial frame with the Sun's center as its origin

Σ' a parallel translation of Σ with a new origin located at the center of a planet influencing the motion of a vehicle

τ region of gravitational influence about a planet

Ω the longitude of an ascending node

ω argument of perihelion

REFERENCES

1. Wintner, A., *Analytical Foundations of Celestial Mechanics*, Princeton University Press, Princeton, New Jersey, 1947.
2. Minovitch, M. A., *A Method for Determining Interplanetary Free-Fall Reconnaissance Trajectories*, Technical Memorandum No. 312-130, Jet Propulsion Laboratory, Pasadena, Calif., August 23, 1961.
3. Battin, R. H., "The Determination of Round-Trip Planetary Reconnaissance Trajectories," *Journal of the Aero/Space Sciences*, Vol. 26, No. 9, September, 1959.
4. Clarke, V. C., Jr., *A Summary of the Characteristics of Ballistic Interplanetary Trajectories, 1962–1977*, Technical Report No. 32-209, Jet Propulsion Laboratory, Pasadena, California, January 15, 1962.
5. Makemson, M. W., Baker, R. M. L., Jr., and Westrom, G. B., "Analysis and Standardization of Astrodynamic Constants," *Journal of Astronautical Sciences*, Vol. 8, No. 1, Spring, 1961.
6. Hammock, D., and Jackson, B., "Vehicle Design for Mars Landing and Return to Mars Orbit," American Astronautical Society, Symposium on the Exploration of Mars, Denver, Colorado, June 6–7, 1963.
7. Dixon, F., and Stimpson, L., "A Systems Approach to Vehicle Design for Earth Reentry From an Interplanetary Mission," American Astronautical Society, Symposium on the Exploration of Mars, Denver, Colorado, June 6–7, 1963.
8. *Planetary Coordinates for the Years 1960–1980*, Her Majesty's Stationery Office, H. M. Almanac Office, London, England, 1958.
9. Clarke, V. C., Jr., *Constants and Related Data Used in Trajectory Calculations at the Jet Propulsion Laboratory*, Technical Report No. 32-273, Jet Propulsion Laboratory, Pasadena, California, May 1, 1962.

APPENDIX A

The Calculation of Planetary Position and Velocity Vectors

In Part II we developed a very convenient calculus for dealing with conic trajectories in three dimensions. We have seen that it is ideally suited for problems in astronautics. Thus, as one might suspect, it can be easily employed to calculate planetary position and velocity vectors for any time t. We shall now give the method that was actually used for the numerical computation of the above trajectories. It has been observed that the accuracy obtained by this method approaches that obtained by the most involved and complicated techniques of classical celestial mechanics.

Let $\mathbf{R}$, which is to be calculated, be the position vector of a particular planet at the time t. Suppose $\mathbf{R}_1$ and $\mathbf{R}_2$ are two position vectors of the planet given in a planetary ephemeris (see Ref. 8) corresponding to t_1 and t_2, respectively, where $t_1 \leq t \leq t_2$. We shall take $t_2 - t_1 = 10$ days for the first six planets. Missions to Uranus, Neptune, and Pluto take too long for elliptic transfer trajectories. In Fig. A-1, the vectors $\mathbf{R}_0$ and $\mathbf{R}_3$ correspond to the planet's position vectors at t_0 and t_3, respectively, which are given as near-by entries in the planetary ephemeris, where $t_0 < t_1 \leq t \leq t_2 < t_3$. These vectors will be used to calculate the planet's osculating elliptic orbit at the time t. This calculated orbit will not be the true osculating orbit at time t because the planet's actual path about the Sun is not elliptic. However, if the arc subtended by $\mathbf{R}_0$ and $\mathbf{R}_3$ is not too large, it may be assumed to be elliptic. This assumption applies even more successfully to the arc subtended by $\mathbf{R}_1$ and $\mathbf{R}_2$, but $\measuredangle (\mathbf{R}_1\ \mathbf{R}_2)$, being small for most planets, will magnify errors in $\mathbf{R}_1$ and $\mathbf{R}_2$ appearing in the ephemeris. Thus, if we choose $t_1 - t_0 = t_3 - t_2 = 10\,k$ days, where k is an integer equal to the kth planet that is being considered, both conditions can be partially satisfied. Hence, one easily finds

Planet	k	$t_3 - t_0$, days
Mercury	1	30
Venus	2	50
Earth	3	70
Mars	4	90

The osculating orbit is then calculated by first finding the semimajor axis by means of Lambert's theorem in the form of Eq. (24), where $t = t_3 - t_0$. The eccentricity is then calculated with the aid of Eq. (30). The $\mathbf{e}$ and $\mathbf{h}$ vectors may now be calculated by means of Eq. (8) to (12). In Fig. A-1, $\mathbf{D} = \mathbf{R}_2 - \mathbf{R}_1$; hence $\mathbf{D}$ lies in the planet's plane of motion and intersects the vector $\mathbf{R}$ at some point Q. The points Q_1 and Q_2 are the positions of the planet at t_1 and t_2, respectively. If $d = \overline{Q_1 Q}$, it is easy to see that

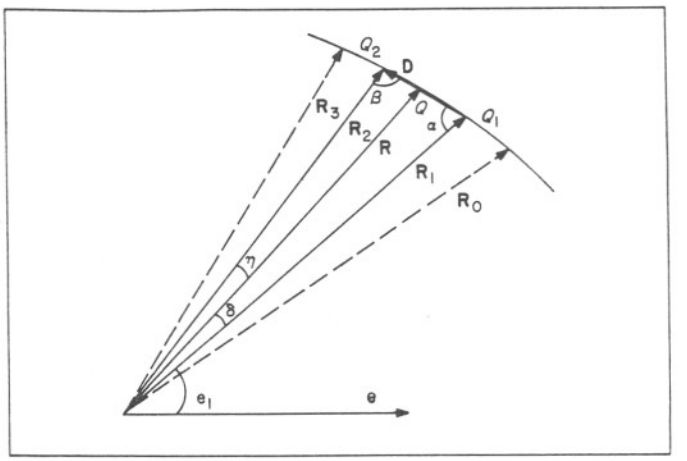

Fig. A-1. Geometry for calculating planet's osculating orbit

$$\hat{\mathbf{R}} = \frac{\mathbf{R}_1 + f\,\mathbf{D}}{|\,\mathbf{R}_1 + f\,\mathbf{D}\,|} \tag{A-1}$$

where $f = d/D$. It is also evident from the Figure that the following trigonometric relations are true:

$$\frac{d}{\sin\delta} = \frac{R_1}{\sin(\beta+\eta)}$$

and

$$\frac{D-d}{\sin\eta} = \frac{R_2}{\sin(\beta+\eta)}$$

Consequently, it follows that

$$f = \left[\,1 + \frac{R_2 \sin(\sigma-\delta)}{R_1 \sin\delta}\,\right]^{-1} \tag{A-2}$$

where $\sigma = \delta + \eta$. This angle σ may easily be calculated by

$$\sigma = \cos^{-1}\left(\frac{\mathbf{R}_1 \cdot \mathbf{R}_2}{R_1 R_2}\right)$$

Now the angle δ is dependent on some scalar function $F(t)$. Since $t_2 - t_1 = 10$ days is small compared to any of the planets' periods about the Sun, $F(t)$ may be expressed as a rapidly converging Taylor series about t_1:

$$\delta = F(t_1) + \frac{dF(t_1)}{dt}(t-t_1) + \frac{1}{2!}\frac{d^2F(t_1)}{dt^2}(t-t_1)^2 + \cdots \qquad \text{(A-3)}$$

Since $\delta = 0$ at $t = t_1$, $F(t_1) = 0$. Let $\theta = \measuredangle\,|\mathbf{e}, \mathbf{R}|$, and suppose that we refer time to the last perihelion passage so that $\theta = 0$ at $t = 0$. Then

$$\delta = F(t) = \theta - \theta_1$$

and it follows, in view of Eq. (34), that

$$\frac{dF(t_1)}{dt} = \frac{h}{l^2}(1 + e\cos\theta_1)^2$$

$$\frac{d^2F(t_1)}{dt^2} = -2\left(\frac{h}{l^2}\right)^2 e\,(1 + e\cos\theta_1)^3 \sin\theta_1$$

and

$$\frac{d^3F(t_1)}{dt^3} = 2\left(\frac{h}{l^2}\right)^3 e\,(1 + e\cos\theta_1)^4 \times [3e\sin^2\theta_1 - (1 + e\cos\theta_1)\cos\theta_1]$$

For all planets except Mercury, the Taylor series converges very rapidly, so that all terms except the first three can be neglected. In the case of Mercury, the fourth term does contribute a small, but sometimes a nonnegligible, amount to the series. The *maximum* contribution of this term has been found to be about 0.1 deg. Thus, for the fourth term, one finds

$$\frac{d^4F(t_1)}{dt^4} = 2e\left(\frac{h}{l^2}\right)^4 \sin\theta_1\,(1 + e\cos\theta_1)^5 \times (24\,e^2\cos^2\theta_1 + 13\,e\cos\theta_1 - 12\,e^2 + 1)$$

The values for $\cos\theta_1$ and $\sin\theta_1$ may be computed from

$$\cos\theta_1 = \frac{\mathbf{R}_1 \cdot \mathbf{e}}{R_1 e}$$

and

$$\sin\theta_1 = S\left(1 - \cos^2\theta_1\right)^{1/2}$$

where S is equal to the sign of $\sin\theta_1$ and is easily seen to be

$$S = \frac{(\mathbf{e} \times \mathbf{R}_1) \cdot \mathbf{h}}{|(\mathbf{e} \times \mathbf{R}_1) \cdot \mathbf{h}|}$$

where $\mathbf{h}$ is the osculating $\mathbf{h}$-vector. Thus, after calculating each term, δ may be obtained by Eq. (A-3). Upon substituting this value into Eq. (A-2) and the resulting value of f into Eq. (A-1), $\mathbf{R}$ can be calculated. The desired position vector of the planet at the time t is obtained by

$$\mathbf{R} = \frac{l}{1 + \mathbf{e}\cdot\hat{\mathbf{R}}}\,\hat{\mathbf{R}}$$

which follows from Eq. (7). The planet's velocity vector $\mathbf{V}$ is immediately calculated by

$$\mathbf{V} = \frac{1}{l}\,\mathbf{h} \times (\hat{\mathbf{R}} + \mathbf{e})$$

APPENDIX B

Constants of the Solar System Used in the Calculations

The following constants have been employed throughout all the numerical computation:

astronomical unit (au) = 1.495990×10^8 km

$GM_{\text{Sun}} = \mu_{\text{Sun}} = 2.9591221 \times 10^{-4} \dfrac{\text{au}^3}{\text{day}^2}$

mean obliquity (for 1950) = 23° 26′ 44.84″

Constants used for the planets were taken from Ref. 5 and 9 and are given in the following table, where R = radius (in km), m = planet's mass, M = Sun's mass, and $\mu = Gm$ (in au^3/day^2). The radius given for Venus includes the visible atmosphere. Thus, the distance of closest approach to Venus given in the numerical tables refers to the distance of closest approach to the planet's cloud layer and not to its actual surface.

Planet	R, km	$(m/M)^{2/5}$	μ, au^3/day^2
Mercury	2330.0	0.00193138	4.835167×10^{-11}
Venus	6100.0	0.00570377	7.241303×10^{-10}
Earth	6378.2	0.00617728	8.887552×10^{-10}
Mars	3415.0	0.00253523	9.582649×10^{-11}